EVOLUTION OF GLACIER-DAMMED LAKES THROUGH SPACE AND TIME; BRADY GLACIER, ALASKA, USA

by

Denny Capps
M.Sc., Montana State University, 2004
B.Sc., Louisiana Tech University, 1997

Dissertation Submitted in Partial Fulfilment of
the Requirements for the Degree of

Doctor of Philosophy

In the
Department of Earth Sciences
Faculty of Sciences

SIMON FRASER UNIVERSITY

Fall 2011

APPROVAL

Name: **Denny Capps**

Degree: **Doctor of Philosophy**

Title of Thesis: **Evolution of glacier-dammed lakes through space and time; Brady Glacier, Alaska, USA**

Examining Committee:

Chair: **Dr. Dan Gibson**
Associate Professor, Department of Earth Sciences

_____

Dr. John Clague
Senior Supervisor
Professor, Department of Earth Sciences

_____

Dr. Gwenn Flowers
Supervisor
Associate Professor, Department of Earth Sciences

_____

Dr. Roger Wheate
Supervisor
Associate Professor, University of Northern BC

_____

Dr. Brent Ward
Internal Examiner
Professor, Department of Earth Sciences

_____

Dr. Wilfried Haeberli
External Examiner
Professor, University of Zurich

Date Defended/Approved: October 21, 2011

Partial Copyright Licence

ABSTRACT

Glacier-dammed lakes and their associated jökulhlaups cause severe flooding in downstream areas and substantially influence glacier dynamics. The goal of this dissertation is to identify and characterize the evolution of glacier-dammed lakes in order to predict their future behaviour using ground-truthed remote sensing techniques and dendrochronology. Brady Glacier in southeast Alaska is particularly well suited for a study of these phenomena because it presently dams ten large (> 1 km^2) lakes and many smaller ones. This dissertation comprises three studies. First, I used interferometric synthetic aperture radar (InSAR) to identify and characterize three previously unknown subglacial lakes. InSAR allowed me to quantify the vertical displacement and volume of water discharged from the three lakes through time. From the fall of 1995 to the spring of 1996, subsidence ranged from 4 to 26 cm/day and the volume of water discharged ranged from 22,000 ± 2000 to 243,000 ± 14,000 m^3/day. Subsidence and discharge rates declined significantly during the winter and continued at a lesser rate through March. Second, I used dendrochronology and precise elevation-constrained mapping to date glacially overridden and drowned trees at the glacier margin. Brady Glacier impounded Spur Lake to an elevation of 83 m a.s.l. around AD 1830 and 121 m a.s.l. around 1839. The glacier continued to advance, thickening by at least 77 m between ca. 1844 and 1859 at a site down-glacier of Spur Lake on the opposite glacier margin. Farther down-glacier, North Trick Lake began to form by 1861 and reached its highest elevation at approximately 130 m a.s.l. when Brady Glacier reached its maximum extent around 1880. Third, I georeferenced a variety of maps, airphotos, and optical satellite imagery to characterize the evolution of the glacier and lakes and also created five bathymetric maps. The main terminus of Brady Glacier has changed little since 1880. However, it downwasted at rates of 2-3 m/yr between 1948 and 2000, more than the regional average. The most dramatic retreat (2 km) and downwasting (123 m) occurred adjacent to glacier-dammed lakes. These lakes will continue to evolve and play a pivotal role in the evolution of Brady Glacier. If downwasting and retreat continue at rates comparable to the past, the glacier may return to a tidewater regimen and retreat catastrophically until it stabilizes in shallow water.

Keywords: glacier-dammed lake; jökulhlaup; Brady Glacier; tidewater glacier; Glacier Bay National Park; Alaska; InSAR; dendrochronology; glacier fluctuation

ACKNOWLEDGEMENTS

This dissertation was funded primarily through a Canon National Parks Science Scholarship to Capps and a Natural Sciences and Engineering Research Council of Canada Discovery Grant to Dr. John Clague. Additional funding was provided by Simon Fraser University's Graduate Fellowship, International Scholarship, and Presidential Research Stipend; a Geological Society of America Graduate Scholarship; a Natural Sciences and Engineering Research Council of Canada Discovery Grant to Dr. Brian Luckman; and a National Science Foundation grant to Dr. Greg Wiles.

I thank Dan Shugar for three seasons of assistance with challenging fieldwork; MacDonald Dettwiler and Associates, specifically Bernhard Rabus and Harold Zwick, for project oversight and Parwant Ghuman for guidance in processing InSAR data; Glacier Bay National Park for maps, aerial photographs, local information, safety checks, and lodging; Jesse Dykstra for pioneering fieldwork; Marmot Mountain outdoor products for providing equipment that kept us safe and warm; G3 – Genuine Guide Gear for backcountry ski equipment; Mike Loverink, owner and pilot of Air Excursions, for his willingness to land a floatplane in iceberg- and snag-infested waters; Drake Olson for flights to and from the glacier under challenging conditions; the European Space Agency provided ERS-1/2 data; Chris Larsen for generously sharing glacier elevation change data; Bill Eichenlaub for a loaning us an inflatable kayak after a bear destroyed ours; Bob Christiansen for help with reconnaissance work in 2006; and lastly, but certainly not least, the Simon Fraser University Department of Earth Sciences staff, in particular Rodney Arnold, Glenda Pauls, Matt Plotnikoff, and Tarja Vaisanen.

Special appreciation goes to Dr. John Clague, primary supervisor and mentor. Never before have I seen such dedication to science and education in an individual. John gives selflessly with his time, knowledge, and resources to all those that show interest in Earth Science. I feel highly privileged to have spent many years under his tutelage. Thank you John.

TABLE OF CONTENTS

Approval ..... **ii**
Abstract iii
Acknowledgements iv
Table of Contents v
List of Figures vii
List of Tables x

1. Introduction **1**
1.1 Background 1
1.2 Research Goals and Objectives 5
1.3 Dissertation Overview 7

2. Identification and characterization of alpine subglacial lakes using InSAR, Brady Glacier, Alaska **9**
Abstract 9
2.1 Introduction 9
2.1.1 Study area 11
2.2 Line-of-sight Displacement 14
2.2.1 Data sets 14
2.2.2 Interferogram processing 16
2.2.3 Interactive unwrapping 18
2.3 Isolating Horizontal and Vertical Displacements 19
2.3.1 Two-dimensional displacement maps 19
2.3.2 One-dimensional displacement maps 20
2.3.3 Error analysis 22
2.4 Displacement Volume Calculation 23
2.5 Discussion 25
2.5.1 Subglacial hydrology 25
2.5.2 Early identification of glacier-dammed lakes 28
2.5.3 Application of technique to other areas 30
2.6 Summary 31

3. Tree-ring dating of the nineteenth-century advance of Brady Glacier and the evolution of two marginal lakes, Alaska **33**
Abstract 33
3.1 Introduction 33
3.2 Study Area 34

3.3 Previous Studies at Brady Glacier 38
3.4 Sample Sites and Chronology Development 40
3.5 Results 42
3.6 Discussion 45
3.6.1 Chronology of last glacier advance and lake damming 45
3.6.2 Comparison with Glacier Bay 49
3.6.3 Differential preservation of subfossil wood 50
3.7 Summary and Conclusions 52

4. Evolution of glacier-dammed lakes through space and time; Brady Glacier, Alaska, USA 53

Abstract 53
4.1 Introduction 54
4.2 Regional Setting 57
4.2.1 Brady Glacier 57
4.2.2 Previous studies 57
4.3 Methods 60
4.3.1 Evolution of Brady Glacier through time 60
4.3.2 Evolution of Brady Glacier's lakes and jökulhlaups through time 61
4.3.3 Current bathymetry of select glacier-dammed lakes 62
4.4 Results 62
4.4.1 Evolution of Brady Glacier through time 62
4.4.2 Evolution of Brady Glacier's lakes and jökulhlaups through time 64
4.4.3 Current bathymetry of select glacier-dammed lakes 75
4.5 Discussion 78
4.5.1 The effect of calving on Brady Glacier 78
4.5.2 Possible jökulhlaup effects on the stability of Brady Glacier 83
4.5.3 Space as a proxy for time 84
4.5.4 Evolution of analogous glacier/lake systems 86
4.6 Conclusion 90

5. Summary 91

5.1 Synthesis 91
5.2 Future Work 94

6. References 98

Appendices 104

Appendix A. Additional interferograms 104
Appendix B. Dendrochronology COFECHA output 112

LIST OF FIGURES

Fig. 1.1. Partially drained Abyss Lake on August 9, 2005. The lake is dammed by Brady Glacier in Glacier Bay National Park and Preserve in southeast Alaska. View is to the southwest (photo by Bruce Molnia). 2

Fig. 1.2. Schematic diagram showing locations of glacier-dammed lakes. (A) supraglacial, (B) subglacial, (C) proglacial, (D) embayment in slope at glacier margin, (E) area of coalescence of two glaciers, (F) tributary valley adjacent to a trunk or tributary glacier, (G) same as F except glaciers dam both ends of the lake, and (H) main valley adjacent to a tributary glacier. Toned area is land; unpatterned area is ice. (Reproduced with permission from Clague and Evans, 1994.) 3

Fig. 1.3. Jökulhlaup on Salmon River near Hyder, Alaska on July 29, 1993 (photo by John Clague) 3

Fig. 2.1. False-color Landsat image of Brady Glacier, southeast Alaska. Topographic contours derived from 2000 SRTM DEM (50-m contour interval). Large lakes dammed by Brady Glacier numbered 1 – 10. Lakes discussed in text: 1) Divide Lake, 2) Hinge Lake, 3) Saddle Lake, 4) Abyss Lake, and 5) Oscar Lake. 12

Fig. 2.2. 1997 digital orthophoto of the study area with contours derived from 2000 SRTM DEM (25-m contour interval). 15

Fig. 2.3. Interferograms for (a) 29 to 30 September 1995 showing substantial displacement over all three subglacial lakes, and (b) 23 to 24 March 1996 showing much less displacement over the same area. For C-band ERS, with a wavelength of 5.6 cm, one fringe corresponds to a difference in line-of-sight (LOS) ground displacement of 2.8 cm. Thus, in Figure 2.3a the line-of-sight displacement at the centre of Hinge Lake over the 24 hour period is 10 cm. 17

Fig. 2.4. (a) Unsuccessfully unwrapped displacement map of Hinge Lake derived using standard techniques (note discontinuity in colour pattern), and (b) successfully unwrapped displacement map derived using an iterative unwrapping technique. 19

Fig. 2.5. Correlation of (a) crevasses seen in 1997 aerial photograph with (b) line-of-sight displacement in the interferogram. 21

Fig. 3.1. Brady Glacier and its surrounding area (after National Park Service, 2009). 36

Fig. 3.2. Terminus of Brady Glacier. The study sites are indicated by red crosses. The interpreted locations of former glacier termini are based on early observations (Klotz, 1899; Davidson, 1904; Derksen, 1976). The red dashed line indicates the present margin of “East Trick” Lake. The red dots indicate

locations of photographs in Figure 3.3. Topographic map – 1961 U.S. Geological Survey; scale 1:63,360; contour interval 100 feet (ca. 30 m). Spur and East Trick lakes are unofficial names. 37

Fig. 3.3. Sample sites: a) glacier margin; view west (person circled for scale). b) North Trick Lake; view east with high strandlines denoted by arrow and red dotted line. c) Spur Lake; view northwest. Photographs taken from viewpoints indicated on Figure 3.2.....41

Fig. 3.4. Crossdate of the composite Brady Glacier chronology (blue solid lines) with Excursion Ridge master chronology (black dotted lines), which was created from living mountain and western hemlock. The upper plot illustrates tree-ring chronologies standardized using a 32-yr spline with persistence removed to emphasize the high-frequency signal. The lower plot shows sample sizes for the two chronologies. Numbers in parentheses are years of overlap (N) and correlation coefficient (R). 43

Fig. 3.5. Outermost ring dates (with critical calendar dates indicated) and elevations of crossdated samples from the three sites. Samples retaining bark are indicated. Outermost rings without bark provide only limiting death dates. At the glacier margin site, the ice reached as high as 260 m a.s.l. Spur Lake could not rise higher than 125 m a.s.l. because of the stable bedrock outlet at that elevation. North Trick Lake elevations reached up to 130 m a.s.l. 44

Fig. 3.6. Inferred terminus of Brady Glacier at three times during the nineteenth century, based on death dates of trees killed by overriding glacier ice and inundated in lakes that were dammed by the advancing glacier. Background Landsat Thematic Mapper 7 multispectral satellite image. 47

Fig. 4.1. False-color Landsat 5 image (bands 7/4/2) of Brady Glacier, southeast Alaska, acquired on August 14, 2010. Topographic contours are derived from 2000 SRTM DEM (50 m contour interval). 56

Fig. 4.2. Inferred terminus of Brady Glacier at three times during the nineteenth century, based on death dates of trees that were killed by overriding glacier ice or drowned in lakes dammed by the advancing glacier (from Capps et al., 2011). Landsat 7 ETM+ image (bands 3/2/1) acquired in 2000. 59

Fig. 4.3. Location of the Brady Glacier terminus through time based on georeferenced maps, airphotos, and Landsat imagery from 1907 to 2010. The background image is a 1997 digitally orthorectified quadrangle. 63

Fig. 4.4. Brady Glacier elevation change from 1948 to 2000. The background image is a 1997 digitally orthorectified quadrangle. 64

Fig. 4.5. Map of large glacier-dammed lakes (>1 km^2) and historic jökulhlaup drainage routes. The background image is a 1997 digitally orthorectified quadrangle. 68

Fig. 4.6. Evolution of North Deception Lake. (a) 1907 International Boundary Commission 1:250,000-scale topographic map; contour interval 250 feet (ca. 75 m). (b) 1948 U.S. Geological Survey 1:63,360-scale topopgraphic map; contour interval 100 feet (ca. 30 m). (c) False-colour Landsat 7 ETM+ image (bands 7/4/2) acquired on September 16, 2010.....70

Fig. 4.7. Evolution of the Trick lakes. (a) 1907 International Boundary Commission 1:250,000-scale topographic map; contour interval 250 feet (ca. 75 m). (b) 1929 U.S. Navy airphoto. (c) 1948 U.S. Geological Survey airphoto. (d) False-colour Landsat 5 image (bands 7/4/2) acquired on September 6, 1986. 71

Fig. 4.8. Evolution of Abyss Lake. (a) 1907 International Boundary Commission 1:250,000-scale topographic map; contour interval 250 feet (ca. 75 m). (b) 1948 1:63,360-scale U.S. Geological Survey topopgraphic map; contour interval 100 feet (ca. 30 m). (c) False-colour Landsat 7 ETM+ image (bands 7/4/2) acquired on September 16, 2010. 74

Fig. 4.9. Bathymetric maps of select Brady Glacier lakes. Patterned area is glacier. (a) Abyss Lake when full to overflow, (b) North Deception Lake when full to overflow, (c) East Trick Lake on August 29, 2005, (d) Bearhole Lake when full to overflow, and (e) Oscar Lake on August 8, 2006. 77

Fig. 4.10. Tidewater glacier cycle (after Trabant et al., 1990; Molnia, 2008). Figures A through D illustrate the four phases of the cycle. (a) Beginning and end of the cycle when the glacier is in a stable position at the head of the fjord. (b) Advancing phase when the glacier pushes the terminal moraine/shoal forward. (c) Glacier at its fully extended phase. (d) Retreat phase with the production of large tabular icebergs.....79

Fig. 4.11. Dixon Lake partially drained during a jökulhlaup in August 2007. The lake is approximately 2.3 km long.....82

Fig. 4.12. Evolution of Excelsior Glacier and Excelsior Lake through time. (a) August 15, 1941 oblique airphoto of Excelsior Glacier, view east. Arrows indicate two areas of subaerial lake water (from Stone, 1963). (b) 1951 U.S. Geological Survey 1:63,360 topographic map of Excelsior Lake, contour interval 100 feet (ca. 30 m). (c) September 3, 1966, oblique airphotos of Excelsior Lake, view west (after Molnia, 2008). (d) August 3, 2009 false-colour Landsat 5 image (bands 7/4/2). 88

Fig. 4.13. False-colour Landsat 5 image (bands 7/4/2) of Baird Glacier acquired on September 19, 2010. Note substantial flow reversals (red arrows), source of past jökulhlaups (red asterisk), outwash plain, and tidewater near southwest edge of image.....89

Fig. 5.1. Custom-built, GPS-enabled, remote-controlled boat (85 cm long).....94

LIST OF TABLES

Table 2.1. ERS images used in this study. 16

Table 2.2. Maximum subsidence at Divide, Hinge, and Saddle lakes in 24 hours. 22

Table 2.3. Minimum and estimated total volume of water displaced from Divide, Hinge, and Saddle lakes in 24 hours. 24

Table 4.1. Approximate lake surface elevations from topographic maps based on airphotos taken in July and August 1948 and in February 2000 when SRTM imagery was acquired. 66

Table 4.2. Approximate calving margin widths. 67

Table 4.3. Interpolated minimum lake volumes. 76

1. INTRODUCTION

1.1 Background

A glacier-dammed lake is a body of water dammed by glacier ice, irrespective of its position relative to the glacier (Fig. 1.1; Blachut and Ballantyne, 1976). A lake can form within, beneath, on top of, or at the margin of a glacier (Fig. 1.2). Glacier-dammed lakes are important because they cause catastrophic floods (Fig. 1.3) and influence glacier dynamics. The floods they produce are referred to by a variety of names: in Iceland they are known as jökulhlaups; in mainland Europe, debacles; in the Himalayas, glacial lake outburst floods (GLOFs); and in South America, aluviónes. However, several of these names can also be applied to floods or flows unrelated to glacier-dammed lakes. Present scientific literature is increasingly using the Icelandic term, jökulhlaup, to describe these catastrophic floods, and I adopt that practice in this dissertation.

Jökulhlaups are a serious hazard in downstream areas, in part because they can have peak discharges orders of magnitude larger than precipitation-induced floods (Clague and Evans, 1994). Jökulhlaups from Glacial Lake Missoula during the waning stages of the last glaciation were the source of the largest known peak flood discharges (17×10^6 m^3/s) in Earth's history (Alho et al., 2010). Jökulhlaups therefore cause substantial erosion and deposition (Post and Mayo, 1971; Russell et al., 2006; Alho et al., 2010) and have historically caused severe damage to infrastructure up to 1200 km from their source (Mason et al., 1930). Consequently, they are the farthest reaching of all terrestrial glacial hazards.

Glacier-dammed lakes and jökulhlaups directly influence glacier dynamics. Jökulhlaups have been responsible for increases in glacier velocities of up to 300% (Anderson et al., 2005; Mayer

et al., 2008), decreases in glacier velocity that have persisted for several years (Magnússon et al., 2010), and temporary, but complete reversal of glacier motion (Sugiyama et al., 2007). Jökulhlaups have also fractured glacier termini, enhancing the mechanical removal of ice fragments and leading to the creation of large supraglacial channels and embayments (Russell et al., 2006).

Fig. 1.1. Partially drained Abyss Lake on August 9, 2005. The lake is dammed by Brady Glacier in Glacier Bay National Park and Preserve in southeast Alaska. View is to the southwest (photo by Bruce Molnia).

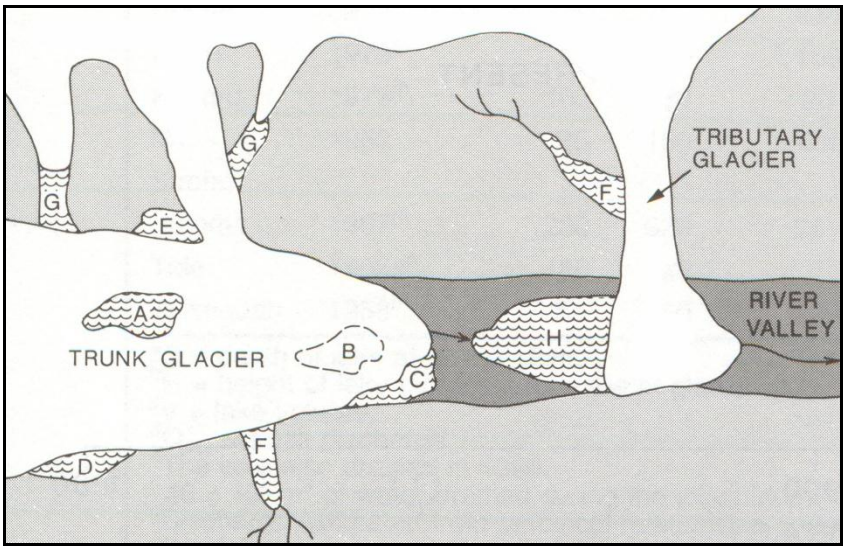

Fig. 1.2. Schematic diagram showing locations of glacier-dammed lakes. (A) supraglacial, (B) subglacial, (C) proglacial, (D) embayment in slope at glacier margin, (E) area of coalescence of two glaciers, (F) tributary valley adjacent to a trunk or tributary glacier, (G) same as F except glaciers dam both ends of the lake, and (H) main valley adjacent to a tributary glacier. Toned area is land; unpatterned area is ice. (Reproduced with permission from Clague and Evans, 1994.)

Fig. 1.3. Jökulhlaup on Salmon River near Hyder, Alaska on July 29, 1993 (photo by John Clague).

Glacier-dammed lakes are common in glacierized mountain regions around the world (Costa and Schuster, 1988; Clague and Evans, 1994); Post and Mayo (1971) identified 750 glacier-dammed lakes in Alaska alone. Many of the lakes they identified have changed dramatically; some no longer exist and many new lakes have formed. Jökulhlaups have caused loss of life or property damage in Alaska, Austria, British Columbia, France, Iceland, India, Italy, Kyrgyzstan, Norway, Pakistan, Peru, Switzerland, Washington, and Wyoming (Eisbacher and Clague, 1984; Costa and Schuster, 1988; Clague and Evans, 1994; Clague and Evans, 1997; Oswald and Wohl, 2007; Mayer et al., 2008). Hundreds of lives have been lost and hundreds of millions of dollars damage have resulted from sudden outbursts of rapidly evolving glacial lakes because the hazard was not been identified until after disasters (Wessels et al., 2002).

Glacier-dammed lakes can change markedly within years or even months, thus their hazard must be assessed regularly. Climate is changing at an unprecedented rate, especially at high latitudes (Trenberth et al., 2007), and glacial lakes evolve rapidly under such conditions; glacier equilibrium is disrupted and hazard zones shift beyond those of historical knowledge (Frey et al., 2010). The recent increase in the rate of retreat and downwasting of alpine glaciers worldwide has accelerated the formation and evolution of glacier-dammed lakes (Kääb et al., 2003; Kargel et al., 2005).

The evolution of glacier-dammed lakes must be documented to fully understand the hazard they pose. Thorarinsson (1939) commented on the life cycle of these lakes, and Clague and Evans (1994) further elucidated the idea and coined the term “jökulhlaup cycle”. As glaciers downwaste and retreat, a critical threshold is reached when they can no longer impound the lake and a cycle of jökulhlaups begins. With continued downwasting or retreat, the frequency of jökulhlaups may increase, but the magnitude decreases until eventually the lake establishes a permanent outlet and jökulhlaups cease. With an improved understanding of the jökulhlaup

cycle and accurate forecasts of future climate, geoscientists may be able to predict the future location of jökulhlaups years, or perhaps decades, before a catastrophic event occurs.

As world population and the demand for natural resources increase, the effect of jökulhlaups on humans and our infrastructure will rise. Scientists and resource managers recognize the need for jökulhlaup hazard assessment. U.S. Geological Survey (USGS) glaciologists Austin Post (retired) and Rod March have argued that current glacier-dammed lakes in Alaska should be identified and characterized. However, no such study is planned by the USGS or other federal or state agencies in the foreseeable future (Post and March, personal communications, 2005).

Brady Glacier in the Fairweather Range of the St. Elias Mountains of Alaska is particularly well suited for a study of glacier-dammed lakes. It presently dams at least 10 large lakes and thus provides a variety of examples for historical and process studies. Six of the lakes are subaerial and four are subglacial. These lakes, and other smaller ones, are in different stages of evolution: incipient, stable and non-draining, and periodically draining. Much surface data are available for Brady Glacier. George Vancouver mapped the terminus in 1794 and made several observations. High-quality topographic maps of the glacier date back to 1907. Sequential airphotos date from 1929 to 1997. Some of the airphotos have been orthorectified and digitized, and thus can be used within a Geographic Information System (GIS). Landsat imagery of the glacier is freely available from 1972 to the present.

1.2 Research Goals and Objectives

The goal of this dissertation is to identify and characterize the evolution of glacier-dammed lakes in order to predict their future behavior using ground-truthed remote sensing techniques and dendrochronology. Traditional hazard assessments are time- and resource-intensive and are

not conducive to regular reassessments. As a result, space-borne remote sensing systems are becoming increasingly important for evaluating hazards (Huggel et al., 2002, Kääb et al., 2003). Glacier-dammed lakes tend to be located in remote, rugged mountains where traditional investigative techniques require large investments of time and resources. Post and Mayo (1971), for example, had to acquire and study over 15,000 airphotos to identify glacier-dammed lakes in Alaska. The combination of radar and optical satellite data offers particular promise for hazard assessment because it capitalizes on the advantages offered by different parts of the electromagnetic spectrum. Radar imagery can bridge temporal gaps in optical imagery due to darkness or cloud cover (Kääb et al., 2003) and can provide measurements presently not attainable with other imagery, such as millimetre-scale surface displacement. Optical imagery is widely available, free or inexpensive, and can be processed with common software packages.

I chose Brady Glacier in southeast Alaska as a study area because of its unique glaciologic and geographic characteristics. The glacier presently dams ten large (>1 km^2) lakes and many smaller ones that are in different stages of development: incipient; stable and non-draining; and periodically draining. Additionally, at least two historic glacier-dammed lakes have drained and are now extinct. Data availability is relatively rich for the region with maps from 1794, topographic maps from 1907, airphotos from 1929, and digitally orthorectified airphotos from 1997. Transportation to the glacier is relatively straightforward from the nearby community of Gustavus via boat and plane.

Dendrochronology, or tree-ring dating, provides an inexpensive and accurate method for dating the advance and retreat of glaciers (Lawrence, 1950; Luckman, 1995; Wiles et al., 1999) and the formation of lakes in previously undammed valleys (Clague and Shilts, 1993; Masiokas et al., 2010). Previous studies have successfully applied dendrochronology at the margins of Brady Glacier (Bengtson, 1962; Derksen, 1976) and more generally in the Glacier Bay area

(Larsen et al., 2005; Lawson et al., 2006). Glacier retreat throughout Alaska is continually exposing new materials suitable for dendrochronology (Barclay et al., 2009b).

1.3 Dissertation Overview

This dissertation comprises, in addition to a brief introduction, three main chapters and a summary. Because Chapters 2 and 3 are published and Chapter 4 will be submitted for publication, the voice will change to first person plural to reflect the contributions of others. Chapter 2 describes the use of interferometric synthetic aperture radar (InSAR) to quantify the vertical displacement of Brady Glacier through time, in order to identify and characterize dynamic alpine subglacial lakes. Important conclusions of this chapter include the positive identification of three previously unidentified subglacial lakes and estimates of discharge from them through time. The technique used in this study can be applied to other glacierized areas to identify and characterize subglacial lakes before they begin to release jökulhlaups and substantially influence glacier dynamics. Drs. Bernhard Rabus and Dan Shugar both contributed significantly to InSAR data processing. Dr. John Clague's oversight, reviews, and comments on drafts greatly improved the manuscript. This chapter was published as a peer-reviewed article in the *Journal of Glaciology*, Vol. 56, No. 199, in 2010.

Chapter 3 describes the use of dendrochronology to date the nineteenth-century advance of Brady Glacier and the evolution of two of its glacier-dammed lakes. Subfossil wood in growth position has been exposed along the margins of Brady Glacier and within the basins of two of its glacial lakes over the past century. I developed a floating tree-ring chronology from this subfossil wood and cross-dated it to master chronologies from the area. Key findings of this study include determining the approximate formation date of Spur Lake (1830) and North Deception Lake (1861). This study is the first to apply elevation-constrained mapping and dendrochronology to

date glacier fluctuations and the evolution of ice-marginal lakes. Drs. Greg Wiles and Brian Luckman assisted with dendrochronology sample collection, preparation, measurement, and dating. Dr. John Clague provided overall supervision, insightful improvements on the manuscript, and also assisted with dendrochronology sample collection. This chapter was published as a peer-reviewed article in *The Holocene* Vol. 21, No. 4, in 2011.

Chapter 4 describes the evolution of Brady Glacier and its glacier-dammed lakes since the first detailed maps were drafted in 1907. An important conclusion of this chapter is that the main terminus of Brady Glacier has remained within several hundred metres of its 1880 extent, but has downwasting substantially. The most dramatic marginal retreat (2 km) and downwasting (123 m) have occurred primarily due to calving into the ten large glacier-dammed lakes that occupy distributary lobes. Calving margins of glacier-dammed lakes share several similarities with tidewater glacier calving margins, which are discussed in this chapter. Significant data for this chapter were provided by Dr. Chris Larsen of the University of Alaska Fairbanks. Dr. John Clague once again provided overall guidance and discerning editorial acumen with drafts of this manuscript. I intend to submit this chapter as a manuscript to the peer-reviewed journal *Geomorphology* after completing the requirements of the degree.

Chapter 5 summarizes the most important results and impacts of the research. It also contains recommendations for future research in the study of glacier-dammed lakes.

2. IDENTIFICATION AND CHARACTERIZATION OF ALPINE SUBGLACIAL LAKES USING INSAR, BRADY GLACIER, ALASKA

Denny M.Capps[1], Bernhard Rabus[1,2], John J. Clague[1], Daniel H. Shugar[1]

[1]Centre for Natural Hazard Research, Simon Fraser University, Burnaby, BC V5A 1S6, Canada

[2]MacDonald Dettwiler and Associates, Ltd., Richmond, BC, V6V 2J3, Canada

Published in *Journal of Glaciology*, Vol. 56, No. 199, December 2010

Abstract

The temporary storage and subsequent release of water at glacial margins can cause severe flooding in downstream areas and substantially influence glacier dynamics. Alpine subglacial lakes may not be identified until they become subaerially exposed or release a jökulhlaup. We use interferometric synthetic aperture radar (InSAR) to identify and characterize three dynamic alpine subglacial lakes of Brady Glacier, Alaska, USA. We quantify changes in vertical displacement of the glacier surface and lake volumes from September 1995 through March 1996 using European Remote-sensing Satellite-1/-2 (ERS-1/-2) tandem data. In the autumn, subsidence ranged from 4 to 26 cm/d and the volume of water discharged ranged from 22,000 ± 2000 to 243,000 ± 14,000 m^3/d. Subsidence and discharge rates declined significantly during the winter and continued at a lesser rate through March. Application of this technique may allow researchers to locate alpine subglacial lakes years or decades before they begin to release hazardous outburst floods and substantially influence glacier dynamics.

2.1 Introduction

The temporary storage and subsequent release of water at glacier margins can cause severe flooding in downstream areas and substantially influence glacier dynamics. Jökulhlaups commonly have peak discharges several orders of magnitude larger than precipitation-induced floods (Clague and Evans, 1994). They alter valley bottoms, channel forms and riparian

ecosystems, cause substantial erosion and aggradation (Post and Mayo, 1971), and have caused severe damage to infrastructure up to 1200km from their source (Mason et al., 1930). Consequently, they are the farthest reaching of all terrestrial glacial hazards. In addition, jökulhlaups and pockets of subglacial water can substantially increase glacier velocity (Fatland and Lingle, 2002; Anderson et al., 2005); some glaciers may not return to their pre-flood velocity for several years (Magnússon et al., 2010).

Researchers have made substantial progress in remotely identifying and characterizing glacier-dammed lakes, including lakes at the base of ice sheets and ice caps (Ridley et al., 1993; Popov and Masolov, 2007; Scharrer et al., 2007; Magnússon et al., 2010), subaerial lakes at the margins of glaciers (Huggel et al., 2002; Bolch et al., 2008), and migrating pockets of subglacial water beneath alpine glaciers (Fatland and Lingle 2002; Lingle and Fatland, 2003). However, alpine subglacial lakes may not be identified until they become subaerially exposed or release a jökulhlaup (Post and Mayo, 1971; Geertsema and Clague, 2005).

We use the term “glacier-dammed lake” in reference to any lake that is dammed by glacier ice, irrespective of its position relative to the glacier (Blachut and Ballantyne, 1976). In contrast, a “subglacial lake” is one that occurs primarily underneath a glacier, whether or not it is at atmospheric pressure (Clague and Evans, 1994; Tweed and Russell, 1999). This primarily morphological definition contrasts with the usages of Siegert (2000), who states that subglacial lakes are “discrete bodies of water that lie at the base of an ice sheet between ice and substrate”, and Hodgson et al. (2009), who further limit the term to lakes sealed off from, and presumably at higher pressure than, the atmosphere.

The goal of this study is to identify and characterize alpine subglacial lakes dammed by Brady Glacier in Alaska using interferometric synthetic aperture radar (InSAR). Specifically our

objectives are to: 1) confirm the existence of suspected subglacial lakes; 2) calculate the vertical displacement of the glacier over the lakes; 3) calculate the volume of water moving into or out of the subglacial lake system; and 4) characterize how these subglacial lakes affect Brady Glacier dynamics. We discuss how the knowledge we have gained can be applied in this and other glacierised areas around the world to minimize hazards posed by alpine subglacial lakes. Early identification and characterization may provide years or decades of warning of future jökulhlaups.

2.1.1 Study area

Brady Glacier is located in the Fairweather Range of the Saint Elias Mountains in Glacier Bay National Park, 125 km west of Juneau, Alaska (Fig. 2.1). It is 51 km long and has an area of 590 km^2. In the early 1990s, the glacier had an accumulation area ratio of 0.65, with an equilibrium line altitude (ELA) of 610 m a.s.l. (Viens, 1995). Brady Glacier terminates on its outwash plain approximately 10 m above sea level; several of its smaller lobes terminate in secondary valleys trending east or west. Peaks up to 3467 m a.s.l. to the northwest supply most of the ice to the glacier. The glacier has deepened the north-northwest-trending, fault-controlled valley in which it lies far below sea level. Ice-penetrating radar measurements near the main axis of Brady Glacier indicate that the bed is at least 200 m below sea level (Barnes and Watts, 1977). This valley is 64 km long and extends from Taylor Bay to the south to near the north end of Glacier Bay. Approximately two-thirds of the ice in this valley flows south-southeast towards Taylor Bay as Brady Glacier and one-third flows north-northwest into Lamplugh and Reid glaciers (Bengtson, 1962; Derksen, 1976). The divide between south- and north-flowing ice lies at approximately 820 m a.s.l. based on the 2000 Shuttle Radar Topography Mission (SRTM) digital elevation model (DEM).

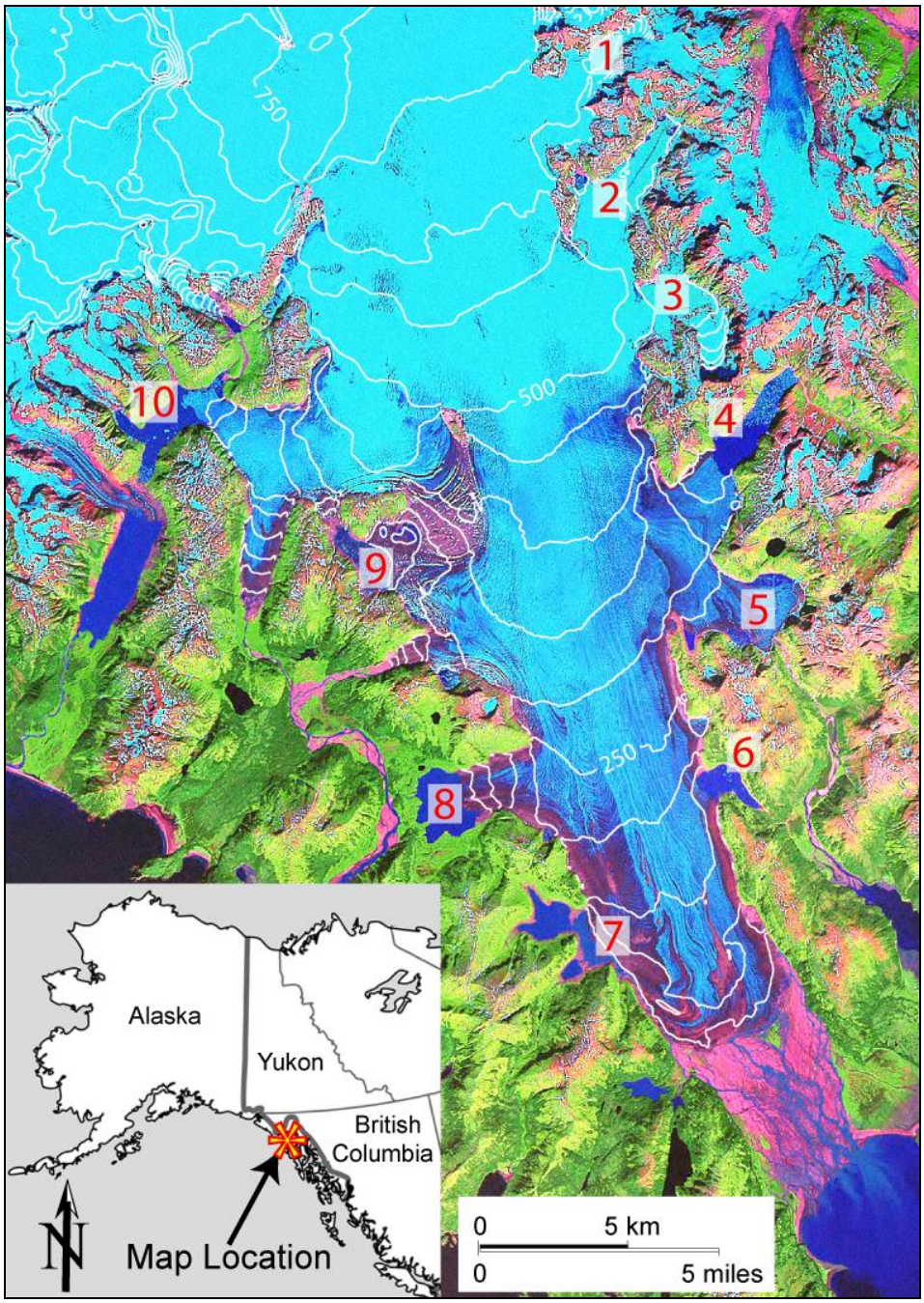

Fig. 2.1. False-color Landsat image of Brady Glacier, southeast Alaska. Topographic contours derived from 2000 SRTM DEM (50-m contour interval). Large lakes dammed by Brady Glacier numbered 1 – 10. Lakes discussed in text: 1) Divide Lake, 2) Hinge Lake, 3) Saddle Lake, 4) Abyss Lake, and 5) Oscar Lake.

The climate at Brady Glacier is cool and moist, typical of the maritime climate throughout southeast Alaska. The strong Aleutian low-pressure system that typically lies offshore in the Gulf

of Alaska dominates the climate. This low-pressure system generates frequent storms that deliver over 280 cm of average annual, water-equivalent precipitation. Snow is common at sea level from late October until early April (Derksen, 1976).

The history of Brady Glacier is broadly similar to that of other glaciers in the region, but there are a few notable differences. Most glaciers in the region reached their Little Ice Age maximum extents in the periods 1540–1710 and 1810–1880, and are now retreating (Larsen et al., 2007; Barclay et al., 2009). In contrast, Brady Glacier reached its current extent around 1880 and its terminus has changed little since then. It was, until relatively recently a tidewater glacier, which may explain its anomalous behaviour (Klotz, 1899; Derksen, 1976; Molnia, 2008). The activity of tidewater glaciers is controlled more by calving dynamics than climate (Post, 1975; Motyka and Begét, 1996). Although Brady Glacier has maintained most of its length and area since the late nineteenth century, it has experienced substantial downwasting. Between 1948 and 2000, the glacier downwasted at an average rate of 2-3 m/yr, which is above the regional average (Larsen et al. 2007). Areas that downwasted the most are adjacent to glacier-dammed lakes; the lakes probably contributed to mass loss through calving. Field observations of the highest Little Ice Age trimline near North Trick Lake (lake 7, Fig. 1), at the southwest margin of the glacier, indicate that the total lowering of the glacier surface in that area is as much as 135 m, which supports the findings of Larsen et al. (2007).

We chose Brady Glacier because it presently dams at least ten large lakes that are in different stages of evolution: incipient, stable and non-draining, periodically draining, and extinct. This allowed us to examine how the lakes have evolved through time. Six of the lakes are subaerial; the other four are primarily subglacial, with more than 50 percent of their areas beneath glacier ice. We estimated the sub-ice extents of the four subglacial lakes from their floating ice ramps, the presence of open water around significant areas of flat or low-gradient

glacier ice, and distinctive crevasses produced by filling and draining of the lakes. We measured water depths of up to 140 m along the margin of Oscar Lake (lake 5, Fig. 2.1).

In this paper, we focus on three previously unidentified subglacial lakes in dead-end valleys on the northeast side of Brady Glacier, which we informally name Divide Lake, Hinge Lake, and Saddle Lake (Fig. 2.2). Other researchers have noted that Brady Glacier flows into these dead-end valleys, but did not identify the lakes (Bengtson, 1962). Only small areas of water are exposed along the glacier margin. Divide Lake at 600 m a.s.l. is the northernmost of the three lakes; it is approximately 1.5 km long and 0.5 km wide. It is near the Brady Glacier ice divide below Divide Peak and underlies a northeast-trending distributary lobe that is confluent with a small, southwest-flowing tributary glacier (Fig. 2.2). Hinge Lake at 450 m a.s.l. is the middle of the three lakes and is 4.2 km long and 1.3 km wide. It has a distinctive hinge-like crevasse that runs along the axis of a northeast-trending distributary lobe. Small areas along the margins of this lobe are open water. Saddle Lake, also at 450 m a.s.l., is the southernmost of the three lakes, is 2.0 km long and 1.6 km wide, and has a saddle-shaped perimeter. The lake underlies a distributary lobe that flows eastward before splaying into embayments to the northeast and southeast. The part of the lake in the southeast embayment underlies the distributary lobe and a small tributary glacier flowing to the north.

2.2 Line-of-sight Displacement

2.2.1 Data sets

Our InSAR measurements are based on four ascending and six descending ERS-1/-2 image pairs of Brady Glacier provided by the European Space Agency (Table 2.1) and the SRTM DEM. The ERS image pairs were acquired in 1995 and 1996, and provide short spatial and temporal baselines. All tandem images were captured 24 hours apart and have a spatial resolution of 20

m. We chose this dataset primarily because short temporal baselines are necessary to avoid decorrelation of the images, which is a common problem on temperate glaciers. The SRTM DEM, acquired in 2000, has a spatial resolution of 30 m.

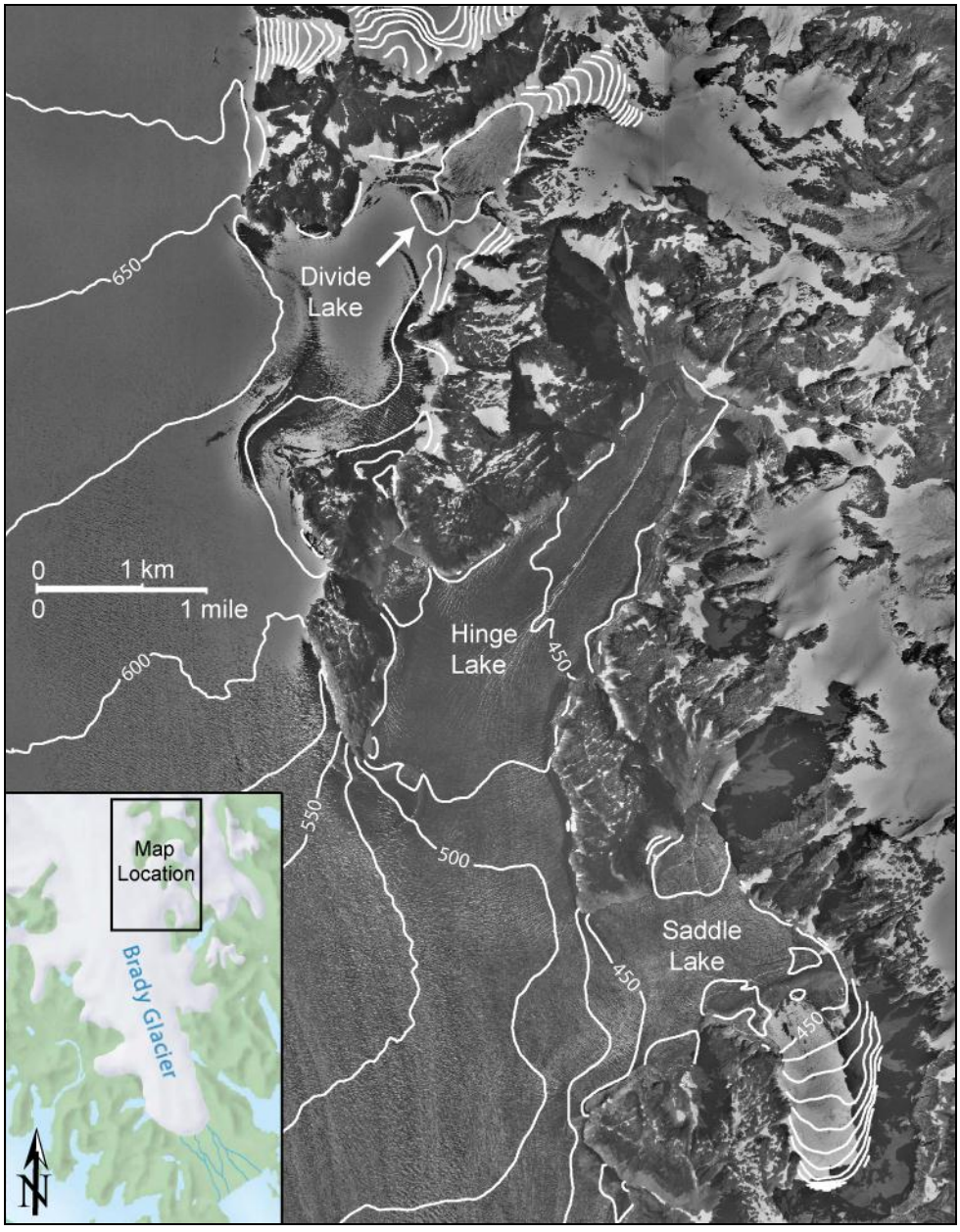

Fig. 2.2. 1997 digital orthophoto of the study area with contours derived from 2000 SRTM DEM (25-m contour interval).

Table 2.1. ERS images used in this study.

Date	ERS	Pass	Track	Perpendicular baseline (m)
11 September 1995	1	Descending	214	64
12 September 1995	2	Descending	214	
29 September 1995	1	Ascending	464	236
30 September 1995	2	Ascending	464	
30 September 1995	1	Descending	486	283
1 October 1995	2	Descending	486	
4 November 1995	1	Descending	486	113
5 November 1995	2	Descending	486	
12 January 1996	1	Ascending	464	117
13 January 1996	2	Ascending	464	
13 January 1996	1	Descending	486	63
14 January 1996	2	Descending	486	
3 March 1996	1	Ascending	192	228
4 March 1996	2	Ascending	192	
4 March 1996	1	Descending	214	90
5 March 1996	2	Descending	214	
22 March 1996	1	Ascending	464	114
23 March 1996	2	Ascending	464	
23 March 1996	1	Descending	486	69
24 March 1996	2	Descending	486	

2.2.2 Interferogram processing

We created ten interferograms from the twenty SAR images using standard InSAR processing techniques (http://www.gamma_rs.ch/uploads/media/gamma_soft_09.pdf). Two interferograms were unusable because of poor coherence. Precipitation recorded at the Elfin Cove meteorological station 23 km southwest of Brady Glacier (http://www.ndbc.noaa.gov/station_history.php?station=cspa2) leads us to suspect that precipitation in the study area caused the decorrelation. The remaining eight interferograms are of good quality and show recurring “bull’s-eye patterns” at the location of each of the

hypothesized subglacial lakes. Figure 2.3a shows an example of substantial displacement from 29 to 30 September 1995 over all three subglacial lakes. Figure 2.3b shows much less displacement from 23 to 24 March 1996 over the three lakes; Hinge Lake experienced negligible displacement during this period (see Appendix A for the remaining eight interferograms).

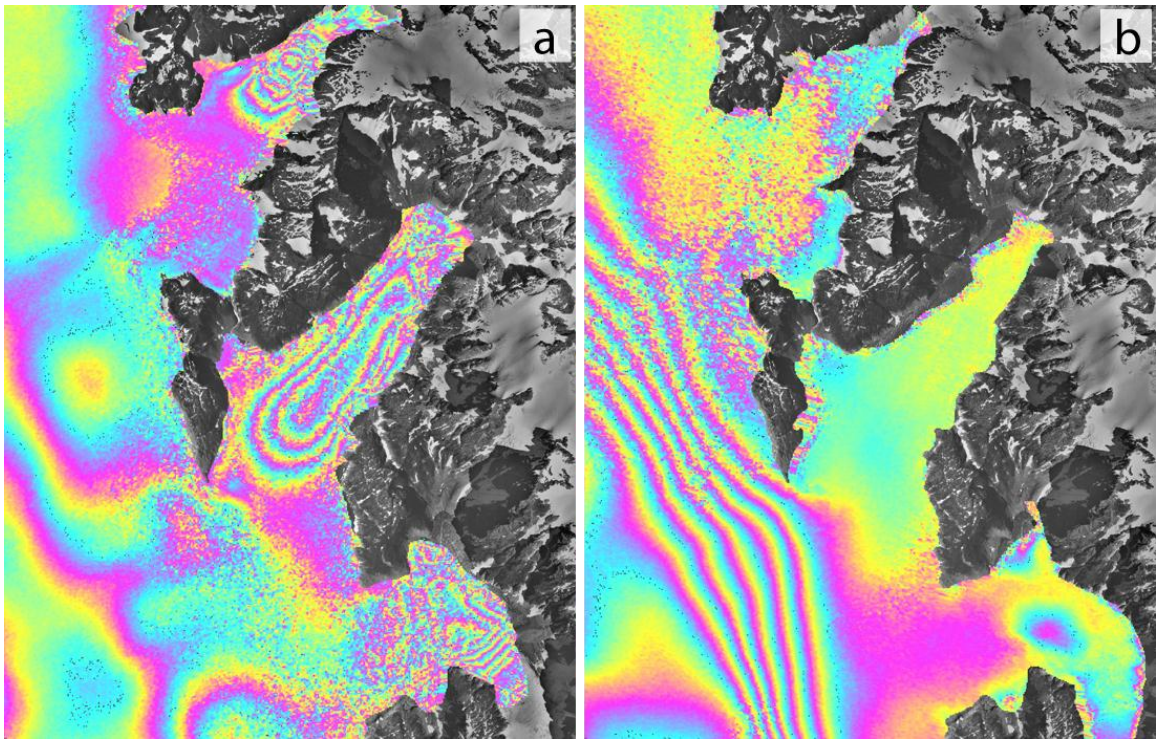

Fig. 2.3. Interferograms for (a) 29 to 30 September 1995 showing substantial displacement over all three subglacial lakes, and (b) 23 to 24 March 1996 showing much less displacement over the same area. For C-band ERS, with a wavelength of 5.6 cm, one fringe corresponds to a difference in line-of-sight (LOS) ground displacement of 2.8 cm. Thus, in Figure 2.3a the line-of-sight displacement at the centre of Hinge Lake over the 24 hour period is 10 cm.

In the case of two of the eight usable interferograms, we encountered localized, but substantial, problems in unwrapping the fringe colour ramp pattern due to areas of low coherence and fringe aliasing (fringes become too dense to unambiguously identify each one). Because all perpendicular baselines are relatively small, only a change in surface scattering at sub-resolution scale can explain low coherence. This change in scattering was likely due to temporal decorrelation caused by precipitation or melt. Unfortunately, the two problematic

interferograms are among the most interesting of the ten. One of them shows the largest observed displacement over the three lakes and the other shows substantial displacement associated with all three lakes. The presence of discontinuous fringes prevented the use of traditional unwrapping routines. To address this problem, we developed a method to improve the unwrapping.

2.2.3 Interactive unwrapping

Although we could not successfully unwrap the fringe colour ramp patterns in all examples with standard techniques, we were able to identify the problematic areas through visual analysis (Fig. 2.4a) and correct them using an iterative process. Wrapped 32-bit interferogram files were exported to 8-bit image files, and individual pixels were manually modified using a standard raster graphics program so that areas of low coherence or high aliasing were clarified. The clarified 8-bit image was cast back to a 32-bit file, masked to remove problematic zones outside the area of interest, and unwrapped with a standard algorithm (Costantini, 1998). This result was then used to demodulate the original image. Figure 2.4b shows the original image unwrapped using this method. The new unwrapping result has an accuracy of better than one fringe in the corrected areas because we used a conservative approach during the clarification process and masked areas where this level of accuracy was not attainable.

Application of this unwrapping technique is limited. It can resolve only localized unwrapping problems and substantial user input during the clarification process precludes its application to larger regions or areas with very low coherence or high aliasing. However, the technique solved localized unwrapping problems caused by mild aliasing and temporal decorrelation.

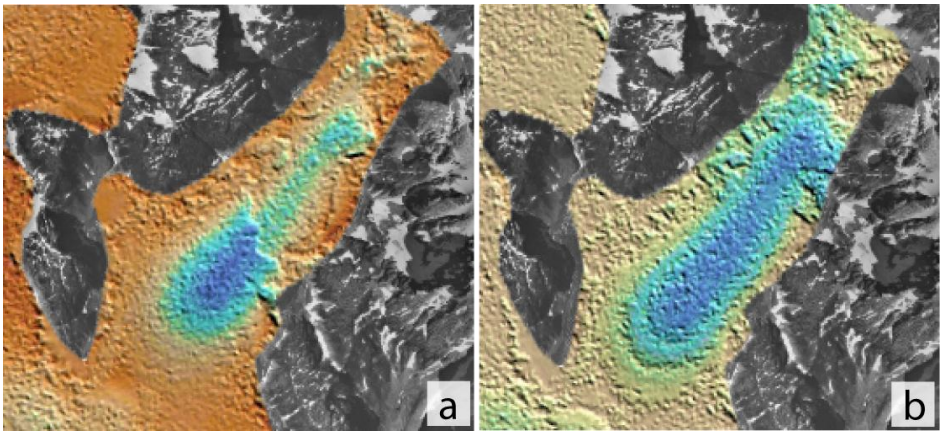

Fig. 2.4. (a) Unsuccessfully unwrapped displacement map of Hinge Lake derived using standard techniques (note discontinuity in colour pattern), and (b) successfully unwrapped displacement map derived using an iterative unwrapping technique.

2.3 Isolating Horizontal and Vertical Displacements

2.3.1 Two-dimensional displacement maps

Displacements in single-track interferograms are LOS; thus, they require additional steps to separate the horizontal and vertical components. Joughin et al. (1998) introduced a technique to discriminate horizontal and vertical displacements that utilizes two interferograms, one ascending and one descending. Two conditions must be met to successfully apply this technique: first, there must be a third constraint on displacement complementing the two interferometric observations; second, glacier motion over the entire interferometric observation period must be constant, that is the two interferograms must represent the same rate and area of displacement despite being acquired at different times. Constraints have been developed to meet the first condition, such as assuming surface-parallel flow (Joughin et al., 1998), applying mass conservation principles (Reeh et al., 2003), or using an ice-flow direction map (Rabus and Lang, 2000, Fatland et al., 2003).

We produced two-dimensional displacement maps for our study area from pairs of near-concurrent (acquired within <1 day), ascending and descending tandem interferograms and an

inferred ice-flow map. Although we were able to meet the first condition by deriving a reliable ice-flow map from ubiquitous flow features in the study area, results with unreasonably large horizontal displacements showed that the second condition was not met - vertical displacement rates over the lakes varied considerably over a single day, precluding use of an averaged 24-hour vertical displacement rate.

2.3.2 One-dimensional displacement maps

Fortunately, we were able to calculate one-dimensional (vertical) displacement using single interferograms because we can demonstrate that horizontal displacement is negligible. One-dimensional displacement maps offer definite advantages because they do not require displacement over the observation period to be constant and because we could obtain as many observations of vertical displacement as there are individual interferograms.

Our argument for negligible horizontal displacement over the subglacial lakes is supported by several lines of evidence. Although unconstrained floating margins can move by lateral spreading and gravitationally driven ice flow, each of the three lobes in the study area flows into a dead-end valley bordered by steep rock walls that do not allow the floating margin to spread. Furthermore, the glacier flows into the valleys very slowly because floating ice must ablate or melt and drain before the glacier can replace it. The vertical displacement patterns in the interferograms closely correlate with distinctive crevasses over the lakes (Fig. 2.5). These patterns are consistent and discernible in aerial photographs from 1948 to the present and over four seasons of fieldwork observations. The crevasses converge towards the areas of maximum vertical displacement and, therefore, are probably caused by repeated inflation and subsidence, not by horizontal displacement. ERS is more sensitive to vertical displacement than horizontal because of its steep average look angle of 23.5° from vertical (Joughin et al., 1998). Most

importantly, regardless of the track angle, subsidence will always create a fringe colour ramp pattern that indicates motion away from the sensor. Depending on the track angle, horizontal displacement will create a pattern that indicates displacement either towards or away from the sensor. The pattern of the lakes in the interferograms in this study shows that all displacement associated with the lakes is away from the sensor, consistent with subsidence. Therefore, we assume that all displacements associated with the lakes are vertical. We calculated total vertical displacement from the edge of the lake, where displacement is zero, to the area of maximum displacement. Results are shown in Table 2.2.

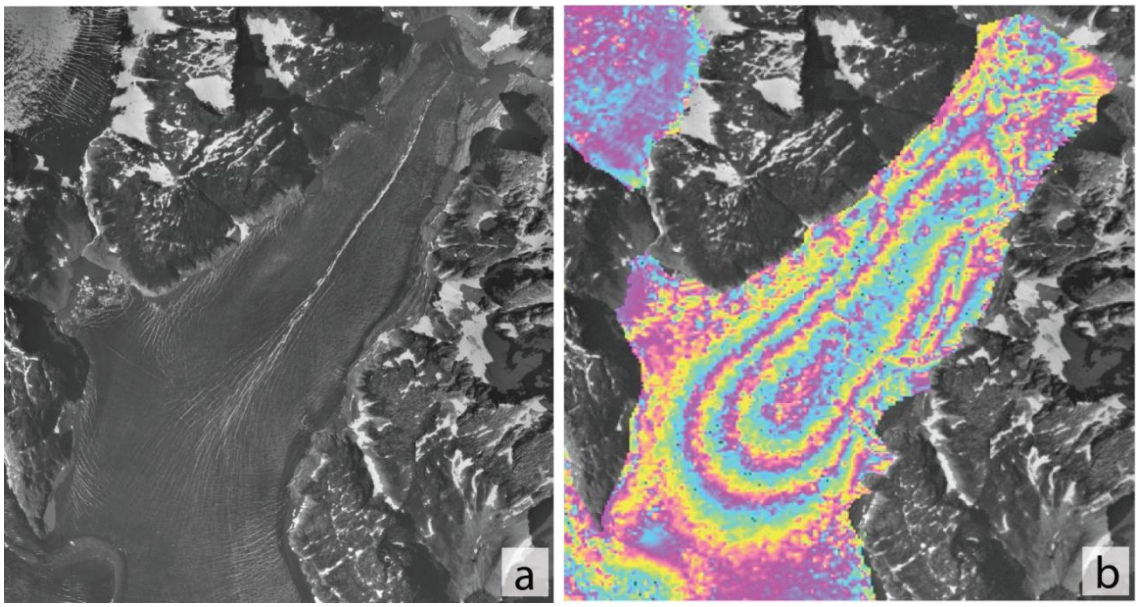

Fig. 2.5. Correlation of (a) crevasses seen in 1997 aerial photograph with (b) line-of-sight displacement in the interferogram.

Table 2.2. Maximum subsidence at Divide, Hinge, and Saddle lakes in 24 hours.

	Maximum subsidence (cm)		
Date	Divide	Hinge	Saddle
11-12 September 1995	*	*	*
29-30 September 1995	13	11	*
30 September - 1 October 1995	5	7	9
4-5 November 1995	*	4	26
12-13 January 1996	*	*	*
13-14 January 1996	0	6	8
3-4 March 1996	0	4	4
4-5 March 1996	0	2	3
22-23 March 1996	0	1	2
23-24 March 1996	0	0	3

* Poor coherence

2.3.3 Error analysis

We estimated the total error by summing the errors associated with the individual components used to calculate the interferometric signal. The interferometric signal is the result of orbit geometry (*o*), surface topography (*t*), atmospheric changes (*a*), sensor noise (*n*), and vertical (d_v) and horizontal (d_h) surface displacement:

$$\phi = \phi_o + \phi_t + \phi_a + \phi_n + \phi_{d_v} + \phi_{d_{h_h}}$$

Errors associated with ERS orbit geometry are small (Mohr and Madsen, 2001); we ignored them in this study. Errors associated with surface topography are the result of inaccuracies in the DEM and changes in the surface elevation of the ice between acquisition of the ERS images and the images used to produce the DEM. Spikes and wells (single pixel errors) in the DEM were removed (http://seamless.usgs.gov/faq/srtm_faq.php#three). Sizeable voids remained in high-relief bedrock areas but were not present over the glacier. Relative vertical error for the DEM was <6 m, of which about one-third was systematic and the remainder random (Rabus et al., 2003). We were unable to measure elevation changes directly between the time the ERS images

were acquired in 1995/96 and the time the images for the DEM were acquired in 2000. Based on thinning rates derived from laser altimetry (Larsen et al., 2007), we estimated the elevation change to be < 8 m — < 0.08 fringes for a 100-m baseline and < 0.16 fringes for a 200-m baseline (Rabus and Fatland, 2000). Thus, we conservatively estimated a maximum of 15 m total elevation error, yielding an error of 0.15 fringes for a 100-m baseline and 0.3 fringes for a 200-m baseline. Under extreme circumstances, atmospheric changes can cause errors of one fringe or larger. Most atmospheric distortions, however, occur over large areas (Rabus and Fatland, 2000). Because we calibrated displacement over the lakes separately and each lake is relatively small, we assume that this source of error is negligible. Noise due to errors associated with sensor noise and temporal decorrelation is spatially random and cancels when ice volume is integrated spatially. The remaining error is the neglected horizontal surface displacement (d_h). If we assume d_h = 0, the total error is:

$$e_{d_v} = \sqrt{\frac{e_{LOS}{}^2}{\cos\theta^2} + e_{d_h}{}^2 \tan\theta^2 \left(\cos(\alpha - \psi)\right)^2} \quad (1)$$

where α, ψ, and θ and are, respectively, the horizontal flow angle, the satellite track angle, and incidence angle where $\theta \approx 23.5^{\circ}$. Assuming a maximum horizontal ice displacement error over the lakes of 1 cm/day and evaluating e_{LOS} for a 200-m baseline and extreme values of α and ψ, equation 1 gives a maximum error of $\leq$ 0.3 cm of vertical displacement over the lakes.

2.4 Displacement Volume Calculation

Using GIS, we calculated the vertical displacement of all pixels over the subglacial lakes and, from those values, the volume of water displaced in discrete 24-hours intervals. We were unable to determine vertical displacements for all pixels and therefore accurate displacement volumes in all interferograms because of substantial areas of poor coherence, fringe aliasing,

and radar layover and shadow. However, we were able to determine the minimum displacement volumes for most of the lakes through the period of data acquisition (Table 2.3). We calculated the volume error by multiplying the systematic error (≤ 0.3 cm) by the masked lake area.

Table 2.3. Minimum and estimated total volume of water displaced from Divide, Hinge, and Saddle lakes in 24 hours.

	Minimum Displacement Volume (m^3)			Estimated Total Displacement Volume (m^3)		
Date	Divide	Hinge	Saddle	Divide	Hinge	Saddle
11-12 Sept 1995	*	*	*	*	*	*
29-30 Sept 1995	34,000 ± 3000	243,000 ± 14,000	*	-	243,000	*
30 Sept - 1 Oct 1995	22,000 ± 2000	127,000 ± 9000	102,000 ± 6000	-	155,000	-
4-5 November 1995	*	89,000 ± 14,000	96,000 ± 21,000	*	88,000	-
12-13 January 1996	*	*	*	*	*	*
13-14 January 1996	≈ 0	44,000 ± 11,000	47,000 ± 4000	≈ 0	133,000	-
3-4 March 1996	≈ 0	75,000 ± 10,000	34,000 ± 4000	≈ 0	88,000	-
4-5 March 1996	≈ 0	50,000 ± 13,000	18,000 ± 4000	≈ 0	44,000	-
22-23 March 1996	≈ 0	23,000 ± 9000	11,000 ± 2000	≈ 0	22,000	-
23-24 March 1996	≈ 0	≈ 0	11,000 ± 3000	≈ 0	≈ 0	-

* Poor coherence

\- Pattern changed too much for estimate

We estimated total displacement volumes for lakes that had to be masked due to poor coherence, fringe aliasing, and radar layover and shadow. We compared interferograms, one with nearly complete coverage and those with substantial masked areas to calculate the estimated total displacement volume using the equation:

$$V_{tot\_t2} = \frac{d_{\max\_t2}}{d_{\max\_t1}} V_{\min\_t1}$$

where V_{tot_t2} is the lake of interest's estimated total displacement volume, $d_{\max\_t2}$ is the lake of interest's maximum vertical displacement, $d_{\max\_t1}$ is the nearly complete lake's maximum vertical displacement, and $V_{\min\_t1}$ is the nearly complete lake's minimum displacement volume.

In some cases, especially at Saddle Lake, complex and temporally inconsistent fringe patterns precluded this approach (Table 2.3).

2.5 Discussion

2.5.1 Subglacial hydrology

All coherent interferograms used in this study show bull's-eye patterns that indicate subsidence of the glacier surface over the lakes. Joughin et al. (1996) also noted bull's-eye patterns in interferograms of a Greenland outlet glacier, but there the patterns were persistent, occurred as conjugate pairs, and resulted from downstream ice flow over subglacial topography. In the Brady Glacier case, the bull's-eye patterns are neither conjugate pairs nor persistently recurring. Like Fatland and Lingle (2002), we interpret this subsidence to result from draining of water at the base of Brady Glacier. Previously, the glacier had separated from its bed when the water reached a sufficient depth to float the ice. Fatland and Lingle (2002) concluded that the bull's-eye patterns of Bering Glacier were distorted due to downstream ice flow. The bull's-eye patterns at Brady Glacier are not located along the axis of flow and are not elongated because of downstream ice flow, but rather because of subglacial bedrock topography. The bull's-eye patterns associated with Divide and Hinge lakes are elongated because the basins in which they lie are elongated and therefore limit the areal extent of the subsidence (Fig. 2.3a). During drainage, the previously level ice surface subsides unevenly onto the glacier bed. Deeper depressions in the northern and southern embayments of the Saddle Lake allow for larger amounts of subsidence in those areas, assuming uniform ice thickness (Fig. 2.3b). The depressions likely were excavated by cirque glaciers in the past, both are still present, but only one remains connected (Fig. 2.2). As a result, these areas continue to subside after the main floating margin becomes grounded, which causes the magnitude and shape of the bull's-eyes in

the interferograms to change over time. Conversely, during lake inflation, the ice cover in the deepest areas of the lake likely begins to rise first. We attempted to determine ice thicknesses and subglacial topography in the lake basins using ice-penetrating radar, but most of the glacier bed was several hundred metres thick and beyond the range of our equipment.

We calculated the volume change per unit area of the three lakes through time. The lakes experienced their highest discharges (Table 2.2) and greatest volume changes per unit area in late September: 0.033, 0.053, and 0.050 m^3/m^2 for Divide, Hinge, and Saddle lakes, respectively. The value for Divide Lake may be lower than those for the other two lakes because Divide Lake is 150 m higher in elevation and near the ELA, and therefore has less meltwater available for draining.

Glacier-dammed lakes typically fill in the spring and early summer and drain in late summer and early fall, although some lakes may drain at any time of the year (Liestøl, 1955; Post and Mayo, 1971). The subglacial lakes in this study exhibit this seasonality, with the largest measured discharges in early fall, although discharge continued through the winter at lower rates (Table 2.2). Generally, the times of highest discharge are also the times of highest meltwater availability. No ERS-1/2 tandem data are available from late March to early September to determine when the lakes fill to their highest levels, although we assume lake levels are highest when melt is greatest during late spring to late summer. Limited field observations showed that the floating margins over the lakes were at their maximum height in early to mid-August of each year from 2005 to 2007. During fieldwork in early April 2007, we observed the floating margins on all three lakes to be at low levels, with Saddle Lake several tens of metres below its full-pool level based on elevations of icebergs at its margins. These icebergs, which previously were floating at the margins of the subglacial lake, were stranded as the lake drained. Assuming that similar processes were operating in 1995/1996 and 2007, we

can compare the 2007 field observations with the 1995/1996 InSAR results to test whether the measured surface displacements are consistent with the lake level lowerings inferred from the stranded icebergs. If we conservatively assume that the level of Saddle Lake fell by 20 cm/day in September and October, 10 cm/day in November and December, and 5 cm/day in January through March (Table 2.2), the lake would drop by more than 22 m. However, we know that the lake fell by as much as 30 cm/day in November. As a result, we conclude that the processes active in 1995/1996 were still active in 2007 and can explain the several tens of metres of difference between the low and high lakes levels that we observed in the field. Based on these field observations, we estimate total annual vertical displacements of 25 m for Divide Lake, 30 m for Hinge Lake, and 35 m for Saddle Lake.

We estimate the total minimum volume displacement from the three lakes to be approximately 1,000,000 ± 129,000 m^3 for the eight days of the 177-day period for which we have measurements. We emphasize, however, that this estimate is conservative because we were unable to quantify some areas due to poor coherence, fringe aliasing, and radar layover and shadow. If we assume that the eight days of measurement (1,000,000 m^3) are representative of discharge through the longer observation period (177 days), about 22,000,000 m^3 of water discharged from the subglacial lake system. Some of this water is derived from melt and precipitation in the lake basins, but without mass balance or subglacial melt measurements, we cannot determine their local contribution to lake level. It is likely that some of the water that accumulates in the lakes is derived from upglacier positions and is brought to the lakes along the glacier margin or via subglacial conduits (see below). Although the volume of water displaced from these lakes is substantial, it is unclear if the discharge significantly affects the motion of a glacier as large as Brady.

We considered the question of whether subglacial lake drainage at Brady Glacier is sudden and catastrophic or continuous and non-catastrophic. We cannot definitively answer this question because coherent radar data are temporally discrete and discontinuous. However, measured drainage from Divide and Hinge lakes slowed markedly from the end of September to the beginning of October (Table 2.2), consistent with catastrophic drainage. Many jökulhlaup hydrographs increase exponentially to a peak, then fall very rapidly (Walder and Costa, 1996). However, the highest measured discharges are in early September and the lakes continued to drain, albeit at lower rates, through the period of the last interferogram in late March. This overall trend supports a hypothesis of slower, more continuous drainage.

The lakes drain through subglacial or englacial conduits or marginal channels. However, determining the type of conduit or channel functioning here is difficult. We did not find any surface expressions of conduits or marginal channels in the interferograms, aerial photographs, or field. There are no gauging stations on any of Brady Glacier's outlet streams. We cannot calculate the most likely drainage path without subglacial topographic data. We suspect, however, that the water drains down-gradient into Abyss Lake (Fig. 2.1). Analogous behaviour exists downglacier where Abyss Lake drains subglacially into informally named Oscar Lake (Grover, 2003).

2.5.2 Early identification of glacier-dammed lakes

Early identification of glacier-dammed lakes is critical to minimizing the hazard of jökulhlaups. Rapid changes in the cryosphere are leading to hazardous situations with few, if any, historical precedents (Frey et al., 2010). Early identification of future jökulhlaups requires an understanding of the jökulhlaup cycle. Many glacier-dammed lakes go through a cycle of jökulhlaup activity as their dams weaken due to downwasting and retreat (Clague and Evans,

1994). A critical threshold is reached when the glacier can no longer impound the lake and a cycle of jökulhlaups begins. With continued downwasting or retreat, the frequency of jökulhlaups may increase, but the magnitude decreases until eventually the water establishes a permanent outlet and jökulhlaups cease.

The subglacial lakes described here will likely enlarge and become subaerial as Brady Glacier continues to downwaste and retreat. Portions of all three lakes already have subaerial exposure and these areas are likely to grow in the future. With continued glacier downwasting and retreat, they will likely enter the jökulhlaup cycle and begin to drain catastrophically. Geertsema and Clague (2005) documented an example of this kind of evolution with Lake No Lake, which is dammed by Tulsequah Glacier in northwest British Columbia. Lake No Lake is not visible in 1948 aerial photographs, but a glacier ramp drops to a floating margin that covered a subglacial lake. This geometry is very similar to that of the lakes described in this study. By 1974, a sizeable subaerial lake had developed, and it is still growing in area. In 1991 the lake began a cycle of jökulhlaups. The volume of water discharged from Lake No Lake remains large, but with continued glacier downwasting and retreat, the lake and its floods will decrease in volume (Geertsema and Clague, 2005).

Brady Glacier's Abyss Lake (Fig. 2.1) has undergone a similar transformation. On the International Boundary Commission's topographic map of the study area, which is based on measurements taken in 1907, the area that is now Abyss Lake appears as a glacier ramp that drops to a floating margin (International Boundary Commission, 1923). Aerial photographs taken in 1948 show Abyss as a large subaerial lake. Since that time, the subaerial part of Abyss has expanded. The lake has partially emptied most years since 1994, draining subglacially into Oscar Lake and over a bedrock sill into the Oscar Creek drainage, where the floodwaters caused widespread damage to the forests. The 1994 jökulhlaup, which caused the level of Abyss Lake to

fall 77 m, released approximately 130,000,000 m^3 of water and was the first discernible flood in that drainage for at least 80 years based on dendrochronological evidence (Grover, 2003). We conducted a bathymetry survey of Abyss Lake in 2006 and determined that when full to overflow, it is at least 270 m deep, very steep-sided, and contains over 500,000,000 m^3 of water. With continued glacier downwasting, jökulhlaups from Abyss Lake eventually will drain subglacially to the Brady Glacier terminus, completely emptying the lake. Jökulhlaups of this magnitude could erode the stabilizing outwash plain and return the glacier to a calving regime, which could have serious implications for the stability of the glacier. The subglacial lakes in this study will likely parallel Abyss Lake's evolution from subglacial and relatively stable to subaerial with catastrophic outbursts. Abyss Lake and the subglacial lakes in this study illustrate how space can be used as a proxy for time in the evolution of glacier-dammed lakes.

Forecasting the evolution of the subglacial lakes reported in this paper is difficult because of the many complicating factors, such as uncertainties in future climate. However, if Brady Glacier continues to downwaste at a rate similar to that of the past 100 years, Saddle and Hinge lakes will likely begin to release jökulhlaups within a few decades, and Divide Lake will enter the jökulhlaup cycle perhaps a few decades later. We base this estimate on the evolutionary history of Abyss Lake and Lake No Lake, which have similar glacier geometries and hydrologic conditions.

2.5.3 Application of technique to other areas

The technique for identifying and characterizing subglacial lakes that we applied in this study can be used in other glacierised areas around the world. For example, it could be used to verify a large subglacial lake in the Witches Cauldron, a tributary to Baird Glacier in southeast Alaska, that Post and Mayo (1971) suggested could drain catastrophically. Post and Mayo (1971)

also identified a subglacial lake beneath Skilak Glacier near Seward, Alaska, based on a distinctive radial crevasse pattern on its surface. Jökulhlaups from this lake have caused extensive damage to downstream infrastructure. We have identified several other large subglacial lakes in southeast Alaska and western British Columbia that have geometries similar to those found at Brady Glacier. Notable examples include the Dead Branch of Norris Glacier near Juneau, Alaska, which has a conspicuous crevasse along its centreline, similar to Hinge Lake (Fig. 2.5), and an unnamed tributary of Patterson Glacier near Petersburg, Alaska. The successful application of this technique to other glacierised alpine areas would allow the identification and quantification of subglacial lakes before they began to release hazardous jökulhlaups. The rapid changes that are occurring in the cryosphere will likely lead to many new lakes forming beneath downwasting alpine glaciers around the world (Frey et al., 2010). The number of such lakes may eventually decrease due to continuing glacier retreat and demise, but in the short term many new lakes will form and evolve in a changing climate. Because 1995/1996 ERS-1/2 tandem mission images are available for most alpine glaciers, our technique could be used to confirm suspected alpine subglacial lakes and to quantify their area and behaviour. Although more recent radar imagery with adequately short temporal baselines is limited, many new InSAR satellites are planned for the future that will extend the usefulness of the technique.

2.6 Summary

We developed a technique to isolate vertical displacements over dynamic alpine subglacial lakes using ERS-1/2 imagery. We assumed, based on several lines of supporting evidence, that horizontal displacement over subglacial lakes in stagnant embayments is negligible. This assumption allowed us to quantify vertical displacement using single interferograms. We were able to determine maximum vertical displacement and displacement volumes for

interferograms with good coherence and minimal aliasing. All interferograms in this study indicate that the lake surfaces are subsiding, but at different rates. Discharge rates are highest in late September, slow dramatically during winter, and continue at lower rates through March.

Our technique can be applied to other glacierised areas around the world. Imagery acquired during the ERS-1/2 tandem mission and imagery provided by future InSAR sensors can be used in conjunction with this technique to identify and characterize alpine subglacial lakes in other glacierised areas. This technique allows researchers to locate subglacial lakes that may cause severe flooding in downstream areas and substantially influence glacier dynamics. Subglacial lakes, years or decades from now, may drain catastrophically, thus our technique may allow time to mitigate the risk from this hazard.

3. TREE-RING DATING OF THE NINETEENTH-CENTURY ADVANCE OF BRADY GLACIER AND THE EVOLUTION OF TWO MARGINAL LAKES, ALASKA

Denny, M. Capps [1], Gregory C. Wiles [2], John J. Clague [1], Brian H. Luckman [3]

[1]Centre for Natural Hazard Research, Simon Fraser University, Burnaby, BC V5A 1S6, Canada

[2] Department of Geology, The College of Wooster, Wooster, OH 44691, USA

[3]Department of Geography, The University of Western Ontario, London, ON N6A 5C2, Canada

Published in *The Holocene,* Vol. 21 No. 4, June 2011

Abstract

We utilized dendrochronology and precise elevation-constrained mapping to date glacially overridden and drowned trees at the margin of Brady Glacier in southeast Alaska. This technique allowed determination of the timing of the former tidewater glacier's last advance and consequent formation and filling of two marginal lakes. The subfossil tree-ring chronology spans the interval from 1370 to 1861 AD. Brady Glacier impounded Spur Lake to an elevation of 83 m a.s.l. around 1830 and 121 m a.s.l. around 1839. Soon after, Spur Lake reached 125 m a.s.l. and began to overflow a stable bedrock sill. The glacier continued to advance, thickening by at least 77 m between ca. 1844 and 1859 at a site down-glacier of Spur Lake on the opposite glacier margin. Farther down-glacier, North Trick Lake began to form by 1861 and reached its highest elevation at approximately 130 m a.s.l. when Brady Glacier reached its maximum extent around 1880. Our findings add precision to the chronology of the last advance of Brady Glacier and provide insight into the evolution of glacier-dammed lakes and calving glaciers.

3.1 Introduction

Brady Glacier is the largest glacier in the Fairweather Range of the St. Elias Mountain in southeast Alaska. Recent downwasting has exposed well preserved subfossil trees that were

overridden by the glacier or inundated by two lakes dammed at the glacier margin. Previous researchers have used dendrochronology to date glacier advances (Lawrence, 1950; Luckman, 1995; Wiles et al., 1999) and the formation of glacier-dammed lakes (Masiokas et al., 2010). In this study, we combine dendrochronologically established death dates with differential GPS mapping of these sub-fossil trees to reconstruct the last advance of Brady Glacier and the filling of the lakes.

Wastage of Alaskan glaciers accounts for the largest measured glacial contribution to recent sea level changes (Arendt et al., 2002). Over 75% of the ice volume lost from glaciers in southeast Alaska and adjacent Canada comes from tidewater and lake-calving glaciers (Larsen et al., 2007). Calving glaciers are susceptible to nonlinear dynamic instability when they terminate in water that is relatively deep compared to ice thickness. Studies that provide insight into calving glacier dynamics are therefore particularly important for forecasting future sea level rise (Meier, et al., 2007). Brady Glacier was formerly a tidewater glacier and it may become one in the future because it is presently grounded well below sea level. Seven distributary lobes of Brady Glacier also have lake-calving margins that exceed 1 km in length. This study provides insight into the evolution of glacier-dammed lakes, the future contribution of Brady Glacier to sea level change, and the dynamics of other calving glaciers.

3.2 Study Area

Brady Glacier is located in Glacier Bay National Park, 125 km west of Juneau, Alaska (Fig. 3.1). It is 51 km long and 590 km^2 in area. In the early 1990s, the glacier had an accumulation area ratio of 0.65, with an approximate equilibrium line altitude (ELA) of 610 m a.s.l. (Viens, 1995). The glacier's major source areas are mountain peaks up to 3467 m a.s.l. to the northwest and the glacier terminates at approximately 10 m a.s.l. on a large outwash plain that extends 4.8

km into Taylor Bay. The glacier occupies a north-northwest-trending, fault-controlled valley 64 km long, that extends from Taylor Bay in the south to near the north end of Glacier Bay (Derksen, 1976). Ice from the Fairweather Range feeds glaciers flowing both south-southeast towards Taylor Bay (Brady Glacier) and north-northwest to Glacier Bay via Lamplugh and Reid glaciers (Bengtson, 1962; Derksen, 1976). The divide between south- and north-flowing ice is at approximately 820 m a.s.l. based on the digital elevation model (DEM) from the 2000 Shuttle Radar Topography Mission (SRTM). Ice-penetrating radar measurements near the axis of Brady Glacier indicate that the bed is at least 200 m below sea level (Barnes and Watts, 1977). Previous dendrochronology studies determined that Brady Glacier reached its current position around 1880 and observations indicate the terminus position has subsequently varied by only a few hundred metres (Klotz, 1899; Bengtson, 1962; Derksen, 1976). Field observations of the highest Little Ice Age trimline near North Trick Lake indicate that the total lowering of the glacier surface in that area is in excess of 135 m.

Presently, the glacier dams at least ten large lakes, six of which are primarily subaerial and four subglacial. These lakes, and other smaller ones, are in different stages of evolution – incipient, stable and non-draining, and periodically draining. This study focuses on North Trick and Spur lakes (Fig. 3.2). Brady Glacier dams North Trick and adjacent South Trick lakes on its southwest side. In the past, North Trick Lake drained subglacially into South Trick Lake and then through either a stable outlet to the southwest into the ocean via Annoksek Creek or subglacially to the terminus (Post and Mayo, 1971; Derksen, 1976). A new body of water, informally named East Trick Lake, has formed as the glacier has retreated due to calving (Fig. 3.2). In August 2007, North and South Trick lakes were dammed at approximately 30 m a.s.l. by moraines and East Trick Lake was glacier-dammed. However, East Trick Lake's surface elevation varies through time. For example, in an August 15, 2010 Landsat image, East Trick and North

Trick Lake were connected by a narrow channel through the moraine, but South Trick Lake remained isolated. Brady Glacier dams Spur Lake on its southeast side (Fig. 3.2). At its maximum level, this lake drains over a bedrock sill to the southeast into Dundas Bay via the Oscar River (informal name). Presently, Spur Lake does not fill to this level, but drains catastrophically along a subglacial path to the outwash plain to the south.

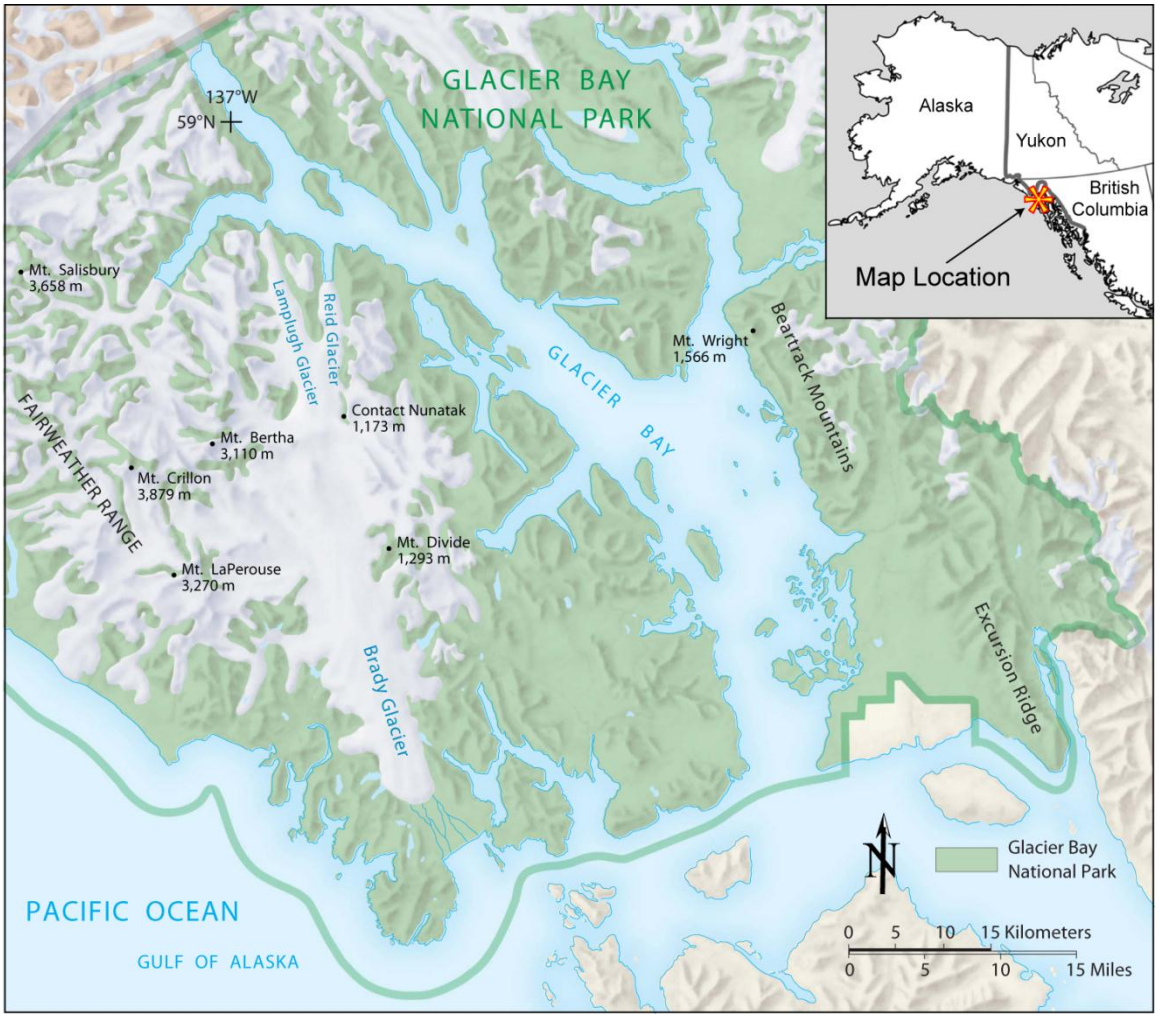

Fig. 3.1. Brady Glacier and its surrounding area (after National Park Service, 2009).

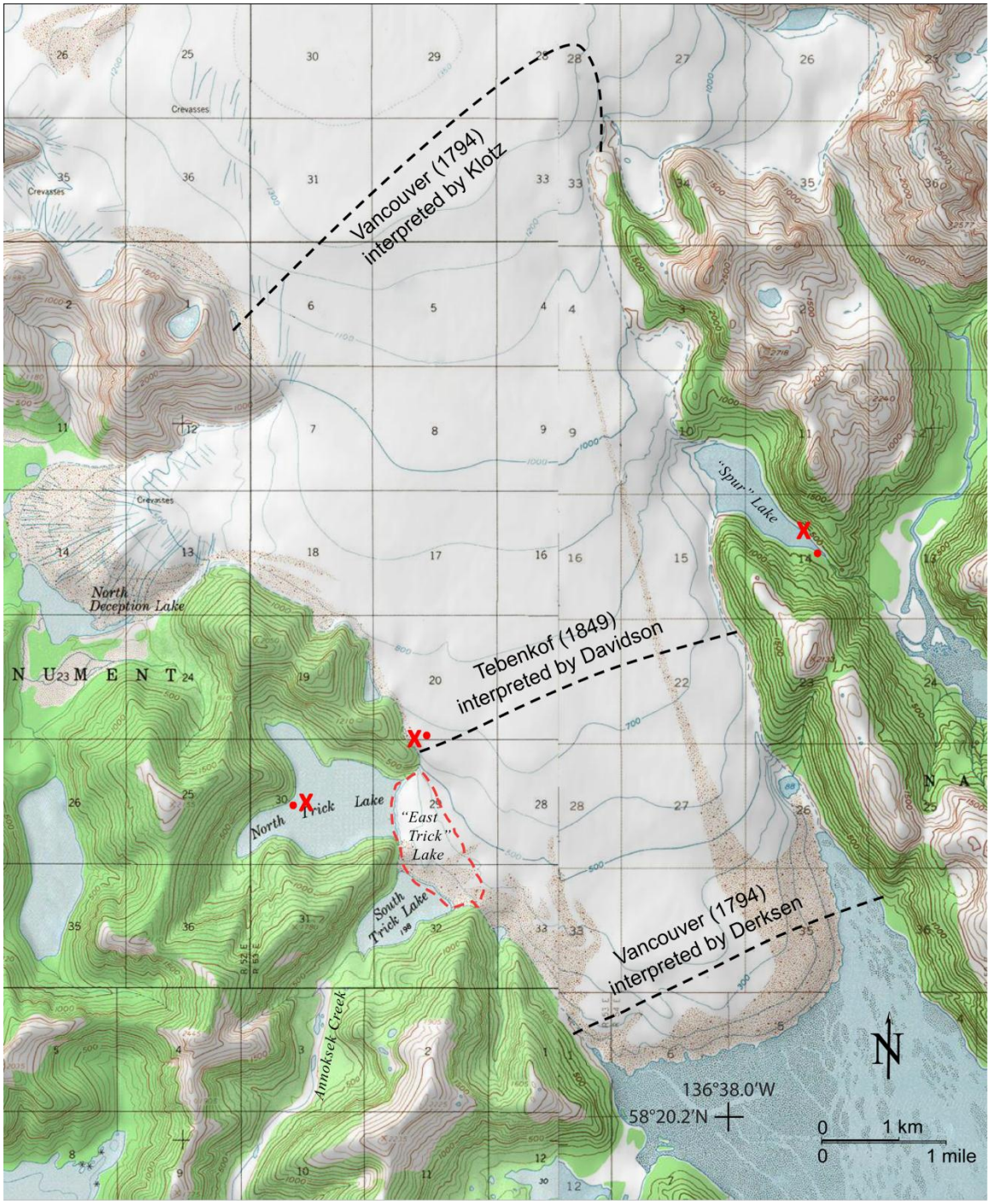

Fig. 3.2. Terminus of Brady Glacier. The study sites are indicated by red crosses. The interpreted locations of former glacier termini are based on early observations (Klotz, 1899; Davidson, 1904; Derksen, 1976). The red dashed line indicates the present margin of "East Trick" Lake. The red dots indicate locations of photographs in Figure 3.3. Topographic map – 1961 U.S. Geological Survey; scale 1:63,360; contour interval 100 feet (ca. 30 m). Spur and East Trick lakes are unofficial names.

The dominant tree species in the area are Sitka spruce (*Picea sitchensis*), western hemlock (*Tsuga heterophylla*), and mountain hemlock (*Tsuga mertensiana*). Sitka spruce and western hemlock are common at low to middle elevations, whereas mountain hemlock is largely restricted to the subalpine zone (Pojar and MacKinnon, 1994).

3.3 Previous Studies at Brady Glacier

Derksen (1976) summarized the late Holocene history of Brady Glacier based on observations dating back to the 1700s and radiocarbon ages from subfossil wood in moraines beyond the maximum extent of the last advance. He postulated an earlier advance beginning no later than 1870 cal yr BP and culminating 1170-1290 cal yr BP. The glacier retreated at least 24 km north of its present terminus by 645-725 cal yr BP, but began to advance shortly thereafter based on radiocarbon ages from subfossil wood in moraines (Bengtson, 1962; Derksen, 1976).

Historical observations of the glacier terminus before the twentieth century are subject to interpretation (Derksen, 1976). Joseph Whidbey, Captain George Vancouver's lieutenant, made the first recorded observations of the terminus in stormy weather on July 10, 1794. The chart produced from his observations roughly reproduces the coastline (Vancouver, 1984), but the perspective is distorted. Klotz (1899) reviewed Vancouver's map and observations and placed the terminus approximately 12 km north of its present location (Fig. 3.2). Later Derksen (1976) disputed Klotz's interpretation and placed the 1794 terminus near its present location (Fig. 3.2). The next recorded observations are based on a map produced by Mikhail Tebenkof in 1849 (Tebenkof, 1981). Davidson (1904) reproduced this map and placed the terminus north of the present margin, but not as far north as Klotz's interpretation of the 1794 terminus (Fig. 3.2). In 1880 John Muir and Samuel Hall Young visited the area. Muir explored lower Brady Glacier and made notes, but inclement weather limited his view. Muir did note that the glacier was

advancing, and he commented on the presence of Spur and North Deception lakes (Fig. 3.2). He did not, however, say anything about the location of the glacier terminus. Young, who stayed near camp while Muir explored the glacier, talked with a Hoonah chief camped at the terminus. The chief complained that, "*The icy mass had been for several years traveling towards the sea at the rate of at least a mile every year*." A few years later, the chief reported that the glacier had begun to retreat (Young, 1915). The changing glacier and inconsistent identification of landforms and reference points complicate interpretation of these early observations.

The terminus location has changed little from the time of the first detailed map in the late nineteenth century. A 1:160,000-scale topographic map of the glacier was made based on survey observations from several summits in 1894 (Klotz, 1899). On this map, the terminus is near its present location and North Trick, South Trick, and Spur lakes are clearly indicated. Subsequent maps from 1907, 1948, 1961, 1971, and 1982 and Landsat imagery from the 1990s and 2000s show that the location of the terminus has varied no more than a few hundred metres from the position it occupied in 1894.

Brady Glacier was previously a tidewater glacier. Several early explorers noted its change from a tidewater glacier to one terminating on an outwash plain. Vancouver, in his account of the 1794 exploration, wrote that, *". . . further progress was now stopped by an immense body of compact perpendicular ice, extending from shore to shore*", which indicates a tidewater terminus. By 1880, however, Muir commented, "*No icebergs are discharged from it, as it is separated from the water of the fiord at high tide by a low, smooth mass of outspread, overswept moraine material . . . The front of the glacier, like all those which do not discharge icebergs, is rounded like a brow, smooth-looking in general views . . .*" (Muir, 1915). Therefore, sometime between 1794 and 1880 the terminus evolved from a calving margin into a non-calving margin. Post and Motyka (1995) described how Taku Glacier, 25 km northeast of Juneau,

evolved in much the same way. When the first detailed map of that area was created in 1890, Taku Glacier was calving into a tidal basin that it had over-deepened during its last advance. By 1931, a morainal shoal had formed that substantially reduced mass loss due to calving. The glacier's rate of advance increased from about 60 m/yr initially to 150 m/yr during 1929-1937. As Taku Glacier continued to advance onto the tidal flat, its terminus spread out and became convex in map view (Post and Motyka, 1995). Brady Glacier's calving margin was probably similar to that of the Taku Glacier in the late 1800s and other present tidewater glacier margins, i.e. perpendicular to or nearly perpendicular to the margins of the fjord in map view. As Brady Glacier built up a stable subaerial shoal and calving diminished, its margin probably became increasingly convex until it resembled the present terminus (Fig. 3.2). The bathymetry of the previous fjord below the shoal is unknown, although it likely affected this evolution. Since Muir's observations in 1880, the outwash plain has grown and now extends almost 5 km beyond the present terminus of the glacier.

3.4 Sample Sites and Chronology Development

We sampled rooted subfossil trunks of glacially overridden trees at the glacier margin and inundated trees at North Trick and Spur lakes in August 2007. The overridden trees, exposed by glacier downwasting in recent decades (Fig. 3.3a), are located approximately 500 m northeast of North Trick Lake above the present glacier margin. Most of the inundated trees are located in the water near the west shore of North Trick Lake (Fig. 3.3b) and on the southeast shore of Spur Lake (Fig. 3.3c). We collected increment cores from rooted subfossil trees at a range of elevations at all three study sites. Samples were collected as low as possible on the trunks and from the least decomposed wood. The location and elevation of the base of each sampled tree were determined with differential GPS. At North Trick Lake we collected samples from partially

submerged, erect trunks directly above the water surface and determined the elevation of the samples above the tree base using a weighted measuring tape. Where available, we selectively sampled trees with preserved bark to ensure recovery of the outermost ring. Very few trees had bark. If no bark was present, the sample was classified as possibly lacking outer rings. However, trees that obviously had abraded or rotten outer layers were not sampled.

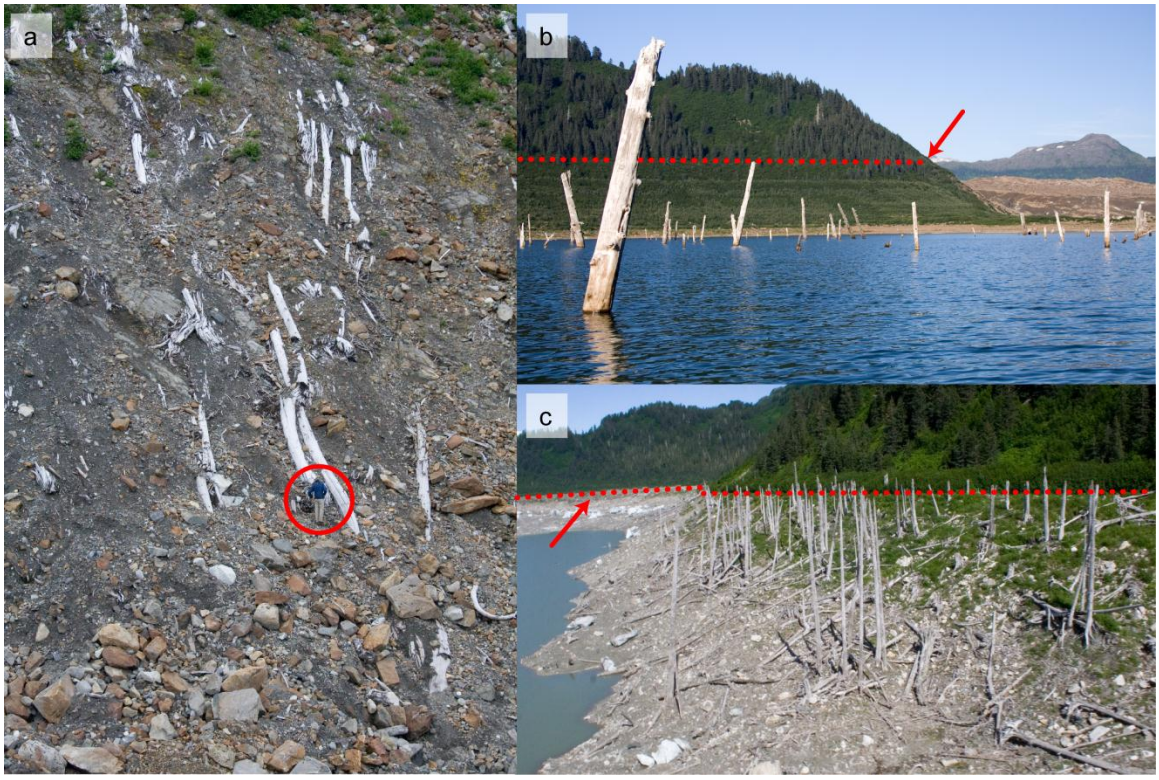

Fig. 3.3. Sample sites: a) glacier margin; view west (person circled for scale). b) North Trick Lake; view east with high strandlines denoted by arrow and red dotted line. c) Spur Lake; view northwest. Photographs taken from viewpoints indicated on Figure 3.2.

Cores were prepared for analysis and crossdated using standard dendrochronological techniques (Stokes and Smiley, 1968). We measured ring widths to the nearest micron using a Velmex measuring system and developed a floating ring-width chronology from all ring-width series using COFECHA (Holmes, 1983; Grissino-Mayer, 2001). Calendar dating of the floating tree-ring chronology was accomplished by comparison with unpublished tree-ring chronologies

of living mountain and western hemlock from sites on Excursion Ridge and the Beartrack Mountains, 65 and 55 km to the east (Fig. 3.1), both within Glacier Bay National Park (Wiles, unpublished). Dating was confirmed by visual comparison of marker rings (Stokes and Smiley, 1968). Samples are archived at Simon Fraser University's Centre for Natural Hazard Research.

3.5 Results

The final chronology is based on radii from 35 subfossil trees at the glacier margin, nine adjacent to Spur Lake, and four in North Trick Lake. Preservation of subfossil wood ranged from good at the glacier margin to poor at North Trick Lake, where no trees had preserved bark. The tree-ring series from all three sites provide a composite tree-ring chronology spanning 492 years, from 1370 to 1861 AD. Correlation of the Brady Glacier chronology with the Excursion Ridge ($R = 0.66$, $n = 344$) and Beartrack ($R = 0.54$, $n = 347$) master chronologies is significant well above the 99% confidence level (Fig. 3.4). The oldest and longest-lived tree grew at 144 m a.s.l. at the glacier margin site, died around 1839 and was at least 469 years of age. Therefore, this glacier margin site had been ice-free since at least 1370. We obtained the pith in only a few samples, thus the innermost sampled ring only provides a minimum date for establishment of the tree. Few sampled trees had surviving bark; consequently the outermost sampled ring only provides a limiting date for the death of the tree in most cases. The limiting outer ring dates of individual samples at Spur Lake range from 1830 at 83 m a.s.l. to 1839 at 121 m a.s.l., at the glacier margin site they range from 1844 at 125 m a.s.l. to 1859 at 202 m a.s.l., and at North Trick Lake they range from 1817 at 16 m a.s.l. to 1861 at 10 m a.s.l. (Fig. 3.5).

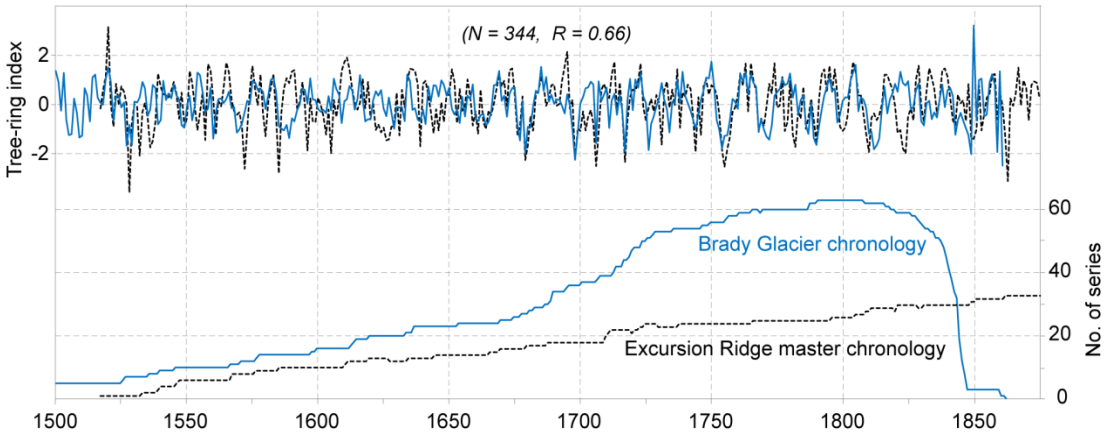

Fig. 3.4. Crossdate of the composite Brady Glacier chronology (blue solid lines) with Excursion Ridge master chronology (black dotted lines), which was created from living mountain and western hemlock. The upper plot illustrates tree-ring chronologies standardized using a 32-yr spline with persistence removed to emphasize the high-frequency signal. The lower plot shows sample sizes for the two chronologies. Numbers in parentheses are years of overlap (N) and correlation coefficient (R).

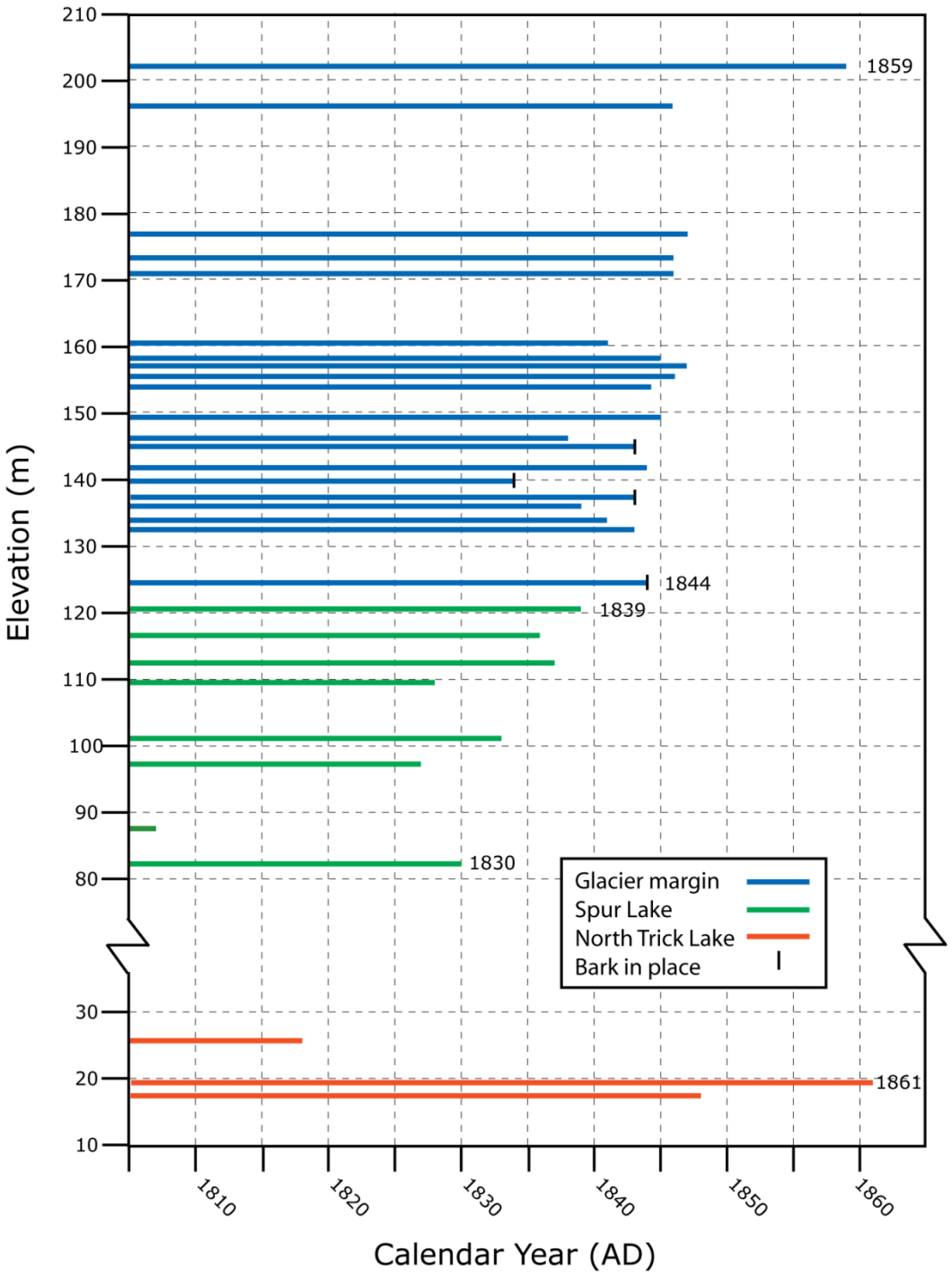

Fig. 3.5. Outermost ring dates (with critical calendar dates indicated) and elevations of crossdated samples from the three sites. Samples retaining bark are indicated. Outermost rings without bark provide only limiting death dates. At the glacier margin site, the ice reached as high as 260 m a.s.l. Spur Lake could not rise higher than 125 m a.s.l. because of the stable bedrock outlet at that elevation. North Trick Lake elevations reached up to 130 m a.s.l.

3.6 Discussion

3.6.1 Chronology of last glacier advance and lake damming

Limiting kill dates of the trees allow us to make inferences about the vertical and horizontal extent of the glacier through time. The trees in the Spur and North Trick lake basins likely were killed when they were inundated by the water dammed by the advancing glacier. Given that glacier-dammed lakes typically drain before lake levels reach 90% of the height of the damming ice (Thorarinsson, 1939; Tweed and Russell, 1999), we assume that the glacier would need to be at least 10% higher in elevation than the associated lake level. The earliest outer ring date related to the most recent advance of Brady Glacier comes from Spur Lake. The lowest sampled tree at 83 m a.s.l. has a limiting date of 1830. To dam the lake to this elevation, the glacier would need to be at least 92 m in elevation at the southern ice-margin of the basin at that time. The highest sampled tree in the Spur Lake basin at 121 m a.s.l. has a limiting date of 1839. This elevation is only 4 m below the stable outlet at 125 m a.s.l. To dam the lake to 121 m a.s.l., the glacier must have been at least 134 m in elevation at the southern ice-margin of the basin. This equates to a thickening of 42 m between 1830 and 1839.

We can calculate horizontal glacier advance from vertical thickening data if we assume a constant surface slope. The average surface slope of Brady Glacier below the divide separating north- and south-flowing ice on the International Boundary Commission's 1907 topographic map is 3.9° (IBC, 1923). Assuming the gradient was the same in the 1830s, an increase in thickness of 42 m would correspond to a horizontal advance of approximately 600 m. This advance, while rapid compared to many glacier advances, is substantially slower than the rate of the Taku Glacier advance of 150 m/yr from 1929-1937 (Post and Motyka, 1995).

Lake level data provide an estimate of the elevation of the ice margin at a given time but it is more difficult to estimate the state of the terminus in the main valley. Most calving glaciers have steep, near-vertical to vertical faces (Molnia, 2008); therefore we can safely assume that Brady Glacier terminated in a near-vertical front several tens of metres high when it was advancing into the sea. For example, the calving front of Hubbard Glacier, 230 km northwest of Brady Glacier, is over 100 m high, 8 km wide, and reaches 125 m a.s.l. within a few hundred metres of the terminus. The calving fronts of Johns Hopkins and Margerie glaciers, 25 and 35 km northwest of Brady Glacier, are over 75 m high, 1.5 and 2.0 km wide, and also reach elevations of 125 m a.s.l. within a few hundred metres of their termini. If Brady Glacier, approximately 4.5 km wide at the study sites, had a 125-m-high calving front when it dammed Spur Lake in 1830, it would quickly raise the level of the lake to 83 m a.s.l. or more. If Brady Glacier was not calving and had a less steep front, several years could have passed between the initial damming of the lake and it eventually reaching 83 m a.s.l. We know from observations cited in the introduction that the glacier was calving in 1794 but not in 1880. Thus, we assume that the terminus was at an intermediate stage between these two states when it reached Spur Lake. We infer that a shoal had begun to form, which limited mass loss due to calving, and the glacier front became slightly convex in map view (Fig. 3.6).

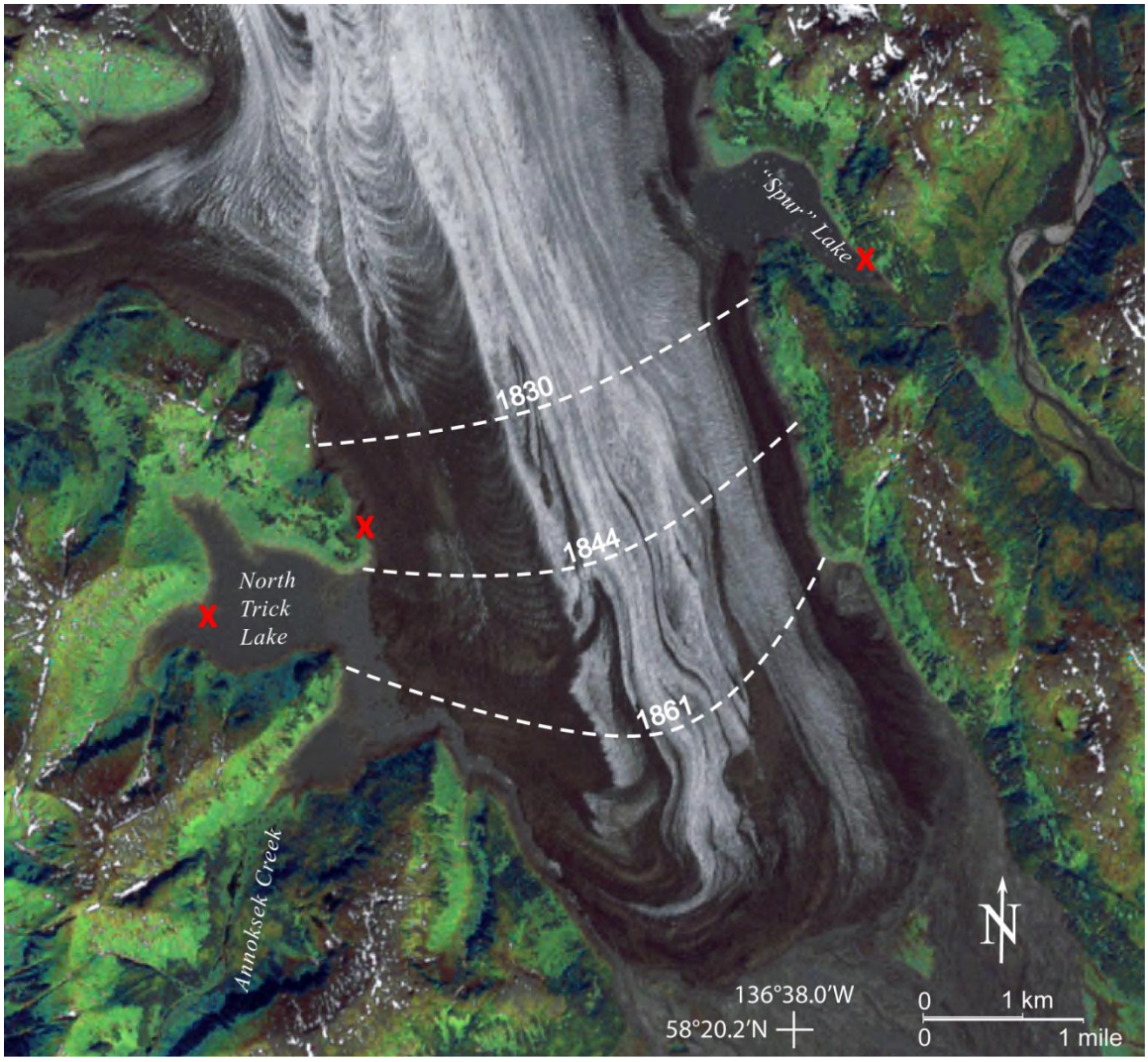

Fig. 3.6. Inferred terminus of Brady Glacier at three times during the nineteenth century, based on death dates of trees killed by overriding glacier ice and inundated in lakes that were dammed by the advancing glacier. Background Landsat Thematic Mapper 7 multispectral satellite image.

The glacier margin site provides evidence for continued thickening and advance of Brady Glacier after the formation and filling of Spur Lake. The limiting date derived from the lowest sample at 125 m a.s.l. is 1844. If the calving front was 125 m high when it reached the site, it would have killed the tree on arrival in 1844. However, if the glacier was not calving and had a less steep front, several years would have passed between the arrival of the ice front at sea level and the death of the tree at 125 m a.s.l. This date and location are in agreement with Davidson's

reproduction of Tebenkof's 1849 map of Brady Glacier (Fig. 3.2). The limiting date derived from the highest sample at 202 m a.s.l. is 1859. Again, assuming a surface slope of 3.9°, an increase in thickness of 77 m corresponds to a horizontal advance of approximately 1100 m over 15 years. We could not find adequate subfossil wood to sample above 202 m a.s.l., although the trimline marking the maximum advance of the glacier is approximately 58 m higher, at 260 m a.s.l. We therefore conclude that the glacier continued to advance for some time after 1859. No scarred or killed trees were found at the highest trimline to provide an absolute date for this maximum position. As in the case of Spur Lake, we cannot determine the exact location of the glacier front at any particular date, we only can estimate its marginal height and terminus location. We hypothesize that the glacier had further developed its stabilizing shoal and its terminus had become more convex in map view (Fig. 3.6).

The final evidence for the timing of glacier advance comes from North Trick Lake. Although we sampled 17 trees in and around North Trick Lake through a vertical range of over 100 m, we were able to crossdate only four samples. These yielded limiting death dates ranging from 1817 at 16 m a.s.l. to 1861 at 10 m a.s.l. The 1861 sample was best preserved and thus provides the most secure limiting date. Because this critical sample is at 10 m a.s.l., glacier advance past this point would have dammed the lake regardless of the frontal profile. An 1861 death date is consistent with the advance recorded at the glacier margin site and Spur Lake. The lake probably rose to the elevation of the highest lake strandline (approximately 130 m a.s.l.) in two to three decades based on the rate of glacier thickening at the other two sites. Thus, we conclude that the glacier continued to thicken and advance until at least 1880, which is consistent with previous tree-ring dates (Bengtson, 1962, Derksen, 1976).

3.6.2 Comparison with Glacier Bay

The piedmont glacier in Glacier Bay attained its maximum size around 1750, completely filling the bay and extending a short distance beyond its mouth (Connor et al., 2009). About 1780, the glacier began a dramatic retreat. Lamplugh Glacier remained connected to the main ice in Glacier Bay until at least 1894 (Klotz, 1899), but no later than 1906 (Molnia, 2008). Glacier Bay ice had retreated over 100 km by 1925 (Molnia, 2008), which is the greatest historic retreat of a glacier on record. Yet part of this retreat occurred at a time when Brady Glacier was advancing.

The ice divide between Brady and Lamplugh-Reid glaciers was probably highest in the mid- to late-1700s, when Glacier Bay ice was thickest. During its last maximum around 1750, ice in Glacier Bay at the present termini of Lamplugh and Reid glaciers was 1000 m a.s.l., 200 m higher than the present ice divide (Bengtson, 1962). As ice in Glacier Bay thinned, Lamplugh and Reid glaciers also thinned, drawing down ice from Brady Glacier. The ice divide thus moved to the south, drawing more ice to the north and away from Brady Glacier. Comparison of an annotated map by Klotz (1899) and the SRTM DEM from 2000 indicates that the divide between the glaciers has migrated approximately 3 km south in the past century.

The concurrent advance of Brady Glacier and retreat of ice in Glacier Bay seems counterintuitive, especially given that the two were connected via Lamplugh and Reid glaciers, as outlined above. We argue that a change in environment at the terminus of Brady Glacier was more important as a determinant of glacier change than the lowering and migration of the ice divide at its head. Past research has demonstrated that the activity of tidewater glaciers is controlled more by calving dynamics than climate (Post, 1975; Motyka and Begét, 1996). As Brady Glacier constructed a stabilizing outwash plain in the nineteenth century, calving ceased. This decrease in mass loss facilitated the further advance of the glacier. It constructed a

morainal embankment, perhaps at a sill, near its present terminus and, from that position, constructed an outwash plain. Brady Glacier has thinned significantly in the twentieth century (Larsen et al., 2007), but has maintained and enlarged its outwash plain, preventing the reestablishment of a calving front.

3.6.3 Differential preservation of subfossil wood

Preservation of subfossil wood at the three sites differs considerably and does not appear to be related to the age of the wood. The trees in the Spur Lake basin died first and are moderately well preserved; those at the glacier margin site were killed next and are the best preserved. The highest trees in North Trick Lake were the last to die, yet are the most poorly preserved; no cores from these higher trees were dateable because of poor preservation.

Different local conditions are thought to be responsible for the differential preservation of wood at the three sites. At the glacier margin site, the subfossil wood was covered by ice and sediment from the time that it was overridden until it became exposed during twentieth-century glacier recession. Burial of the trees minimized weathering and erosion. Barclay et al. (2009) describe similar preservation of trees buried by Tebenkof Glacier in southern Alaska over 1700 years ago.

Water covered the subfossil wood for differing amounts of time at the two lake sites. Spur Lake filled to near its stable outlet in 1839, or shortly thereafter, and the glacier continued to thicken for approximately 40 years. With a thick glacier dam and a stable outlet, Spur Lake does not appear to have drained by jökulhlaup until recently. Available evidence from maps, aerial photographs, satellite imagery, and published and unpublished research show Spur Lake filled to overflow prior to 2002. The first evidence of the lake below its stable outlet is a Landsat image acquired in March 2002. Since then, jökulhlaups have periodically drained the lake, the lake has

not filled to overflow, and vegetation is becoming established below the highest strandline. Stranded icebergs in the basin in 2007 (Fig. 3.3c) show that jökulhlaups have continued. The lake level defined by the stranded icebergs was only 89 m a.s.l., 36 m below the stable outlet. This history suggests that the subfossil wood we sampled in Spur Lake has only been exposed to air for a short time and thus was relatively well preserved. Clague and Shilts (1993) described similar preservation of trees in two stable landslide-dammed lakes where the trees were preserved for at least 800 years.

Most of the trees in North Trick Lake were killed after 1861 as the glacier continued to advance and raise the lake to successively higher levels. By 1929, the date of the first U.S. Navy aerial photographs, the glacier was downwasting. In these images, vegetation is colonizing the area between the lakeshore and the highest strandline. Aerial photographs taken in 1948 show a lower lake and at least three, progressively less-densely-vegetated strandlines above the shoreline. South Trick Lake had drained catastrophically to the terminus before the 1948 photographs were taken, which allowed North Trick Lake to drain to lower levels. Therefore, most of the trees in the basin have been subaerially exposed discontinuously for at least 59 years. Post and Mayo (1971) and Derksen (1976) state that North Trick Lake had a long history of jökulhlaups. The lowest non-glaciated outlet of the basin is approximately 247 m a.s.l. or about 117 m higher than the highest strandline. Without a stable outlet, the lake would fill and drain quasi-periodically throughout its life cycle. The highest and longest exposed subfossil wood at this site was the most decomposed, whereas the trees in the present moraine-dammed lake are the best preserved because they have been exposed to subaerial processes for the shortest time.

In both North Trick and Spur lakes, there is a clear concordance in height of the tops of standing, formerly inundated trees (Fig. 3.3). Most of the inundated trees in Spur Lake are

cropped at approximately 125 m a.s.l, and those in North Trick Lake do not extend above approximately 35 m a.s.l. We postulate that the height of these cropped trees results from trimming by winter lake ice at elevations where the lakes were maintained for relatively long periods of time.

3.7 Summary and Conclusions

We developed a tree-ring chronology spanning the period from 1370-1861 AD from subfossil wood at three sites bordering Brady Glacier and used it to document the history of glacier fluctuations and glacier-dammed lake evolution. Our data confirm that the study sites were not occupied by the glacier or lakes for at least 450 years prior to 1830. Spur Lake was impounded by the advancing glacier no later than 1830 and had filled to an elevation of approximately 121 m a.s.l. by 1839. The glacier continued to advance, reaching a site about 1.4 km farther south by 1844, and dammed North Trick Lake another 1.1 km down valley by 1861. Brady Glacier did not reach its maximum extent until at least the 1860s, and probably not until 1880. We postulate that this advance was made possible by establishment of a morainal shoal, similar to the behavior observed at Taku Glacier in the 1900s, which caused a major reduction in ablation due to cessation of terminal calving. This study is the first to apply elevation-constrained mapping and dendrochronology to date glacier fluctuations and the evolution of ice-marginal lakes.

4. EVOLUTION OF GLACIER-DAMMED LAKES THROUGH SPACE AND TIME; BRADY GLACIER, ALASKA, USA

Denny M. Capps and John J. Clague

Abstract

Glacier-dammed lakes and their associated jökulhlaups cause severe flooding in downstream areas and substantially influence glacier dynamics. Brady Glacier in southeast Alaska is well suited for a study of these phenomena because it presently dams ten large (> 1 km^2) lakes. Our objectives are to demonstrate how Brady Glacier and its lakes have co-evolved in the past and to apply this knowledge to predict how the glacier and its lakes will likely evolve in the future. To accomplish these objectives, we georeferenced a variety of maps, airphotos, and optical satellite imagery to characterize the evolution of the glacier and lakes. We also collected bathymetry data and created bathymetric maps of select lakes. Despite small advances and retreats, the main terminus of Brady Glacier has changed little since 1880. However, it downwasted at rates of 2-3 m/yr between 1948 and 2000, more than the regional average. The most dramatic retreat (2 km) and downwasting (123 m) have occurred adjacent to glacier-dammed lakes. The retreat and downwasting are primarily the result of calving into ten large glacier-dammed lakes. Calving margins of glacier-dammed lakes share several similarities with tidewater glacier calving margins. After tidewater glaciers reach equilibrium, a perturbation such as a change in climate can thin the glacier so that it no longer is grounded on the stabilizing shoal, triggering more mass to be lost through calving than is replenished. The glacier may then catastrophically retreat. Brady Glacier is a former tidewater glacier with many glacier-dammed lakes that are contributing to mass loss. Eventually, Brady Glacier will return to a tidewater regimen and enter into a phase of catastrophic retreat. The situation at Brady Glacier is not unique, and the lessons learned here can be applied elsewhere to identify future glacier-dammed lakes, jökulhlaups, and glacier instability.

4.1 Introduction

Glacier-dammed lakes and the catastrophic outburst floods (jökulhlaups) that emanate from them cause severe flooding in downstream areas and substantially influence glacier dynamics. Jökulhlaups commonly have peak discharges orders of magnitude larger than precipitation-induced floods (Clague and Evans, 1994). Additionally, large jökulhlaups can fracture and uplift glacier termini. The fracturing enhances mechanical removal of ice fragments, which can lead to the creation of large supraglacial channels and embayments (Russell et al., 2006). Jökulhlaups cause substantial erosion and deposition, alter riparian ecosystems (Post and Mayo, 1971), and have caused severe damage to infrastructure up to 1,200 km from their source (Mason et al., 1930). Consequently, they are the farthest reaching of all terrestrial glacial hazards.

In the past decade, research has confirmed that glacier-dammed lakes and jökulhlaups can directly affect glacier motion. Anderson et al. (2005) documented a jökulhlaup that increased glacier velocity by a factor of 2.4 in the Wrangell Mountains of Alaska. Sugiyama et al. (2007) recorded a temporary, but complete, reversal of glacier motion during a jökulhlaup in the Swiss Alps. Magnússon et al. (2010) noted an Icelandic glacier that did not return to pre-flood velocity for several years after a jökulhlaup. Mayer et al. (2008) documented a jökulhlaup from a glacier-dammed lake in the Tian Shan Mountains of Kyrgyzstan that was preceded by flotation of the ice dam; flotation, in turn, caused a substantial intensification in calving and a threefold increase in glacier velocity. For two months after the jökulhlaup, the glacier experienced higher velocities into the former lake basin.

Brady Glacier, the largest glacier in the Fairweather Range of the St. Elias Mountains of Alaska, is well suited for a study of the evolution of glacial lakes. The main terminus of Brady Glacier has varied little over the past 130 years but, between 1948 and 2000, the lobate margins of the glacier retreated up to 2 km and downwasted up to 120 m adjacent to ten large (> 1 km^2)

ice-dammed lakes (Larsen, et al., 2007; Capps et al., 2010). Six of the ten lakes are primarily subaerial (Fig. 4.1), and four are subglacial; we define a lake as subglacial if it occurs primarily underneath the glacier, whether or not it is at atmospheric pressure (Clague and Evans, 1994; Tweed and Russell, 1999). In seven of the ten lakes, the glacier has a calving margin that exceeds 1 km in width. These lakes, and many smaller ones, are in different stages of evolution – incipient, stable and non-draining, and periodically draining.

Our goals in this paper are to demonstrate how Brady Glacier and the numerous lakes that it dams have co-evolved in the past and to apply this knowledge to predict how the glacier and its lakes will likely evolve in the future. Our specific objectives are to: (1) compile and interpret previous observations, research, maps, airphotos, and optical satellite imagery to define the last advance of Brady Glacier and the evolution of its lakes; (2) describe the present state of the glacier and its lakes through the use of field-based measurements and recent optical satellite imagery; (3) predict how the glacier and its lakes will evolve in the future based on analogous past behaviour in similar glacier systems in the region; and (4) discuss how this information can be applied to forecast the future evolution of other glaciers and lakes in the region and elsewhere.

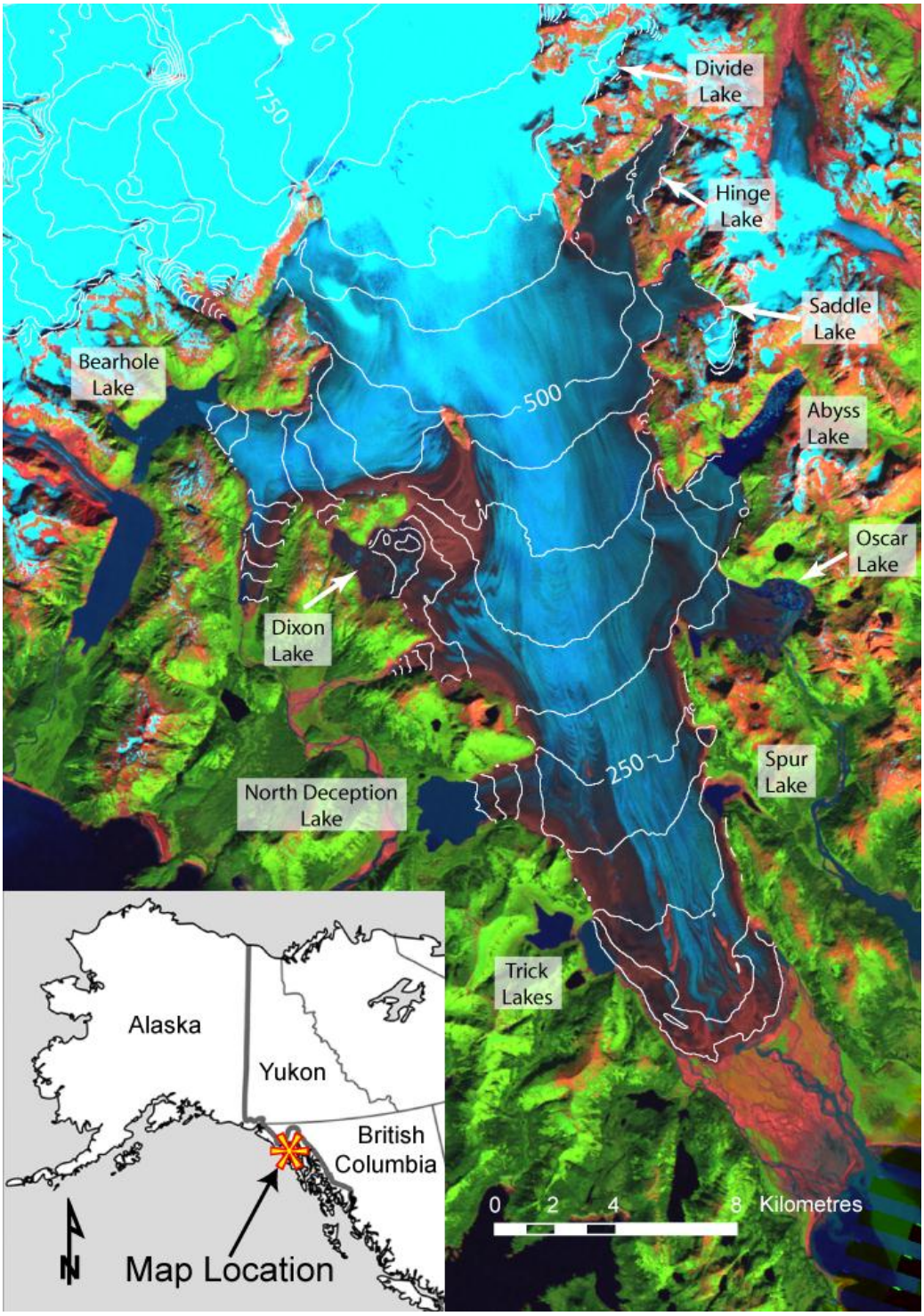

Fig. 4.1. False-color Landsat 5 image (bands 7/4/2) of Brady Glacier, southeast Alaska, acquired on August 14, 2010. Topographic contours are derived from 2000 SRTM DEM (50 m contour interval).

4.2 Regional Setting

4.2.1 Brady Glacier

Brady Glacier is located in Glacier Bay National Park, 125 km west of Juneau, Alaska (Fig. 4.1). It is 51 km long and 590 km^2 in area. In the early 1990s, the glacier had an accumulation area ratio of 0.65, with an equilibrium line altitude (ELA) of approximately 610 m a.s.l. (Viens, 1995). Peaks up to 3467 m a.s.l. to the northwest supply most of the ice to the glacier. The glacier terminates approximately 10 m a.s.l. on a large outwash plain that extends 4.8 km into Taylor Bay.

Brady Glacier has excavated a north-northwest-trending, fault-controlled valley (Derksen, 1976) that is 64 km long and extends from Taylor Bay on the south to near the north end of Glacier Bay. Approximately two-thirds of the ice flows south-southeast towards Taylor Bay as Brady Glacier and one-third flows north-northwest into Lamplugh and Reid glaciers, which terminate in Glacier Bay (Bengtson, 1962; Derksen, 1976). The divide between south- and north-flowing ice lies at approximately 820 m a.s.l. based on the 2000 Shuttle Radar Topography Mission (SRTM) digital elevation model (DEM). Ice-penetrating radar measurements near the main axis of Brady Glacier indicate that the bed is well below sea level and the valley might be a continuous fjord if the glaciers and outwash plain were not present (Barnes and Watts, 1977).

4.2.2 Previous studies

The late Holocene extent of Brady Glacier has been a subject of debate. The glacier had retreated at least 24 km north of its present terminus by 645-725 cal yr BP, but began to advance shortly thereafter based on radiocarbon ages from subfossil wood in till (Bengtson, 1962; Derksen, 1976). Historical observations of the glacier terminus date back to 1794 when Joseph Whidbey, Captain George Vancouver's lieutenant, made the first recorded observations

of the terminus. The chart produced from his observations roughly reproduces the coastline (Vancouver, 1984), but the perspective is distorted. Numerous other explorers mapped the terminus area, but the changing glacier and inconsistent identification of landforms and reference points complicate interpretation of these early observations. Accurate maps of the area were not produced until detailed measurements were recorded in 1907.

Capps et al. (2011) determined the timing of the glacier's last advance and related formation and filling of North Trick and Spur lakes, which formerly were probably marine embayments (Fig. 4.2). Their inferred evolution is based on dendrochronology and precise elevation-constrained mapping of overridden and drowned trees at the glacier margin. Brady Glacier impounded Spur Lake to an elevation of 83 m a.s.l. ca. 1830 and to 121 m a.s.l. by ca. 1839. Soon after, Spur Lake reached 125 m a.s.l. and began to overflow across a stable bedrock sill to the southeast. The glacier continued to advance, thickening by at least 77 m between ca. 1844 and 1859 at a site 500 m northeast of North Trick Lake. North Trick Lake began to form by 1861 and reached its highest elevation at approximately 130 m a.s.l. when Brady Glacier reached its maximum extent ca. 1880. By 1929, the glacier had begun to downwaste and vegetation was colonizing the area between the lakeshore and the highest strandline of North Trick Lake (Capps et al., 2011).

Several early explorers noted Brady Glacier's change from a tidewater glacier to one terminating on an outwash plain. Vancouver, in his account of the 1794 exploration, wrote that, ". . . further progress was now stopped by an immense body of compact perpendicular ice, extending from shore to shore", which indicates a tidewater terminus. By 1880, however, Muir commented, "No icebergs are discharged from it, as it is separated from the water of the fiord at high tide by a low, smooth mass of outspread, overswept moraine material . . . The front of the glacier, like all those which do not discharge icebergs, is rounded like a brow, smooth-

looking in general views . . .” (Muir, 1915). Therefore, sometime between 1794 and 1880 the terminus evolved from a calving margin into a non-calving margin.

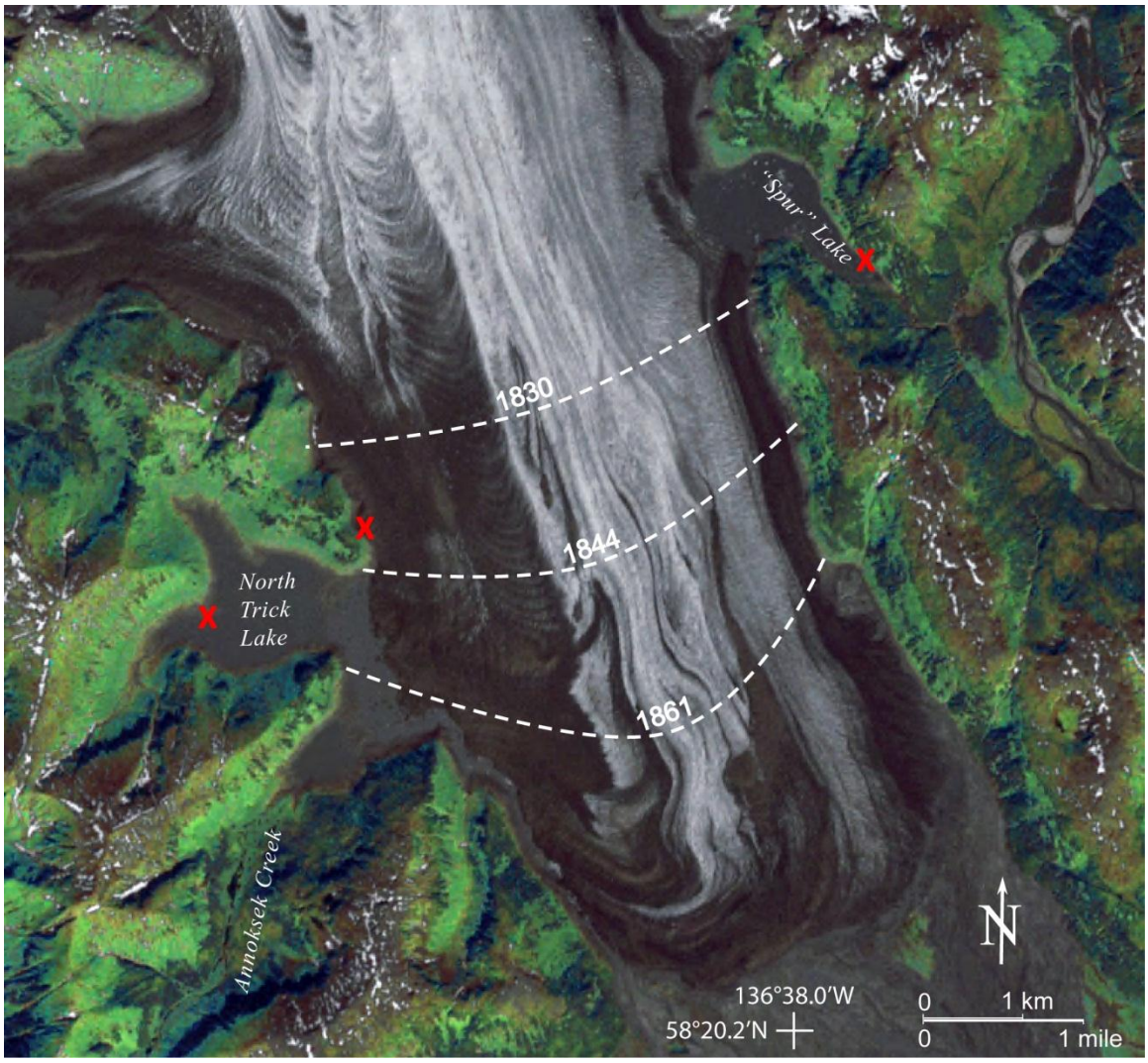

Fig. 4.2. Inferred terminus of Brady Glacier at three times during the nineteenth century, based on death dates of trees that were killed by overriding glacier ice or drowned in lakes dammed by the advancing glacier (from Capps et al., 2011). Landsat 7 ETM+ image (bands 3/2/1) acquired in 2000.

4.3 Methods

4.3.1 Evolution of Brady Glacier through time

We georeferenced a variety of maps, airphotos, and optical satellite imagery to characterize Brady Glacier from the beginning of the twentieth century to 2010. As previously noted, the earliest map of the area is from 1794, but the first topographic map with ice contours was made in 1907 during the Canada-U.S. International Boundary Survey. We scanned this map at a resolution of 600 dots per inch (dpi). The first airphotos of the area were taken in 1929 by the United States Navy, but these only cover the lowest 10 km of the glacier. The first large-scale, high-quality maps of the entire glacier were produced from airphotos taken in 1948. More airphotos were taken periodically through 1997. Glacier Bay National Park provided us with 600 dpi scans of the 1929 airphotos and 1997 digitally orthorectified black-and-white airphotos. The 1997 airphotos were the foundation for our GIS work because of their high spatial resolution (1 m). We obtained 600 dpi digital scans of the 1948 and 1979 airphotos and Landsat imagery from the U.S. Geological Survey's EarthExplorer web server (http://edcsns17.cr.usgs.gov/EarthExplorer/). The earliest satellite imagery used here is from Landsat 1, acquired in 1972. Repeat Landsat 5 and 7 imagery is available to the termination of our study in 2010. Using the georeferencing tool in ArcGIS 9.3 and techniques outlined in Hughes et al. (2006), we identified at least eight ground control points (GCPs) per airphoto or map, applied a second-order polynomial transformation, and resampled pixels through cubic convolution. From these georeferenced products, we manually outlined the glacier terminus for the years 1907 and 1929, and the glacier below the ELA for the years 1948, 1979, 1997, and 2010.

We determined the volume change of the glacier through time using elevation change data supplied by Dr. Chris Larsen of the University of Alaska Fairbanks. Larsen et al. (2007)

differenced the 2000 SRTM DEM from the National Elevation Dataset DEM, which is based on the airphotos taken in 1948, to determine elevation and volume changes of Brady Glacier and other glaciated areas of southeast Alaska and adjacent British Columbia, Canada. They published a regional map of glacier elevation changes that includes Brady Glacier; however, the scale was too small for the detail needed in this study. They also plotted volume change rates of Brady Glacier in comparison to other glaciers in the region, but did not provide numerical values. Regardless, we wanted to calculate separate values of volume change in the ablation and accumulation zones. Therefore, using a GIS, we created an elevation change map of all pixels over the glacier from Larsen's data and calculated from those values the glacier volume change between 1948 and 2000. We calculated the volume error by multiplying the DEM differencing error (±0.3 m/yr below the ELA and ±0.6 m/yr above the ELA) by the glacier area. The differencing error is greater in the accumulation zone because of the larger error associated there with photogrammetric mapping (Larsen et al., 2007).

4.3.2 Evolution of Brady Glacier's lakes and jökulhlaups through time

We identified and characterized the glacier-dammed lakes from the beginning of the twentieth century to 2010 using the same georeferenced GIS data that we used to delineate the glacier. Quantified attributes include area, width of calving front, and elevation. We also compiled evidence of past jökulhlaups and drainage routes based on previous research, field observations, and optical imagery. Earlier jökulhlaups were recorded primarily by Post and Mayo (1971) and Derksen (1976). Since the mid-1970s, most evidence of jökulhlaups consists of coincidental observations of unusually turbid, debris- and iceberg-laden water adjacent to the glacier made by Glacier Bay National Park personnel or reported to the park by passing boat captains.

4.3.3 Current bathymetry of select glacier-dammed lakes

We collected bathymetry data and created bathymetric maps of Abyss, Bearhole, East Trick, North Deception, and Oscar lakes using a sonar-equipped floatplane and a custom-built, remote-controlled boat. We used the floatplane to collect data in larger stretches of open water at a relatively safe distance from the calving front of the glacier. We used the remote-controlled boat to collect data near the more hazardous calving fronts. With one exception, we created bathymetry maps using the default settings of Golden Software Surfer 9 software and the minimum curvature gridding method. In the case of North Deception Lake, the default setting produced an unnatural "cross" shape in the bathymetry. To produce a more realistic interpretation, we changed the internal tension settings from 0 to 1.

4.4 Results

4.4.1 Evolution of Brady Glacier through time

Changes in the position of Brady Glacier terminus have been small compared to those of other glaciers in the region (Larsen et al., 2007; Barclay et al., 2009). The greatest change occurred between 1948 and 1979, when the glacier advanced by as much as 600 m (Fig. 4.3). After 1979, the terminus began a spatially discontinuous retreat that continued to 2010. In the late 2000s and 2010, small lakes began to form at the terminus (Fig. 4.1).

Although the main Brady Glacier terminus has moved little since 1907, the glacier has downwasted substantially, particularly in areas adjacent to the glacier-dammed lakes (Fig. 4.4). Glacier volume loss between 1948 and 2000 is 8.4 ± 2.9 km^3 in the ablation zone and 4.1 ± 8.1 km^3 in the accumulation zone, for a total volume loss of 12.5 km^3 ± 11.1 km^3. The greatest downwasting is adjacent to Dixon Lake (123 m ± 16 m), Saddle Lake (111 m ± 16 m), and North Deception Lake (103 m ± 16 m). Despite the overall pattern of downwasting, some areas seem

to have thickened. Figure 4.4 shows 40-50 m of inflation at the southeast margin of the terminus. This result is supported by Figure 4.3, which shows that the glacier advanced in this area from 1948 to 1979. Figure 4.4 also shows as much as 30-40 m of thickening in the northwest part of the map, which is in the accumulation zone. We were unable to verify if this apparent thickening is real or an error associated with photogrammetric mapping.

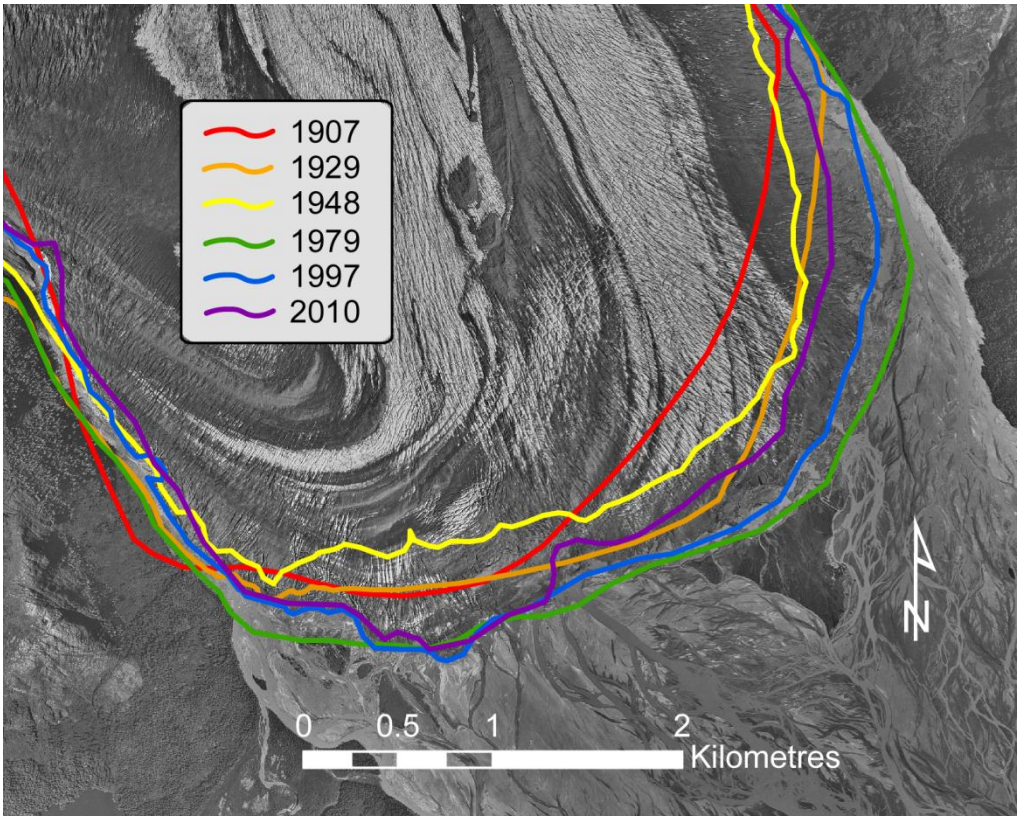

Fig. 4.3. Location of the Brady Glacier terminus through time based on georeferenced maps, airphotos, and Landsat imagery from 1907 to 2010. The background image is a 1997 digitally orthorectified quadrangle.

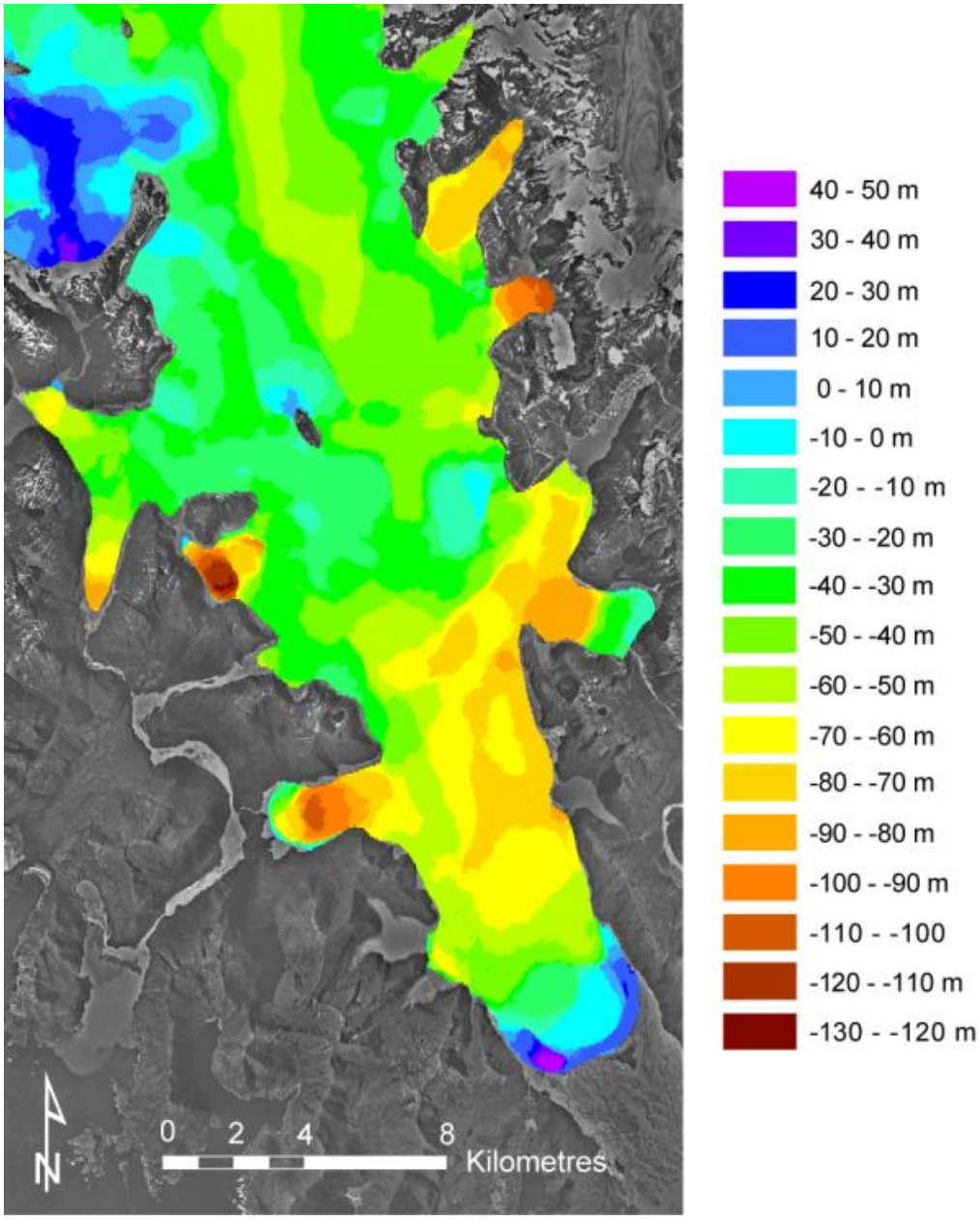

Fig. 4.4. Brady Glacier elevation change from 1948 to 2000. The background image is a 1997 digitally orthorectified quadrangle.

4.4.2 Evolution of Brady Glacier's lakes and jökulhlaups through time

Direct comparisons of Brady Glacier's lakes and jökulhlaups through time are difficult because they are dynamic features and events. An airphoto or satellite image only shows a lake's condition at a specific time and does not indicate whether the lake is filling, stable, or

rapidly draining. To address this issue, the lakes and their associated jökulhlaups must be discussed individually in the larger context of their histories and settings.

Bearhole Lake. Bearhole Lake is first identifiable in airphotos from 1948, when it appears as three lobes of open water between Brady and Palma glaciers and tributary valleys. At that time, the lake had a combined surface area of 0.8 km^2, was dammed to an elevation of 204 m a.s.l. by both Palma and Brady glaciers (Table 4.1), and had a combined calving front over 2300 m long (Table 4.2). Jökulhlaups drained subglacially under Palma Glacier into Palma River (Fig. 4.5). Dendrochronology indicates that catastrophic floods from this lake denuded the floodplain of Palma River around 1918, and floods continued to at least 1976 (Derksen, 1976). The lake continued to be dammed by Palma Glacier at least through 1979, but by 1997, Palma Glacier had retreated and downwasted enough that Bearhole Lake was dammed by a bedrock sill to the southwest and Brady Glacier to the southeast. The lake has not experienced further jökulhlaups since that time. In 2010, the lake had an area of 3.2 km^2 and the calving margin had retreated into a relatively stable position in a constriction in the Bearhole lobe of Brady Glacier (Fig. 4.1).

Dixon Lake. Dixon Lake is first evident in the 1948 airphotos as a 0.8 km^2 iceberg-choked subaerial lake. The lake drains subglacially to the south, then west before emerging subaerially into Dixon River (Fig. 4.5). Photographs taken from adjacent peaks in 1894 by the International Boundary Commission show the valley floor of Dixon River stripped of vegetation and full of sediment, suggesting that the lake was dammed and releasing jökulhlaups at that time. It was either subglacial or not properly surveyed on the 1907 topographic map. Dixon Lake underwent major change in the 1980s when a large area around its margin began to float. By the 1990s, the floating margin was beginning to break up, and then, during the 2000s, subaerial Dixon Lake grew rapidly in size. In 2007, one of us (DMC) witnessed the draining of the lake, the discharge of floodwaters from the lobe of the glacier, inundation of the floodplain of Dixon River, and

large standing waves and a sediment plume where the river entered Dixon Harbour. By 2010, Dixon Lake had grown to 3.6 km^2 and is now the largest lake dammed by Brady Glacier.

Table 4.1. Approximate lake surface elevations from topographic maps based on airphotos taken in July and August 1948 and in February 2000 when SRTM imagery was acquired.

Lake	m a.s.l.	
	1948	2000
Bearhole	204	165
Dixon	274	170
North Deception	23	18
North Trick	60	30
East Trick	x	30
South Trick	60	30
Spur	133	133
Oscar	198	198
Abyss	269	230
Saddle	507*	411*
Hinge	501*	430*
Divide	624*	584*

x – lake did not exist at that time, * - elevation of ice shelf

Table 4.2. Approximate calving margin widths.

Lake	m	
	1948	2010
Bearhole	2360	1850
Dixon	940	2820
North Deception	2150	1270
North Trick	760	*
East Trick	*	1660
South Trick	920	*
Spur	1190	1140
Oscar	770	6400
Abyss	890	1240
Saddle	900	1300
Hinge	610	610
Divide	*	*

* - No calving margin

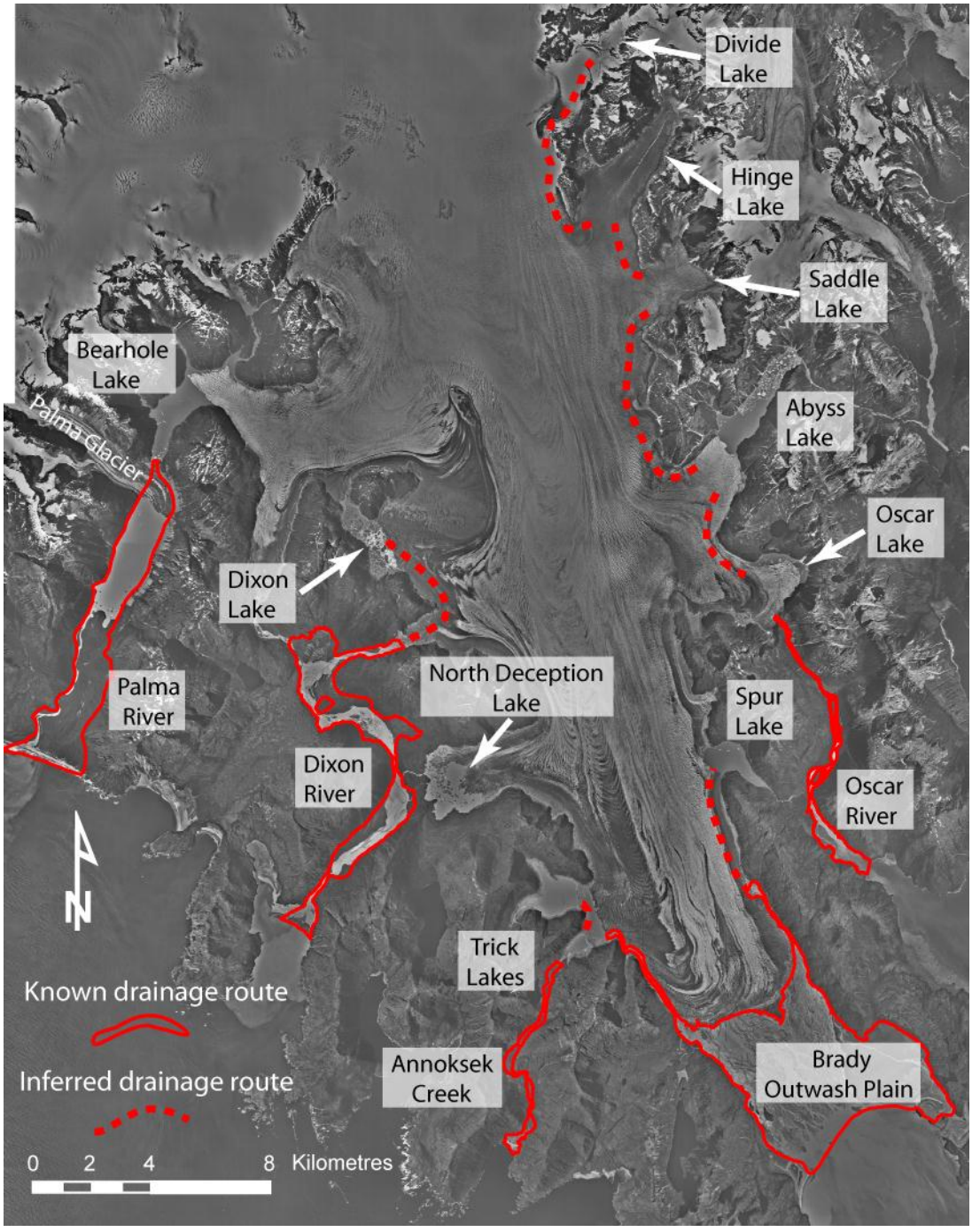

Fig. 4.5. Map of large glacier-dammed lakes (>1 km^2) and historic jökulhlaup drainage routes. The background image is a 1997 digitally orthorectified quadrangle.

North Deception Lake. This lake was originally dammed between the west-flowing North Deception lobe and a north-northeast trending ridge, as shown on the 1907 topographic map (Fig. 4.6a). We found no documented evidence for jökulhlaups, but any such floods would have

drained into adjacent Dixon River (Fig. 4.5). When full, the lake may have backed up into South Deception Lake. By 1929, the glacier had begun to retreat and North Deception Lake occupied an overdeepened depression produced by the North Deception lobe. The lake entered a phase of relative stability for several decades, but beginning in the mid-1990s, the North Deception lobe began to break up rapidly and retreat to the east. By 2004, the ice margin had retreated to a more stable position where the lobe narrows, and it has remained near that position since. The surface area of the lake increased from 0.5 km^2 in 1948 to 3.2 km^2 in 2010. Comparison of the contours in Figure 4.6b and the glacier recession in Figure 4.6c indicates that over 150 m of ice thickness has been lost at North Deception Lake between 1948 and 2010. This thinning is consistent with the findings of Larsen et al. (2007). The lake surface has lowered slightly since 1948 because the lake established a lower outlet during glacier retreat. We have found no evidence that North Deception Lake has produced any jökulhlaups.

North Trick Lake. Dendrochronologic evidence indicates that North Trick Lake formed by 1861 when the glacier was advancing (Capps et al., 2011). North Trick Lake is clearly indicated on the 1907 topographic map, but its basin was not accurately mapped to true scale (Fig. 4.7a). By 1929, the glacier was downwasting, the lake was dammed to a lower level, and vegetation was colonizing the area between the lakeshore and the highest strandline (Fig. 4.7b). 1948 airphotos show the lake at an even lower level, with at least three, progressively less densely vegetated strandlines above the shoreline (Fig. 4.7c). Post and Mayo (1971) and Derksen (1976) noted that North Trick Lake has a long history of jökulhlaups. The lowest non-glaciated outlet of the basin is at approximately 247 m a.s.l., or about 117 m higher than the highest strandline. Therefore, because it does not have a stable outlet, the lake would fill and drain repeatedly. By the mid-1980s, Brady Glacier had retreated sufficiently that it no longer dammed North Trick Lake (Fig. 4.7d). Today, North Trick Lake is a stable 1.0 km^2 moraine-dammed lake.

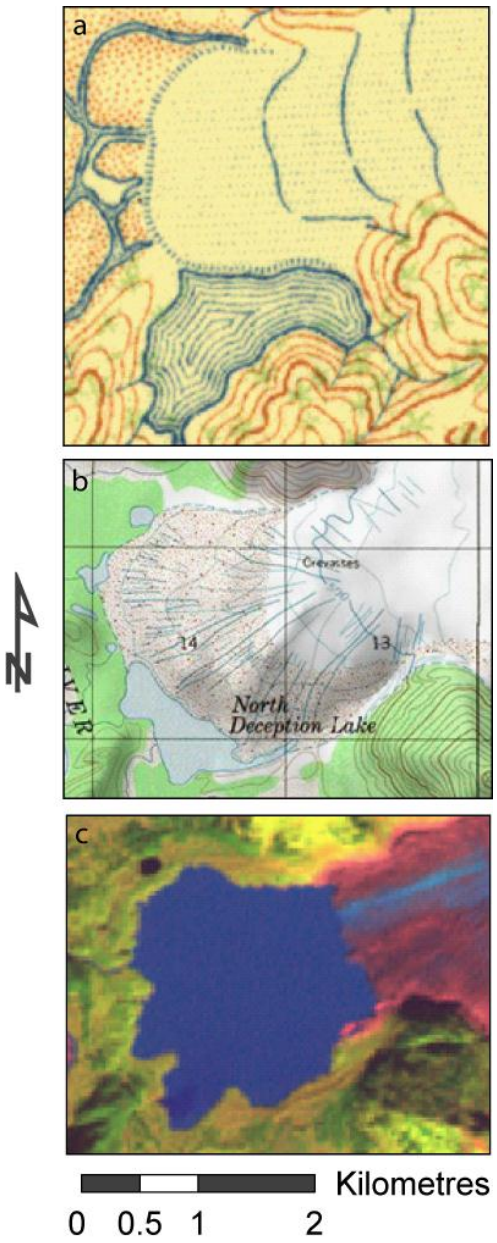

Fig. 4.6. Evolution of North Deception Lake. (a) 1907 International Boundary Commission 1:250,000-scale topographic map; contour interval 250 feet (ca. 75 m). (b) 1948 U.S. Geological Survey 1:63,360-scale topopgraphic map; contour interval 100 feet (ca. 30 m). (c) False-colour Landsat 7 ETM+ image (bands 7/4/2) acquired on September 16, 2010.

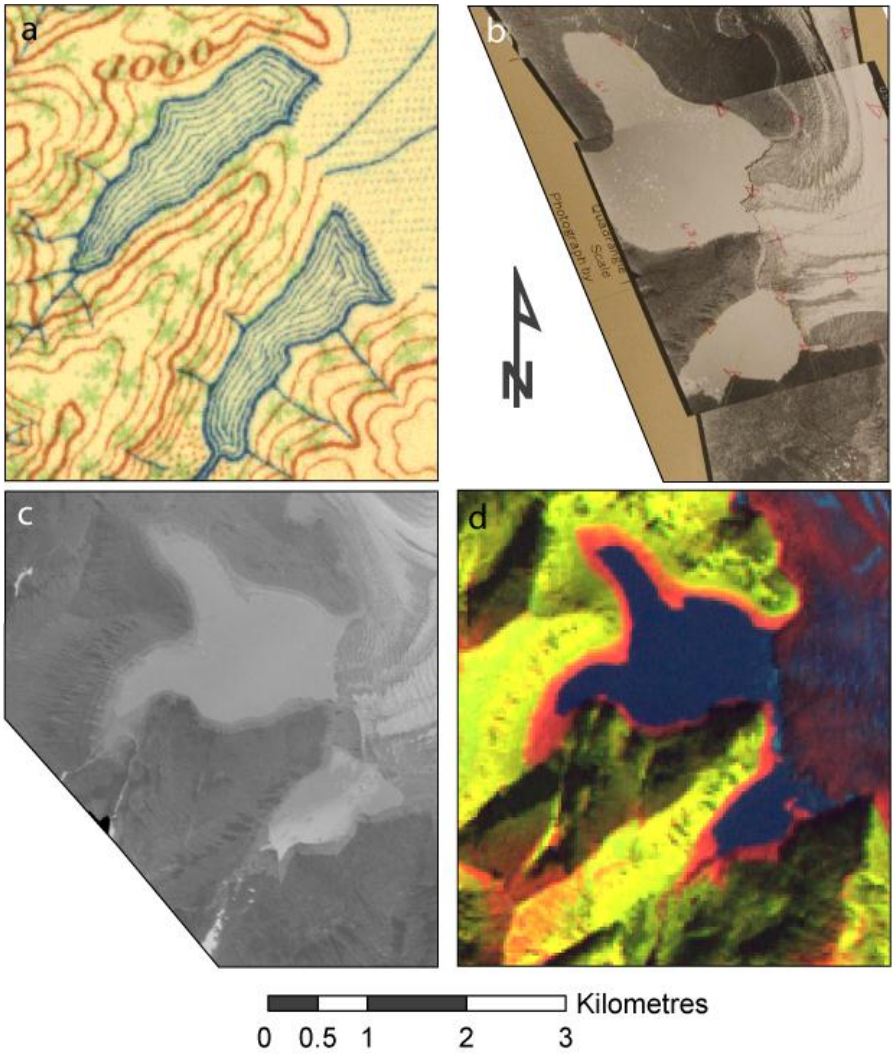

Fig. 4.7. Evolution of the Trick lakes. (a) 1907 International Boundary Commission 1:250,000-scale topographic map; contour interval 250 feet (ca. 75 m). (b) 1929 U.S. Navy airphoto. (c) 1948 U.S. Geological Survey airphoto. (d) False-colour Landsat 5 image (bands 7/4/2) acquired on September 6, 1986.

South Trick Lake. This lake formed a few years after North Trick Lake, but before the glacier reached its maximum extent in ca. 1880 (Bengtson, 1962; Derksen, 1976; Capps et al., 2011). It is shown on the 1907 topographic map, but, like North Trick Lake, its basin is not to true scale (Fig. 4.7a). In the 1929 airphotos, the lake had an area of 0.7 km^2 and was full and overflowing into Annoksek Creek (Fig. 4.5). In the 1948 airphotos, it was lower and not overflowing into Annoksek Creek. At that time, however, it still had an area of 0.7 km^2 because the glacier front

had retreated. By the mid-1980s, the glacier had retreated farther and no longer dammed South Trick or North Trick lakes; the two lakes began to merge into one larger lake that we call East Trick Lake. Based on changes in vegetation evident in Landsat imagery between 1986 and 1990, East Trick Lake no longer achieved an elevation that allowed it to overflow into Annoksek Creek; instead it drained catastrophically onto Brady Glacier's outwash plain. Beginning in the early 2000s, East Trick Lake was no longer dammed to sufficient elevations to be confluent with South Trick Lake. South Trick Lake was left as an isolated 0.2 km^2 moraine-dammed lake. As late as 2009, East Trick Lake occasionally reached a level at which it became confluent with North Trick Lake.

Spur Lake. Spur Lake began to form no later than 1830 and had filled to near its stable outlet at 125 m a.s.l. by ca. 1839 (Capps et al., 2011). Spur Lake had an area of 0.4 km^2 in 1929. By 1948 the area of the lake had increased to 0.8 km^2 through retreat of the calving glacier margin while maintaining the same elevation. With a thick glacier dam and a stable outlet, Spur Lake does not appear to have produced a jökulhlaup until recently. The lake apparently remained full prior to a Landsat image acquired in March 2002, which showed it partially drained. Since then, jökulhlaups have partially drained the lake, the lake has not filled to overflow, and vegetation is becoming established below the highest strandline. Stranded icebergs observed in the basin in 2007 by DMC indicate that jökulhlaups have continued. When at lower levels, a portion of Spur Lake is moraine-dammed (Fig. 4.1). The area of the lake on September 16, 2010, was 0.6 km^2.

Oscar Lake. This lake appears as a small (0.1 km^2) subaerial lake on the 1907 topographic map. It is about the same size on the 1948 topographic map. The lake probably had a much larger subglacial area in 1948, based on the relatively flat surface of the adjacent ice lobe. The very low surface slope of the ice is characteristic of a floating margin. Since 2000, the width of

the calving front and the subaerial area of the lake have increased rapidly due to thinning and breakup of ice evident in Landsat imagery. By 2010, the surface area had increased to 2.6 km^2. The level of the lake has remained constant because it is controlled by a bedrock sill at approximately 200 m a.s.l. Oscar Lake has no known history of jökulhlaups.

Abyss Lake. The area that is now Abyss Lake appears as flat or nearly flat ice on the 1907 topographic map (Fig. 4.8a). The 1948 map shows a 2.6 km^2 subaerial lake dammed by Brady Glacier to the southwest and overflowing across a bedrock sill to the east at 269 m a.s.l. (Fig. 4.8b). The lake has partially emptied most years since 1994, draining subglacially into Oscar Lake and over a bedrock sill into the Oscar Creek drainage, where the floodwaters have caused widespread damage to forest. The 1994 jökulhlaup, which caused the level of Abyss Lake to fall 77 m, released approximately 130 x 10^6 m^3 of water and was the first known flood in the Oscar Creek catchment for at least 80 years based on dendrochronological evidence (Grover, 2003). The elevation of the lake was 39 m lower in 2000 than in 1948, although the former level was measured in February, a time of year when the lake is commonly lower after a summer outburst. Nonetheless, observations during three seasons of fieldwork (2005-2007) and satellite imagery indicate that the lake may no longer fill to a level where it overflows the stable bedrock sill to the east. The width of the calving front in Abyss Lake has increased by almost 40% from 1948 to 2010. The surface area was 2.7 km^2 in 2010, an increase of only 4% from 1948. Although almost 0.4 km^2 of ice has been lost in the Abyss embayment, the westward expansion of the lake has been offset by the fall in lake level and the consequent smaller surface area around its perimeter (Fig. 4.8c). Abyss Lake probably extends far underneath Brady Glacier based on the extensive, flat ice shelf at the margin of the lake.

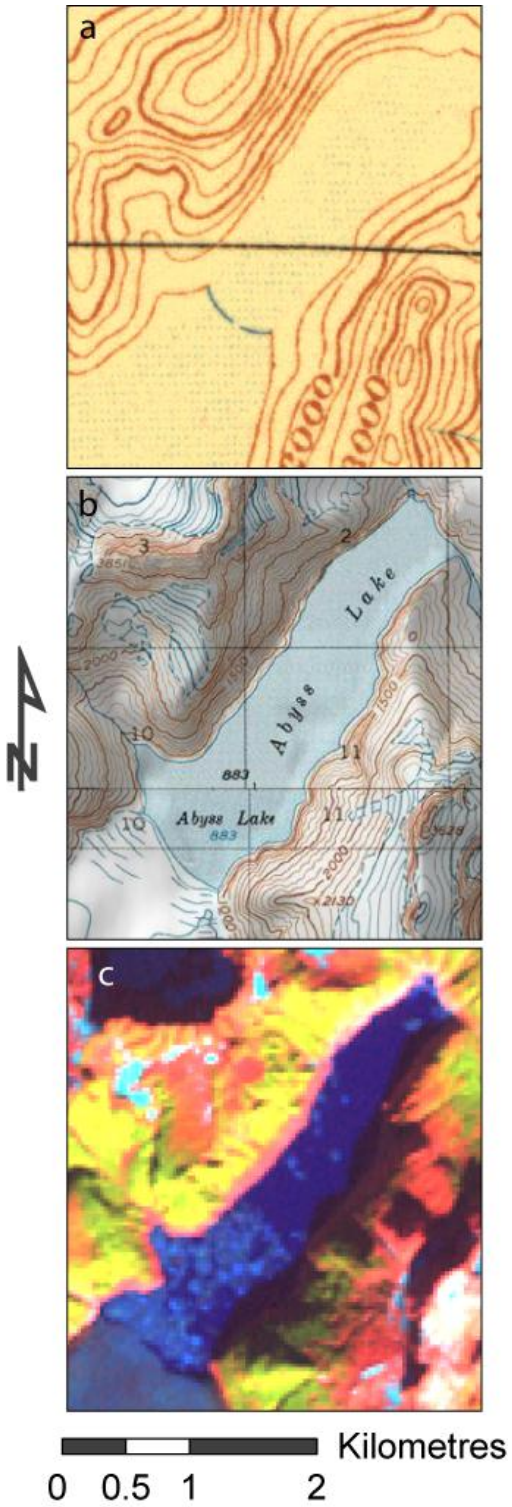

Fig. 4.8. Evolution of Abyss Lake. (a) 1907 International Boundary Commission 1:250,000-scale topographic map; contour interval 250 feet (ca. 75 m). (b) 1948 1:63,360-scale U.S. Geological Survey topopgraphic map; contour interval 100 feet (ca. 30 m). (c) False-colour Landsat 7 ETM+ image (bands 7/4/2) acquired on September 16, 2010.

Capps et al. (2010) identified three subglacial lakes north of Abyss Lake – informally named Saddle, Hinge, and Divide lakes. Only small areas of water are exposed seasonally along the margins of each of these lakes. Saddle Lake is approximately 2.0 km long and 1.6 km wide and has a saddle-shaped perimeter. The lake underlies a distributary lobe that flows eastward before splaying into embayments to the northeast and southeast. The part of the lake in the southeast embayment underlies the distributary lobe and a small tributary glacier flowing to the north. The suture zone between the two glaciers is evidenced by an accumulation of surface debris (Fig. 4.1). Hinge Lake is approximately 4.2 km long, 1.3 km wide, and has a distinctive hinge-like crevasse that runs along the axis of a northeast-trending distributary lobe. The crevasse is likely the result of repeated filling and draining of the lake. Divide Lake is approximately 1.5 km long and 0.5 km wide. It is near the Brady Glacier ice divide below Divide Peak and underlies a northeast-trending distributary glacier. None of the lakes has a known history of jökulhlaups. However, analysis of InSAR data has shown that, from September 1995 to March 1996, Saddle Lake discharged over 300,000 m^3 of water, Hinge Lake over 600,000 m^3, and Divide Lake over 50,000 m^3 (Capps, et al., 2010).

4.4.3 Current bathymetry of select glacier-dammed lakes

We collected sonar depth data (Table 4.3) and created bathymetric maps of Abyss, North Deception, East Trick, Bearhole, and Oscar lakes (Fig. 4.9). Collecting bathymetry data in glacier-dammed lakes can be hazardous and difficult. Lakes drain with little warning and may vary in depth and area from year-to-year. For example, the bathymetry map of Abyss Lake (Fig. 4.9a) represents the depths of the lake when it is full, although the lake was partially drained when we conducted the survey. Icebergs pose additional challenges because they can suddenly roll over and they often block access to large areas of the lake. Due to the low data density, interpolation likely underestimates actual lake volumes. For example, in the bathymetry map of

Bearhole Lake (Fig. 4.9d), the northwest and northeast arms are illustrated as ≤25 m deep. However, no bathymetry data were collected in these parts of the lake, and the interpolation probably underestimates the depths and thus volumes. Therefore, the volume calculations should be considered minimum estimates.

Table 4.3. Interpolated minimum lake volumes.

Lake	Interpolated minimum volume (m^3)
Abyss	3.45×10^8
North Deception	9.5×10^7
East Trick	1.5×10^7
Bearhole	1.3×10^8
Oscar	6.5×10^7

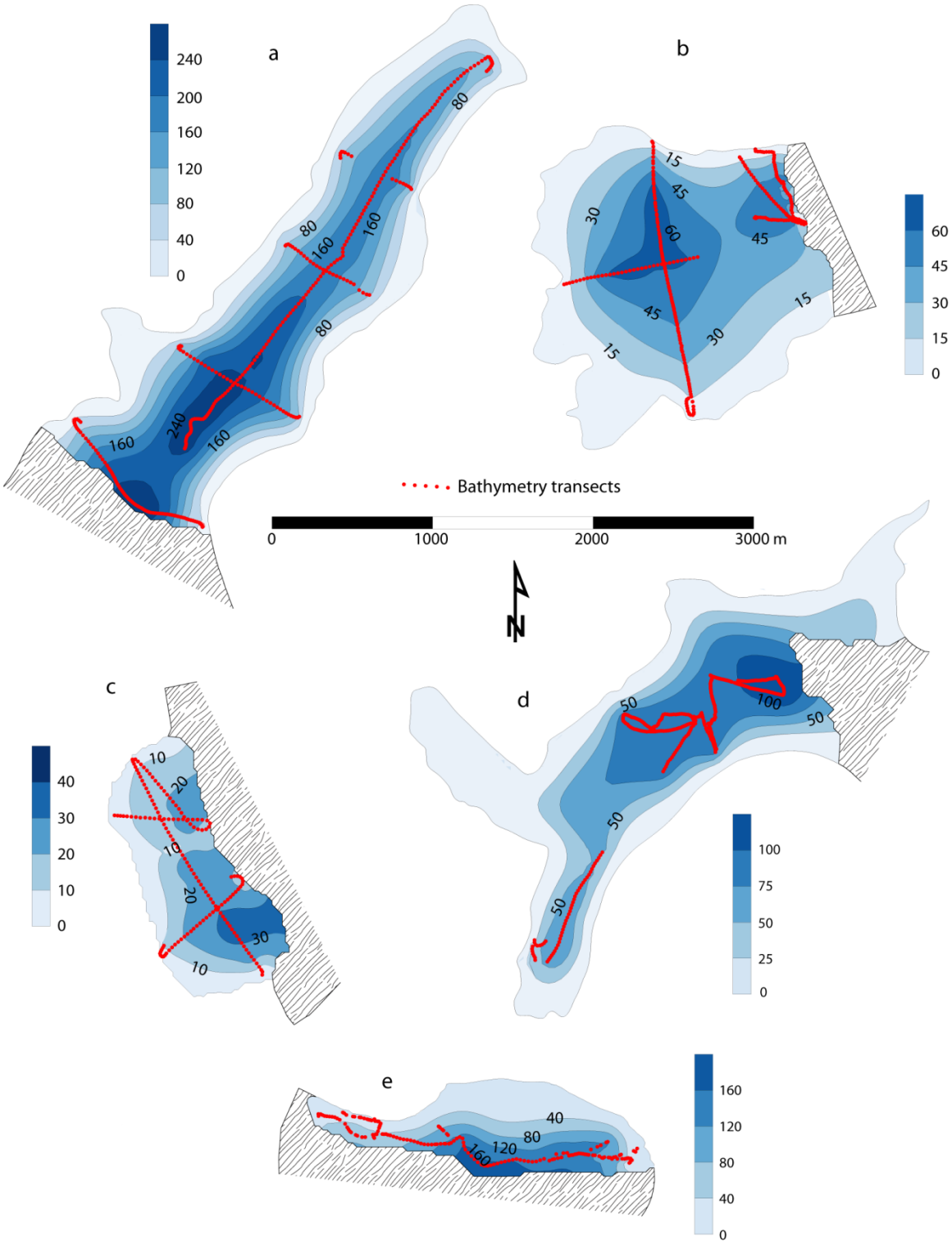

Fig. 4.9. Bathymetric maps of select Brady Glacier lakes. Patterned area is glacier. (a) Abyss Lake when full to overflow, (b) North Deception Lake when full to overflow, (c) East Trick Lake on August 29, 2005, (d) Bearhole Lake when full to overflow, and (e) Oscar Lake on August 8, 2006.

4.5 Discussion

The greatest retreat (2 km) and downwasting (123 m) of Brady Glacier have occurred adjacent to glacier-dammed lakes. In the discussion that follows, we examine the ways in which glacier-dammed lakes can affect glacier retreat and downwasting.

4.5.1 The effect of calving on Brady Glacier

4.5.1.1 Terminal calving

Unlike most glaciers, which are primarily controlled by climate, tidewater glaciers are strongly influenced by the nature of the terminus. When a morainal shoal or a fjord constriction limits mass loss due to calving, a tidewater glacier may remain stable or even advance in a warming climate (Post, 1975; Motyka and Begét, 1996). Contemporary examples from the region include Hubbard and Taku glaciers, which have advanced for at least the last century while most land-terminating glaciers have retreated (Molnia, 2008). However, once a tidewater glacier reaches equilibrium, a perturbation such as a brief climatic change can cause the glacier to retreat from the stabilizing shoal (Figure 4.10). If more mass is lost through calving than is replenished, the glacier catastrophically retreats (Post, 1975). This instability, to a large degree, results from a reversed bed slope behind the shoal.

The activity of tidewater glaciers can be out of phase with climatic cycles, depending on glacier response time. Response time depends on glacier size, geometry, topography, bathymetry, and the magnitude and duration of the disturbance. Many tidewater glaciers are large, so their response times to climate forcing can lag by 100 or more years (Meier and Post, 1987). Although tidewater glaciers constitute less than 0.1% of the total number of glaciers in Alaska (Molnia, 2008), they account for 36% of the total glacier area in the state (Viens, 1995)

and are therefore significant because of their contribution to sea level rise and the large number of icebergs that they discharge.

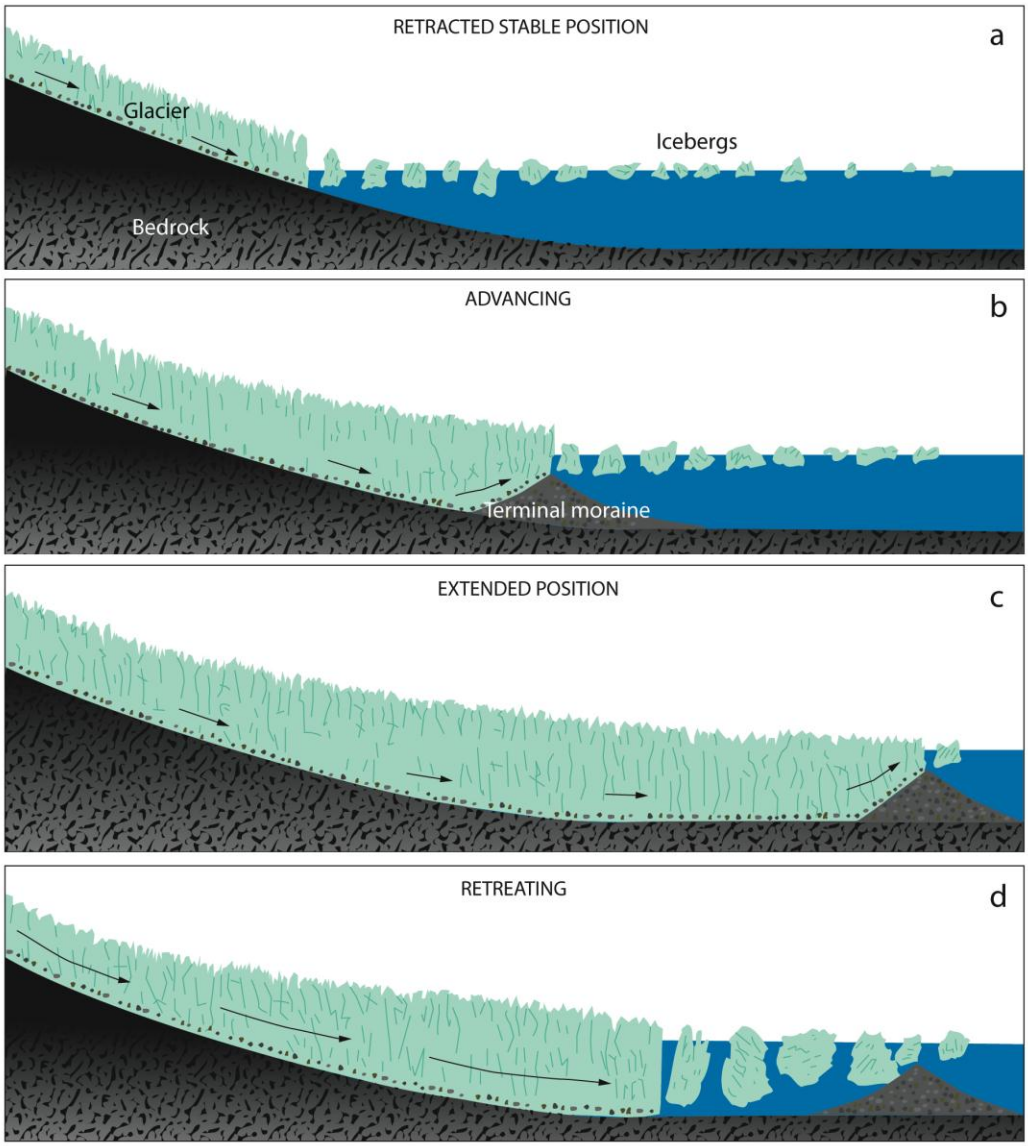

Fig. 4.10. Tidewater glacier cycle (after Trabant et al., 1990; Molnia, 2008). Figures A through D illustrate the four phases of the cycle. (a) Beginning and end of the cycle when the glacier is in a stable position at the head of the fjord. (b) Advancing phase when the glacier pushes the terminal moraine/shoal forward. (c) Glacier at its fully extended phase. (d) Retreat phase with the production of large tabular icebergs.

Studies that provide insight into calving glacier dynamics are particularly important, not only for predicting the amount and rate of sea level rise (Meier et al., 2007) but also the evolution of glacier-dammed lakes. Iceberg calving may account for over 70% of the mass lost from glaciers worldwide, but the uncertainties around this estimate are large (van der Veen, 2002). Even though Brady Glacier currently terminates on land, eight lobes have calving margins longer than 1 km. Tidewater- and lake-calving glaciers account for over 75% of the ice volume loss in southeast Alaska and adjacent northwest British Columbia (Larsen et al., 2007). Rapid wastage of Alaska glaciers accounts for some of the largest measured glaciological contributions to sea level rise (Arendt et al., 2002, Berthier, et al., 2010). Tidewater, former tidewater, and overdeepened glaciers in the region are catastrophically retreating and have downwasted by as much as 640 m between 1948 and 2000 (Larsen et al., 2007).

Brady Glacier is different from most other glaciers in the region in that its terminus has changed little over the past 11 decades in spite of extensive downwasting. If the glacier continues to downwaste, which is likely in the prevailing climate, its terminus must eventually retreat. Brady Glacier is grounded well below sea level, which keeps the terminus in an extended position even though it is actively downwasting. Assuming that other variables do not change, downwasting causes a decrease in effective pressure at the bed. A decrease in effective pressure can cause a glacier to flow faster (Meier and Post, 1987). Alternatively, Brady Glacier may have maintained a constant velocity with a reduced surface slope, while maintaining an extended terminus.

Brady Glacier is beginning to retreat in sensitive areas, evidenced by small lakes that are beginning to form around the perimeter of the main terminus. If these small lakes grow in size, they may eventually coalesce with enlarging East Trick Lake 3 km to the north and become large enough to return the main terminus of the glacier to a calving regime. The removal of back-

pressure due to calving at the ice front can also cause an increase in velocity, which may initiate a positive feedback cycle (Meier and Post, 1987). If the glacier returned to a calving regimen, it would retreat until the terminus stabilized in shallower water. Adjacent Glacier Bay is the site of the greatest documented glacier retreat in history; the tidewater glacier there retreated over 100 km in 155 years until it stabilized in shallow water (Molnia, 2008). Catastrophic retreat is currently in progress at Columbia Glacier and is projected to continue until it encounters shallower water 32 km upstream from the pre-retreat terminus, or another 15 km beyond its 2005 terminus (O'Neel et al., 2005). As Brady Glacier begins to retreat, its outwash plain will act as a stabilizer by confining icebergs in a small area, which will slow the calving process (van der Veen, 2002). Through time, however, this effect will diminish as the terminal lake grows larger and the outwash plain possibly is eroded.

4.5.1.2 Glacier-dammed-lake calving margins

Glacier-dammed lake margins, like tidewater margins, are major foci of ice loss. The areas of Brady Glacier that have experienced the greatest downwasting and retreat over the past 130 years are adjacent to glacier-dammed lakes. If other factors are constant, an increase in calving width will cause an increase in mass loss. In 1948, the large lakes described in this study had a combined calving width of 11.5 km; by 2010, the width had increased to 18.3 km. Two of the lakes with the greatest increases in size and associated downwasting and retreat, Dixon and North Deception lakes, had geometries that made their margins prone to collapse. Both lake basins are circular and deepen towards the main lobe of the glacier, which make them susceptible to positive feedback cycling. As more ice calved, the calving margin grew longer, which, in turn, facilitated further calving. We know the bathymetry of North Deception Lake from SONAR data and the generalized bathymetry of Dixon Lake from aerial observations when it was partially drained (Fig. 4.11). As the calving margins retreated into deeper water, larger

icebergs calved, which facilitated further mass loss. These properties combined to contribute to the large downwasting and retreat at Dixon and North Deception lakes.

Fig. 4.11. Dixon Lake partially drained during a jökulhlaup in August 2007. The lake is approximately 2.3 km long.

Although the geometries of other lakes dammed by Brady Glacier were not as favourable for collapse, enhanced downwasting occurred at all lakes. We know from field observations and satellite imagery (Fig. 4.1) that North Trick, South Trick, and Spur lakes had substantial subaqueous moraines that were built where the glacier margin was stable for an extended period. Once the glacier margin retreated from these moraines, ice loss increased because

thicker blocks of ice could calve in the deeper water. Divide Lake experienced the least downwasting, probably because it did not have a calving margin like the other lakes.

Glacier-dammed lakes can cause large amounts of ice-mass loss by calving. Many glacier-dammed lakes have a floating ice tongue that collapses when the lake begins to drain (Marcus, 1960; Mayer et al., 2008). Jökulhlaups at Tulsequah Lake and Lake No Lake, both of which are dammed by Tulsequah Glacier in northwestern British Columbia, generated so much calved ice that the water was obscured (Marcus, 1960; Geertsema and Clague, 2005). The senior author observed this phenomenon during the 2007 draining of Dixon Lake. In previous days the lake had large areas that were iceberg-free. As the lake drained and the floating ice tongue was no longer supported, the basin became choked with icebergs (Fig. 4.11). After an ice tongue fragments in such a scenario, the ice melts faster and is more readily transported out of the lake during a jökulhlaup, thus removing mass more rapidly from the glacier. This process is repeated each time the lake drains and refills as long as a floating tongue reforms.

4.5.2 Possible jökulhlaup effects on the stability of Brady Glacier

A large jökulhlaup or series of jökulhlaups could erode Brady Glacier's terminus and the adjacent outwash plain. Russell et al. (2006) noted that mechanical break-up of glacier ice is one of the most distinctive effects of jökulhlaups. Processes that could impact Brady Glacier include: (1) large-scale tunnel collapse; (2) hydraulic jacking along the glacier margin and surface; and (3) undercutting of the margin, causing ice-cliff collapse. A catastrophic jökulhlaup from the combined Abyss-Oscar lake system poses the greatest risk to the stability of the main terminus of Brady Glacier. We know from past jökulhlaups that Abyss Lake is hydraulically connected to Oscar Lake through a subglacial conduit or conduits. Even after Abyss Lake has drained into Oscar Lake, as it has in past years, it contains at least 2.1×10^8 m^3 of water. Oscar Lake contains

at least 9.5 x 10^7 m^3 of water based on limited bathymetry data collected along the margin of the subaerial lake that existed in 2006. The subaerial portion of the lake has expanded rapidly since then, and the lake likely extends a substantial distance underneath the glacier. If Oscar Lake drained to the terminus, Abyss Lake would almost certainly drain with it. The combined volume of the two lakes would be at least 3.2 x 10^8 m^3, but the actual value is probably closer to 1.0 x 10^9 m^3 or 1.0 km^3 of water or more based on the underestimation of the interpolation and an estimation of the volume of water that we were unable to account for underneath the floating ice shelves. A jökulhlaup of this size would mechanically erode ice from the terminus by large-scale tunnel collapse, hydraulic jacking, ice-cliff collapse, and other processes.

Russell (2006) also noted that jökulhlaups can incise and extend outwash plains. Stream power and therefore erosion potential are greatest where the jökulhlaup exits the glacier. After a large jökulhlaup, subsequent ones will be more channelized, further focusing stream power and potentially causing more extensive erosion (Russell, 2006). The amount of erosion or deposition at any one location is controlled by slope, discharge, and sediment availability. On the Brady Glacier outwash plain, slope is known and discharge can be estimated, but subglacial sediment availability and potential jökulhlaup routing are unknown. Therefore, we cannot predict the location or magnitude of erosion or deposition at and away from the terminus. Nevertheless, a combined jökulhlaup from Abyss and Oscar lakes could incise the stabilizing outwash plain adjacent to the terminus and cause the glacier to lose contact with it. Repeated events could trigger a return to a tidewater regimen.

4.5.3 Space as a proxy for time

Kastens and Ishikawa (2006) state that *"... it is fairly common in thinking about the Earth to find that variation or progression through space is closely connected with variation or*

progression though time." As a result we often think about distance in space instead of duration of geologic time. Data displayed in a spatial dimension can be used as a visual analogy to reveal or emphasize causal relationships. For example, the greater the distance away from a mid-ocean ridge spreading center, the greater the time since formation of that strip of seafloor (Kastens and Ishikawa, 2006).

An example of substituting space for time at Brady Glacier comes from using the evolution of South Trick Lake, the lake nearest the terminus and lowest in elevation, to illustrate how lakes higher on Brady Glacier may respond if the glacier continues to downwaste or begins to retreat. We have described how South Trick Lake was dammed by the advancing glacier, released jökulhlaups for decades, then eventually was no longer dammed by the glacier as it downwasted and retreated. Clague and Evans (1994) identified that many glacier-dammed lakes go through a similar cycle of jökulhlaup activity as their glacier dams weaken due to downwasting and retreat. A critical threshold is reached when the glacier can no longer impound the lake and a cycle of jökulhlaups begins. With continued downwasting or retreat, the frequency of jökulhlaups may increase, but the magnitude decreases until eventually the water establishes a permanent outlet and jökulhlaups cease. Using knowledge of the jökulhlaup cycle learned from previous behaviour of Brady and similar glacier systems, we can predict how lakes more distant from the terminus and higher in elevation will evolve through time.

The clearest example of applying the concept of space as a proxy for time in understanding the evolution of Brady Glacier's lakes is the four subglacial lakes. Based on the results of this study and the conclusions reached by Capps et al. (2010), these lakes will become increasingly subaerial if Brady Glacier continues to downwaste and retreat, especially as the calving fronts increase in width and depth, thereby creating a positive feedback cycle for more ice loss. Oscar Lake recently began a rapid subaerial expansion. We expect this expansion to continue until the

calving margin retreats to where the lobe of ice flowing into the basin narrows and lateral shear stress provides sufficient drag to once again stabilize the calving margin. Depending on where this stable location is, the retreat could destabilize ice that dams the lake and trigger the first jökulhlaup of record. Saddle and Hinge lakes will likely begin to release jökulhlaups several years after, with Divide Lake beginning last because it is the farthest from the terminus and highest in elevation. As previously noted in the results, Abyss Lake has also undergone a similar transformation from a floating margin that covered a subglacial lake in 1907, to a largely subaerial lake by the time the first airphotos were taken in 1948, and then began releasing damaging jökulhlaups in 1994. The four subglacial lakes will likely parallel Abyss Lake's evolution from subglacial and relatively stable to subaerial with catastrophic outbursts.

Geertsema and Clague (2005) documented an example of this type of evolution with Lake No Lake dammed by Tulsequah Glacier in northwest British Columbia. In 1948 airphotos there is no subaerial Lake No Lake, but a glacier ramp drops to a floating margin that covered a subglacial lake. This geometry and setting are similar to that of the subglacial lakes described here. By 1974, a substantial subaerial lake had developed and it continues to grow in area. In 1991 the lake began a cycle of jökulhlaups. The volume of water discharged from Lake No Lake remains large, but, with continued glacier downwasting and retreat, the lake and its floods will decrease in volume much like adjacent Tulsequah Lake has through time (Geertsema and Clague, 2005).

4.5.4 Evolution of analogous glacier/lake systems

4.5.4.1 Past

There are analogous glacier and lake systems that have evolved in much the same manner that we predict for Brady Glacier. An excellent example is the evolution of Excelsior Glacier and

Excelsior Lake in the Kenai Mountains of southern Alaska. In 1913, Excelsior Glacier terminated on an outwash plain about 1 km from Johnstone Bay. In 1941 Excelsior Lake was in the initial stages of development 8 km north-northeast of its 1913 terminus (Fig. 4.12a; Stone, 1963). The debris-covered ice visible on a 1941 airphoto is likely a suture zone between west-flowing ice from tributary glaciers to the east and east-flowing ice from a distributary of Excelsior Glacier. Also visible in this photo, as indicated by the arrows, are two areas of subaerial lake exposure. By 1951, the terminus of the glacier had retreated as much as 4.3 km into a terminal lake, the area of Excelsior Lake itself had expanded dramatically, and Excelsior Lake had drained (Fig. 4.12b). Excelsior Lake grew to fill most of its potential tributary basin by the 1960s (Fig. 4.12c; Marcus, 1968) and is now an embayment in the rapidly enlarging terminal lake (Fig. 4.12d). We do not know if jökulhlaups from the lake contributed to the breakup of the terminus of the glacier, but the calving dynamics at Excelsior Lake certainly contributed to enhanced breakup of the glacier evident in Figure 4.12d.

The geometry of the Excelsior Lake basin is similar to that of the Abyss and Hinge lake basins. In particular, the state of Excelsior Lake in 1941 is similar to the present state of Hinge Lake, which also has small subaerial lakes like those shown in Figure 4.12a. Abyss and Hinge lakes and Brady Glacier may go through an evolution similar to that of Excelsior Lake and Excelsior Glacier.

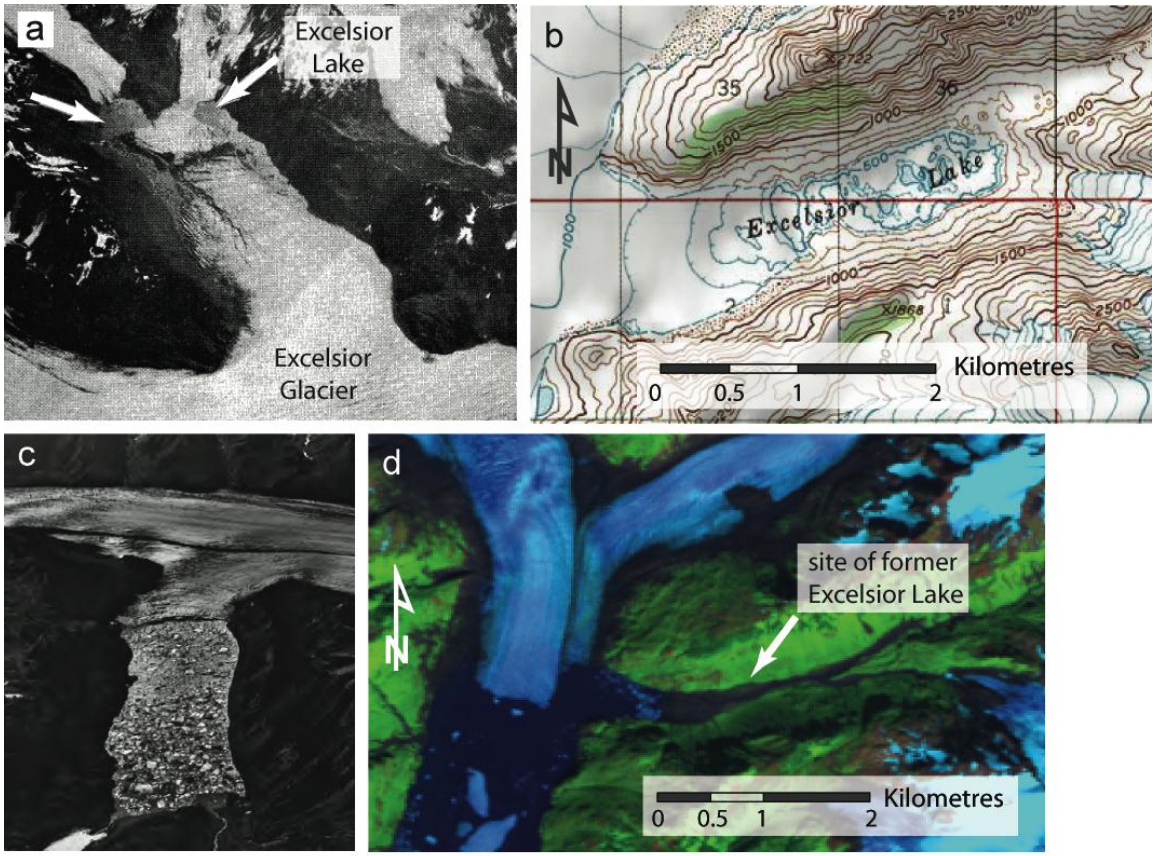

Fig. 4.12. Evolution of Excelsior Glacier and Excelsior Lake through time. (a) August 15, 1941 oblique airphoto of Excelsior Glacier, view east. Arrows indicate two areas of subaerial lake water (from Stone, 1963). (b) 1951 U.S. Geological Survey 1:63,360 topographic map of Excelsior Lake, contour interval 100 feet (ca. 30 m). (c) September 3, 1966, oblique airphotos of Excelsior Lake, view west (after Molnia, 2008). (d) August 3, 2009 false-colour Landsat 5 image (bands 7/4/2).

4.5.4.2 Future

There are analogous glacier and lake systems that may experience an evolution comparable to that at Excelsior Glacier and to that we predict for Brady Glacier. An example is Baird Glacier and a series of lakes that it dams near Petersburg, Alaska (Fig. 4.13). Baird Glacier currently terminates against a 2-km-long outwash plain about 10 m above Thomas Bay. The glacier downwasted substantially between 1948 and 2000 (Larsen et al., 2007). It presently impounds large volumes of water in the Witches Cauldron, a tributary in which there has been a 9.5-km reversal of ice flow. We infer that jökulhlaups have occurred from a lake at the head of this

tributary based on observations of stranded icebergs in previous Landsat imagery (Fig. 4.13). If Baird Glacier continues to downwaste, glacier-dammed lakes in the Witches Cauldron and other tributaries will grow in size and number and the terminus may retreat off the stabilizing outwash plain. Abandonment of the outwash plain could trigger a catastrophic retreat because Baird Glacier, like Brady Glacier, is grounded well below sea level.

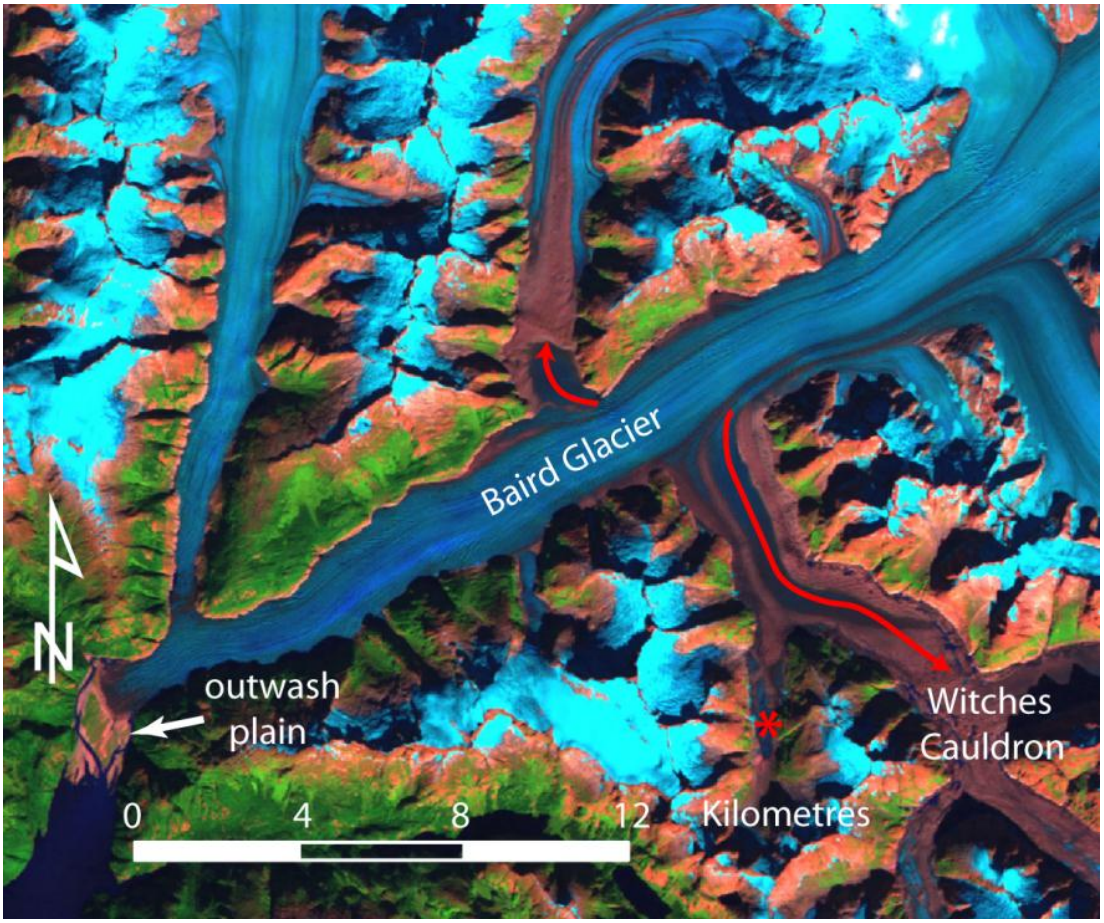

Fig. 4.13. False-colour Landsat 5 image (bands 7/4/2) of Baird Glacier acquired on September 19, 2010. Note substantial flow reversals (red arrows), source of past jökulhlaups (red asterisk), outwash plain, and tidewater near southwest edge of image.

There are numerous other examples of glacier-dammed lakes and their associated jökulhlaups that are likely to play a key role in the evolution of glaciers. Examples are the Dead Branch of Norris Glacier near Juneau, which has a conspicuous crevasse along its centre line

similar to that at Hinge Lake, Tulsequah Glacier near Juneau, a series of glaciers that dam lakes in the Desolation Valley north of Lituya Bay, and Battle Glacier near Alsek River.

4.6 Conclusion

Despite small advances and retreats, the main terminus of Brady Glacier has changed little since 1880. However, it has downwasted substantially, more than the regional average of 2-3 m/yr, between 1948 and 2000. The most dramatic retreat (2 km) and downwasting (123 m) have occurred adjacent to glacier-dammed lakes. Retreat and downwasting are primarily the result of calving into ten large glacier-dammed lakes. Between 1948 and 2010, the combined calving width of the glacier-dammed lakes increased from 11.5 km to 18.3 km. Calving margins of glacier-dammed lakes share several similarities with tidewater glacier calving margins. Bathymetry surveys revealed that some lakes contain at least 3.45×10^8 m^3 of water, and jökulhlaups from one or more lakes could have a significant influence on the terminus of the glacier. After tidewater glaciers reach equilibrium, a perturbation such as a climatic change can thin the glacier so that it no longer is grounded on the stabilizing shoal, triggering more mass loss through calving than is replenished. The glacier may then catastrophically retreat. Brady Glacier is a former tidewater glacier with many glacier-dammed lakes that are contributing to mass loss. Eventually, Brady Glacier will return to a tidewater regimen and enter into a phase of catastrophic retreat. The situation at Brady Glacier is not unique, and the lessons learned here can be applied elsewhere to identify future glacier-dammed lakes, jökulhlaups, and glacier instability.

5. SUMMARY

5.1 Synthesis

The late Holocene history of Brady Glacier had been the subject of debate. The glacier retreated at least 24 km north of its present terminus by 645-725 cal yr BP, but began to advance shortly thereafter based on radiocarbon ages from subfossil wood in till (Bengtson, 1962; Derksen, 1976). Recorded historical observations date back to 1794, but fluctuations in the glacier terminus and inconsistent identification of landforms and reference points complicate interpretation of these early observations.

Recent downwasting and retreat of Brady Glacier has exposed subfossil wood along the glacier margins and at two glacier-dammed lakes. Research that constituted one module of this dissertation determined the timing of the nineteenth-century advance of Brady Glacier and the evolution of Spur and North Deception lakes using precise elevation-constrained mapping and dendrochronology. I developed a floating tree-ring chronology and cross-dated it with master chronologies from the Glacier Bay region. The resulting chronology spans the period from AD 1370 to 1861. The data confirm that the study sites were not occupied by the glacier or lakes for at least 450 years prior to 1830. Spur Lake was impounded by the advancing glacier no later than 1830 and had filled to an elevation of approximately 121 m a.s.l. by 1839. The glacier continued to advance, reaching a site about 1.4 km farther south by 1844, and dammed North Trick Lake another 1.1 km down valley by 1861. Brady Glacier continued to advance for many more years, but the exact timing of this phase of the advance could not be determined from the subfossil wood sampled in this study because it was too decomposed for reliable dating.

However, other dendrochronology research indicates that the glacier continued to advance until 1880 (Bengtson, 1962; Derksen, 1976).

This study better constrains the time of Brady Glacier's advance and margin fluctuations since AD 1370 and settles previous debate about the location of the glacier margin during recorded history. Previous researchers have used dendrochronology to date glacier advances and the formation of glacier-dammed lakes, but this study is the first to combine precise, elevation-constrained mapping and dendrogeomorphology.

The terminus of Brady Glacier has remained within several hundred metres of its present position since 1880. Although the terminus has maintained its position, the glacier downwasted 2-3 m/yr between 1948 and 2000, which is more than the regional average (Larsen et al., 2007). The most dramatic change, however, has occurred in the numerous distributary lobes, where terminal retreat of 2 km or more and downwasting up to 123 m have occurred adjacent to glacier-dammed lakes. The retreat and downwasting are primarily the result of calving into ten large glacier-dammed lakes. Glacier-dammed lake calving margins share several similarities with tidewater glacier calving margins. Once a tidewater glacier reaches equilibrium, a perturbation can thin the glacier so that it no longer is grounded on the stabilizing shoal, triggering the loss of more mass through calving than is replenished. The glacier will then enter a phase of catastrophic retreat (Post, 1975). Both types of calving margins induce large amounts of ice loss that can contribute to or cause catastrophic retreat. Adjacent Glacier Bay is the site of the greatest documented glacier retreat in history; the tidewater glacier there retreated over 100 km in 155 years (Molnia, 2008). Brady Glacier is a former tidewater glacier. Eventually, as the glacier continues to downwaste and retreat, it will return to a tidewater regimen and begin a phase of catastrophic retreat.

In preliminary studies for this dissertation, I noted what appeared to be three previously unidentified subglacial lakes at the northeast margin of Brady Glacier. To map and characterize these suspected subglacial lakes, I developed an InSAR technique that isolated vertical displacements of the overlying ice using ERS-1/-2 tandem imagery. Citing several different sources of supporting evidence, I assumed that horizontal displacement in the dead end distributary valleys is negligible. This simplifying assumption allowed me to quantify vertical displacement and displacement volumes using single interferograms instead of more complicated calculations that involve two interferograms. All interferograms in this study indicate that the lake surfaces are subsiding, but at different rates. Discharge rates are highest in late September, slow dramatically during winter, and continue at lower rates through March. I would expect inflation of the lake surfaces during the ablation season, but unfortunately tandem imagery was not available for the early summer months. The technique used in this study is particularly valuable because it allows researchers to locate subglacial lakes that might otherwise go undetected. Previous researchers have made substantial progress in remotely identifying and characterizing glacier-dammed lakes in other settings, however I developed the first technique applicable to alpine subglacial lakes. Subglacial lakes can significantly influence glacier dynamics and may begin to drain catastrophically years or decades from now, thus use of this technique may allow time to mitigate the risk from jökulhlaups.

I designed and custom-built a remote-controlled boat to collect bathymetric and GSP data in a range of conditions (Fig. 5.1). Bathymetric surveys on glacier-dammed lakes are difficult because the lakes may drain rapidly, usually contain large icebergs, and are generally difficult to access. Because of these difficulties and safety issues, the bathymetry of very few glacier-dammed lakes is known. I used the remote-controlled boat in areas that were too dangerous or too small to access with a floatplane. To build the boat, I first chose a fibreglass shell with the

appropriate amount of flotation to support the necessary equipment and the capability of surviving a roll if upset by a rotating iceberg or calving glacier. Second, I mounted a 12-volt battery in the bottom to keep the centre of gravity as low as possible, so that the boat would right itself if it turned over. The battery powered the electric motor/propeller and GPS-enabled sonar that recorded data to a memory card that I downloaded after the survey. The boat was controlled by a standard RC transmitter and receiver. Finally, I painted the 85 cm boat safety orange and affixed a removable flag on a mast to assist in locating it at long distances.

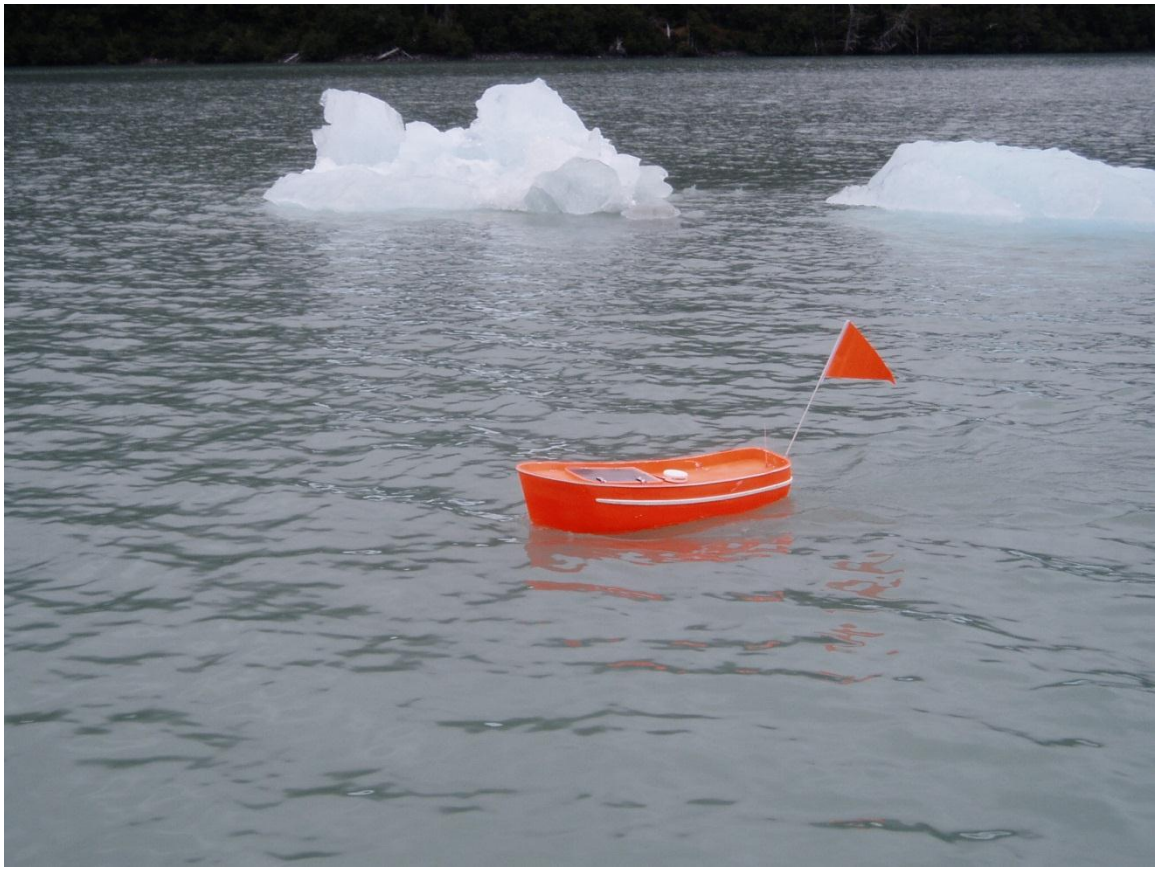

Fig. 5.1. Custom-built, GPS-enabled, remote-controlled boat (85 cm long).

5.2 Future Work

Downwasting and retreat of Brady Glacier are continually exposing new subfossil wood that is suitable for dendrochronology, thus providing an opportunity to further date the history of

the glacier. The wood, however, decays rapidly once it is exposed to the atmosphere. Decayed wood is difficult to impossible to date, therefore the glacier margins should be revisited and sampled at regular intervals in the future to provide a more comprehensive history of the glacier. It is possible that Bearhole, Oscar, or Abyss lakes may also contain rooted subfossil wood similar to that found in North Deception and Spur lakes. If so, the evolution of these lakes could be determined once they enter the jökulhlaup cycle and begin to drain.

Precise elevation-constrained mapping and dendrochronology can easily be applied in other glacierized areas to determine the timing of glacier advances and the evolution of glacier-dammed lakes. The technique is useful in areas where the only dateable subfossil wood may be on the fjord walls. The technique can be applied in lakes of all types to determine the date of formation and rate of filling, if sufficient number of in-situ subfossil tree stems exists over a range of elevations.

The InSAR technique that I developed to identify and characterize alpine subglacial lakes could also be applied to other glacierized areas. Imagery acquired during the ERS-1/-2 tandem mission covers much of the alpine glacierized terrain of the world, and next-generation InSAR sensors with sufficiently short temporal baselines could extend the usefulness of the technique well into the future.

There are numerous locations on Brady Glacier where ice-penetrating radar (IPR) surveys could provide a wealth of information about the thickness of the glacier that would aid in interpreting glacier and lake processes. These data could be used to infer the depth of subglacial lakes, determine volumes of water beneath floating ice tongues, locate ice dams, and determine glacier thickness in critical areas such as the terminus. I successfully deployed a Sensors & Software pulseEKKO 100 ground penetrating radar with a 50 MHz antennae on Divide, Hinge,

and Saddle lakes. The ice on the lakes, however, was thicker than the equipment was able to image – greater than 225 m. In future surveys, lower frequency antennae and higher power transmitters should be used to increase the depth of useful data.

Glacier-dammed lakes may store large amounts of water underneath the floating ice tongue of the damming glacier. An ice-penetrating radar survey of a floating ice tongue could determine the subglacial topography and aid in at least a first-order estimation of subglacial water volumes. More precise volumes cannot be calculated without bathymetry data. A complimentary or alternative method would be side-scan sonar survey performed in the lake perpendicular to the floating ice tongue, which would allow accurate volume calculations.

IPR could also be used to determine the stability of the ice dam at Oscar Lake. By determining where the glacier effectively seals the lake and how much downwasting or recession would be necessary to destabilize the lake, one might be able to predict when the lake would enter the jökulhlaup cycle and release large jökulhlaups that could destabilize the terminus and cause catastrophic glacier retreat. However, uncertainties in this evaluation would be large, allowing only a first-order approximation.

Lastly, IPR could be used to determine ice thickness in critical areas such as the terminus of Brady Glacier. This information is required to predict the future evolution of the glacier. If the terminus is several hundred metres thick, it will likely remain stable for decades. If it is tens of metres thick, however, it may begin to retreat rapidly in the near future.

Glacier Bay National Park natural resources managers or U.S. Geological Survey Alaska hydrology personnel could easily add the georeferenced materials in this dissertation to their GIS databases and update them with new georeferenced Landsat imagery as it becomes

available. Cursory monitoring of the imagery could provide insight into the evolution of the glacier and its lakes and potentially warn managers of developing hazardous situations.

Brady Glacier presents numerous opportunities for interesting modelling results. Relatively simple modelling exercises could: 1) estimate glacier thickness in the main and tributary lobes using assumed bed shear stresses; 2) estimate subglacial discharge routing from both subglacial and subaerial lakes; and 3) estimate the discharge from potential future jökulhlaups.

Brady Glacier and the lakes that it dams are dynamic features. The research I conducted for this dissertation only captured part of a continually unfolding story. The glacier-dammed lakes will continue to progress through the different stages of the jökulhlaup cycle and will play a pivotal role in the evolution of the glacier. In the coming years, perhaps decades, Brady Glacier will return to a tidewater regimen and retreat catastrophically until it stabilizes in shallower water. The stabilizing position is unknown because the subglacial topography is largely undetermined; however, it will likely be many tens of kilometres upglacier of the present terminus.

6. REFERENCES

Alho, P., Baker, V.R., Smith, L.R., 2010. Paleohydraulic reconstruction of the largest Glacial Lake Missoula draining(s). *Quaternary Sci. Rev*. 29 (23-24), 3067-3078.

Anderson, R.S., Walder, J.S., Anderson, S.P., Trabant, D.C., Fountain, A.G., 2005. The dynamic response of Kennicott Glacier, Alaska, USA, to the Hidden Creek Lake outburst flood. *Ann. Glaciol.,* 40 (1), 237-242.

Arendt, A.A., Echelmeyer, K.A., Harrison, W.D., Lingle, C.S., Valentine, V.B., 2002. Rapid wastage of Alaska glaciers and their contribution to rising sea level. *Science* 297 (5580), 382-86.

Barclay, D.J., Wiles, G.C., Calkin, P.E., 2009. Holocene glacier fluctuations in Alaska. *Quaternary Sci. Rev*., 28 (21-22), 2034-2048.

Barclay, D.J., Wiles, G.C., Calkin, P.E., 2009b. Tree-ring crossdates for a First Millennium AD advance of Tebenkof Glacier, southern Alaska. *Quaternary Res.* 71 (1), 22–26.

Barnes, D.F., Watts, R.D., 1977. Geophysical surveys in Glacier Bay National Monument. *US Geol. Surv. Circ.* 751-B.

Bengtson, K.B., 1962. Recent history of the Brady Glacier, Glacier Bay National Monument, Alaska, U.S.A. *Inter. Assoc. Sci. Hydr., Inter. Union Geodesy Geophys., Symp. Obergurgl*, 58, 78-87.

Berthier, E., Schiefer, E., Clarke, G.K., Menounos, B., Rémy, F., 2010. Contribution of Alaskan glaciers to sea-level rise derived from satellite imagery. *Nature Geosci.* 3, 92-95.

Blachut, S.P., Ballantyne, C.K., 1976. Ice-dammed lakes: A critical review of their nature and behaviour. *McMaster Univ. Dep. Geogr. Disc. Pap. 6*.

Bolch, T., Buchroithner, M.F., Peters, J., Baessler, M., Bajracharya, S., 2008. Identification of glacier motion and potentially dangerous glacial lakes in the Mt. Everest region/Nepal using spaceborne imagery. *Nat. Hazard Earth Systems,* 8 (6), 1329-1340.

Capps, D.M., Rabus, B., Clague, J.J., Shugar, D.H., 2010. Identification and characterization of alpine subglacial lakes using interferometric synthetic aperture radar (InSAR): Brady Glacier, Alaska, USA. *J. Glaciol.* 56 (199), 861-870.

Capps, D.M., Wiles, G.C., Clague, J.J., Luckman, B.H., 2011. Tree-ring dating of the nineteenth-century advance of Brady Glacier and the evolution of two ice-marginal lakes, Alaska. *Holocene*. 21 (4), 641-649.

Clague, J.J., Shilts, W.W., 1993 Two landslide-dammed lakes in the Cascade Mountains, southwestern British Columbia. In: *Current Research*, Part E. Geological Survey of Canada, Paper 93–1E, 47–54.

Clague, J.J., Evans, S.G., 1994. Formation and failure of natural dams in the Canadian Cordillera. *Geol. Surv. Can. Bull.* 464.

Clarke, G.K., 1982. Glacier outburst floods from “Hazard Lake”, Yukon Territory, and the problem of flood magnitude prediction. *J. Glaciol.* 28 (98), 3-21.

Connor, C., Streveler, G., Post, A., Monteith, D., Howell, W., 2009 The Neoglacial landscape and human history of Glacier Bay, Glacier Bay National Park and Preserve, southeast Alaska, USA. *Holocene* 19, 381-93.

Costa, J.E., Schuster, R.L., 1988. The formation and failure of natural dams. *Geol. Soc. Am. Bull.* 100 (7), 1054-1068.

Costantini, M., 1998. A novel phase unwrapping method based on network programming. *IEEE Trans. Geosci. Remote Sensing*., 36 (3), 813-821.

Davidson, G., 1904 The glaciers of Alaska that are shown on Russian charts or mentioned in older narratives. *Geographic Society of the Pacific Transactions and Proceedings* Series II, Volume 3.

Derksen, S.J., 1976. Glacial geology of the Brady Glacier region, Alaska. *Inst. Polar Studies Rep.* 60.

Fatland, D.R., Lingle, C.S., 2002. InSAR observations of the 1993-95 Bering Glacier (Alaska, U.S.A.) surge and a surge hypothesis. J. Glaciol., 48 (162), 439-451.

Fatland, D.R., Lingle, C.S., Truffer, M., 2003. A surface motion survey of Black Rapids Glacier, Alaska, U.S.A. *Ann. Glaciol.*, 36, 29-36.

Frey, H., Haeberli, W., Linsbauer, A., Huggel, C., Paul, F., 2010. A multi-level strategy for anticipating future glacier lake formation and associated hazard potentials. *Nat. Hazards Earth Syst. Sci.* 10 (2), 339-352.

Geertsema, M., Clague, J.J., 2005. Jökulhlaups at Tulsequah Glacier, northwestern British Columbia, Canada. *Holocene,* 15 (2), 310-316.

Grissino-Mayer, H.D., 2001. Evaluating crossdating accuracy: a manual and tutorial for the computer program COFECHA. *Tree-Ring Res.* 57, 205-21.

Grover, J.S., 2003. An investigation of glacier outburst floods from Abyss Lake, Glacier Bay National Park, Alaska. *Nat. Park Serv., Nat. Res. Water Res. Div., Nat. Res. Tech. Report* 312.

Hodgson, D.A., Roberts, S.J., Bentley, M.J., Smith, J.A., Johnson, J.S., Verleyen, E., Vyverman, W., Hodson, A.J., Leng, M.J., Cziferský, A., Fox , A.J., Sanderson, D.C.W., 2009. Exploring former subglacial Hodgson Lake, Antarctica Paper I: Site description, geomorphology and limnology. *Quaternary Sci. Rev*., 28 (23-24), 2295-2309.

Holmes, R.L., 1983. Computer-assisted quality control in tree-ring dating and measurement. *Tree-Ring Bull.* 43, 69-78.

Huggel, C., Kääb, A., Haeberli, W., Teysseire, P., Paul, F., 2002. Remote sensing based assessment of hazards from glacier lake outbursts: A case study in the Swiss Alps. *Can. Geotech. J.,* 39 (2), 316-330.

Hughes, M.L., McDowell, P.F., Marcus, W.A., 2006. Accuracy assessment of georectified aerial photographs: implications for measuring lateral channel movement in a GIS. *Geomorphology* 74 (1-4), 1-16.

International Boundary Commission, 1923. Alaska Boundary Tribunal Map Series (1907): #10 from Cape Muzon to Mount St. Elias. *Intern. Boundary Comm*., Ottawa, ON, scale 1:250,000.

Joughin, I.R., Winebrenner, D., Fahnestock, M., Kwok , R., Krabill, W., 1996. Measurement of ice-sheet topography using satellite-radar-interferometry. *J. Glaciol.*, 42 (140), 10-22.

Joughin, I.R., Kwok , R., Fahnestock, M.A., 1998. Interferometric estimation of three-dimensional ice-flow using ascending and descending passes. *IEEE Trans. Geosci. Remote Sensing,* 36 (1), 25-37.

Kääb, A., Wessels, R., Haeberli, W., Huggel, C., Kargel, J., Khalsa, S., 2003. Rapid ASTER imaging facilitates timely assessment of glacier hazards and disasters. *Eos* 84 (13), 117, 121.

Kargel, J., Abrams, M., Bishop, M., Bush, A., Hamilton, G., Jiskoot, H., Kääb, A., Kieffer, H., Lee, E., Paul, F., Rau, F., Raup, B., Shroder, J., Soltesz, D., Stainforth, D., Stearns, L., Wessels, R., 2005. Multispectral imaging contributions to global land ice measurements from space. *Remote Sens. Environ.* 99, 187 – 219.

Kastens, K.A., Ishikawa, T., 2006. Spatial thinking in the geosciences and cognitive sciences: A cross-disciplinary look at the intersection of the two fields. In: Manduca, C.A., Mogk, D.W. (Eds.), Earth and Mind: How Geologists Think and Learn about the Earth. *Geol. Soc. Am. Special Paper* 413, 53-76.

Klotz, O.J., 1899. Notes on glaciers of southeastern Alaska and adjoining territory. *Geogr. J.,* 14 (5), 523-534.

Larsen, C.F., Motyka, R.J., Freymueller, J.T., Echelmeyer, K.A., Ivins, E.R., 2005. Rapid viscoelastic uplift in southeast Alaska caused by post-Little Ice Age glacier retreat. *Earth Planet. Sc. Lett.* 237, 548–60.

Larsen, C.F., Motyka, R.J., Arendt, A.A., Echelmeyer, K.A., Geissler, P.E., 2007. Glacier changes in southeast Alaska and northwest British Columbia and contribution to sea level rise. *J. Geophys. Res.,* 112 (F01007), 1-11.

Lawrence, D.B., 1950. Estimating dates of recent glacier advances and recession rates by studying tree growth layers. *Trans. Am. Geophys. Union* 31, 243–48.

Lawson, D., Wiles, G., Conkey, L., Finnegan, D., 2006. A dendroclimatic record of paleoclimate of the last 10,000 years, Glacier Bay National Park and Preserve: Progress understanding climate change in southeast Alaska. Annual Report 2006 to National Park Service, 33 pp.

Liestøl, O., 1955. Glacier-dammed lakes in Norway. Norsk Geogr. Tidsskr, 15 (3-4), 122-149.

Lingle, C.S., Fatland, D.R., 2003. Does englacial water storage drive temperate glacier surges? *Ann. Glaciol.*, 36 (1), 14-20.

Luckman, B.H., 1995. Calendar-dated, early Little Ice Age glacier advance at Robson Glacier, British Columbia, Canada. *Holocene* 5, 149-159.

Magnússon, E., Björnsson, H., Rott, H., Pálsson, F., 2010. Reduced glacier sliding caused by persistent drainage from a subglacial lake. *Cryosphere*, 4 (2), 13-20.

Marcus, M.G., 1960. Periodic drainage of glacier-dammed Tulsequah Lake, British Columbia. *Geog. Rev.* 50 (1), 89-106.

Marcus, M.G., 1968. Effects on glacier-dammed lakes in the Chugach and Kenai Mountains. In National Research Council. Division of Earth Sciences. Committee on the Alaska Earthquake. *The great Alaska earthquake; hydrology.* Part A. Washington, D.C., National Academy of Sciences, 329-347.

Masiokas, M.H., Luckman, B.H., Villalba, R., Ripalta, A., , Rabassa, J., 2010. Little Ice Age fluctuations of Glaciar Río Manso in the north Patagonian Andes of Argentina. *Quaternary Res.* 73, 96-106.

Mason, K., Gunn, J.P., Todd, H.J., 1930. The Shyok flood, 1929. *Himalayan J.,* 2, 35-47.

Mayer, C., Lambrecht, A., Hagg, W., Helm, A., Scharrer, K., 2008. Post-drainage ice dam response at Lake Merzbacher, Inylchek Glacier, Kyrgyzstan. *Geogr. Ann.* 90A (1), 87–96.

Meier, M.F., Post, A., 1987. Fast tidewater glaciers. *J. Geophys. Res.* 92 (B9), 9051-9058.

Meier, M.F., Dyurgerov, M.B., Rick, U.K., O'Neel, S., Pfeffer, W.T., Anderson, R.S., Anderson, S.P., Glazovsky, A.F., 2007. Glaciers dominate eustatic sea-level rise in the 21st century. *Science* 317 (5841), 1064–1067.

Mohr, J.J., Madsen, S.N., 2001. Geometric calibration of ERS satellite SAR images. *IEEE Trans. Geosci. Remote Sensing.,* 39 (4), 842-850.

Molnia, B.F., 2008. Satellite image atlas of glaciers of the world; glaciers of North America; glaciers of Alaska. *US Geol. Surv. Prof. Pap.* 1386-K.

Motyka, R.J., Begét, J.E., 1996. Taku Glacier, southeast Alaska, U.S.A.: late Holocene history of a tidewater glacier. *Arctic Alpine Res.* 28 (1), 42-51.

Muir, J., 1915. *Travels in Alaska.* New York, Houghton Mifflin Company.

National Park Service. 2009. U.S. National Park Service, "Glacier Bay National Park." In http://www.nps.gov/glba/planyourvisit/upload/GLBA_map-2.pdf.

Nye, J.F., 1976. Water flow in glaciers: Jökulhlaups, tunnels and veins*. J. Glaciol.* 17 (76), 181–207.

O'Neel, S., Pfeffer, W.T., Krimmel, R., Meier, M., 2005. Evolving force balance at Columbia Glacier, Alaska, during its rapid retreat. *J. Geophys.* Res. 110 (F3), 1-18.

Pojar, J., , MacKinnon, A., 1994. Plants *of the Pacific Northwest Coast: Washington, Oregon, British Columbia, and Alaska*. Vancouver, BC, Lone Pine Publishing.

Popov, S.V., Masolov, V.N., 2007. Forty-seven new subglacial lakes in the 0-110 degrees E sector of east Antarctica. *J. Glaciol.,* 53 (181), 289-297.

Post, A., 1975. Preliminary hydrography and historic terminal changes of Columbia Glacier, Alaska. *US Geol. Surv. Hydrol. Invest. Atlas* HA-559.

Post, A., Mayo, L.R., 1971. Glacier dammed lakes and outburst floods in Alaska. *US Geol. Surv. Hydrol. Invest. Atlas* HA-455.

Post, A., Motyka, R.J., 1995. Taku and Le Conte glaciers, Alaska: calving-speed control of late-Holocene asynchronous advances and retreats. *Phys. Geogr.* 16, 59-82.

Rabus, B.T., Fatland, D.R., 2000. Comparison of SAR-interferometric and surveyed velocities on a mountain glacier: Black Rapids Glacier, Alaska, U.S.A. *J. Glaciol.,* 46 (152), 119-128.

Rabus, B.T., Lang, O., 2000. Ice motion and topography in the Siachen Glacier area, Central Kashmir, derived with an operational processing system for INSAR-DEMs. *Proc. Fringe '99: Advancing ERS SAR Interferometry from Applications towards Operations,* Liege, Belgium, p. 10-12.

Rabus, B., Eineder, M., Roth, A., Bamler, R., 2003. The shuttle radar topography mission - A new class of digital elevation models acquired by spaceborne radar. *J. Photogrammetry Remote Sensing.,* 57 (4), 241-262.

Reeh, N., Mohr, J.J., Madsen, S.N., Oerter , H., Gundestrup, N.S., 2003. Three-dimensional surface velocities of Storstrømmen Glacier, Greenland, derived from radar interferometry and ice-sounding radar measurements. *J. Glaciol.,* 49 (165), 201-209.

Ridley, J.K., Cudlip, W., Laxon, S.W., 1993. Identification of subglacial lakes using ERS-1 radar altimeter. *J. Glaciol.,* 39 (133), 625-634.

Russell, A.J., Roberts, M.J., Fay, H., Marren, P.M., Cassidy, N.J., Tweed, F.S., Harris, T., 2006. Icelandic jökulhlaup impacts: Implications for ice-sheet hydrology, sediment transfer and geomorphology. *Geomorphology* 75 (1-2), 33-64.

Scharrer, K., Malservisi, R., Mayer, C., Spieler, O., Münzer, U., 2007. Combination of SAR remote sensing and GIS for monitoring subglacial volcanic activity – recent results from Vatnajökull ice cap (Iceland). Nat. Hazards Earth Syst. Sci., 7 (6), 717-722.

Siegert, M.J., 2000. Antarctic subglacial lakes. Earth-Sci. Rev., 50 (1-2), 29-50.

Stokes, M.A., Smiley, T.L., 1968. *An introduction to tree-ring dating*. Chicago, Illinois, University of Chicago Press.

Sugiyama, S., Bauder, A., Weiss, P., Funk, M., 2007. Reversal of ice motion during the outburst of a glacier-dammed lake on Gornergletscher, Switzerland. *J. Glaciol.* 1 (181), 75-84.

Tebenkof, M.D., 1981. *Atlas of the northwest coasts of America: From Bering Strait to Cape Corrientes and the Aleutian Islands with several sheets on the northeast coast of Asia*. Kingston, Ontario, Limestone Press.

Thorarinsson, S., 1939. The ice-dammed lakes of Iceland, with particular reference to their value as indicators of glacier oscillations. *Geogr. Ann.* 21A, 216–42.

Trenberth, K.E., Jones, P.D., Ambenje, P., Bojariu, R., Easterling, D., Klein Tank, A., Parker, D., Rahimzadeh, F., Renwick, J.A., Rusticucci, M., Soden, B., Zhai, P., 2007. Observations: Surface and Atmospheric Climate Change. In: Climate Change 2007: The Physical Science Basis. Contribution of Working Group I to the Fourth Assessment Report of the Intergovernmental Panel on Climate Change [Solomon, S., D. Qin, M. Manning, Z. Chen, M. Marquis, K.B. Averyt, M. Tignor and H.L. Miller (eds.)]. Cambridge University Press, Cambridge, United Kingdom and New York, NY, USA.

Tweed, F.S., Russell, A.J., 1999. Controls on the formation and sudden drainage of glacier-impounded lakes: Implications for jökulhlaup characteristics. Progr. Phys. Geog., 23 (1), 79-110.

van der Veen, C.J., 2002. Calving glaciers. *Prog. Phys. Geog.* 26 (1), 96-122.

Vancouver, G., 1984. In: Lamb, W.K. (Ed.), *A Voyage of Discovery to the North Pacific Ocean and Round the World, 1791-1795.* London, Hakluyt Society.

Viens, R.J., 1995. Dynamics and mass balance of temperate tidewater calving glaciers of southern Alaska. M.S. dissertation, University of Washington, Seattle, WA, 149 p.

Walder, J.S., Costa, J.E., 1996. Outburst floods from glacier-dammed lakes; the effect of mode of lake drainage on flood magnitude. Earth Surf. Proc. Landforms, 21 (8), 701-723.

Wessels, R., Kargel, J., Kieffer, H., 2002. ASTER measurement of supraglacial lakes in the MountEverest region of the Himalaya. *Ann. Glaciol.* 34, 399-408.

Wiles, G.C., Barclay, D.J., Calkin, P.E., 1999. Tree-ring dated 'Little Ice Age' histories of maritime glaciers from western Prince William Sound, Alaska. *Holocene* 9, 163-73.

Young, S.H., 1915. *Alaska days with John Muir*. New York, Fleming H. Revell Company.

APPENDICES

Appendix A. Additional interferograms

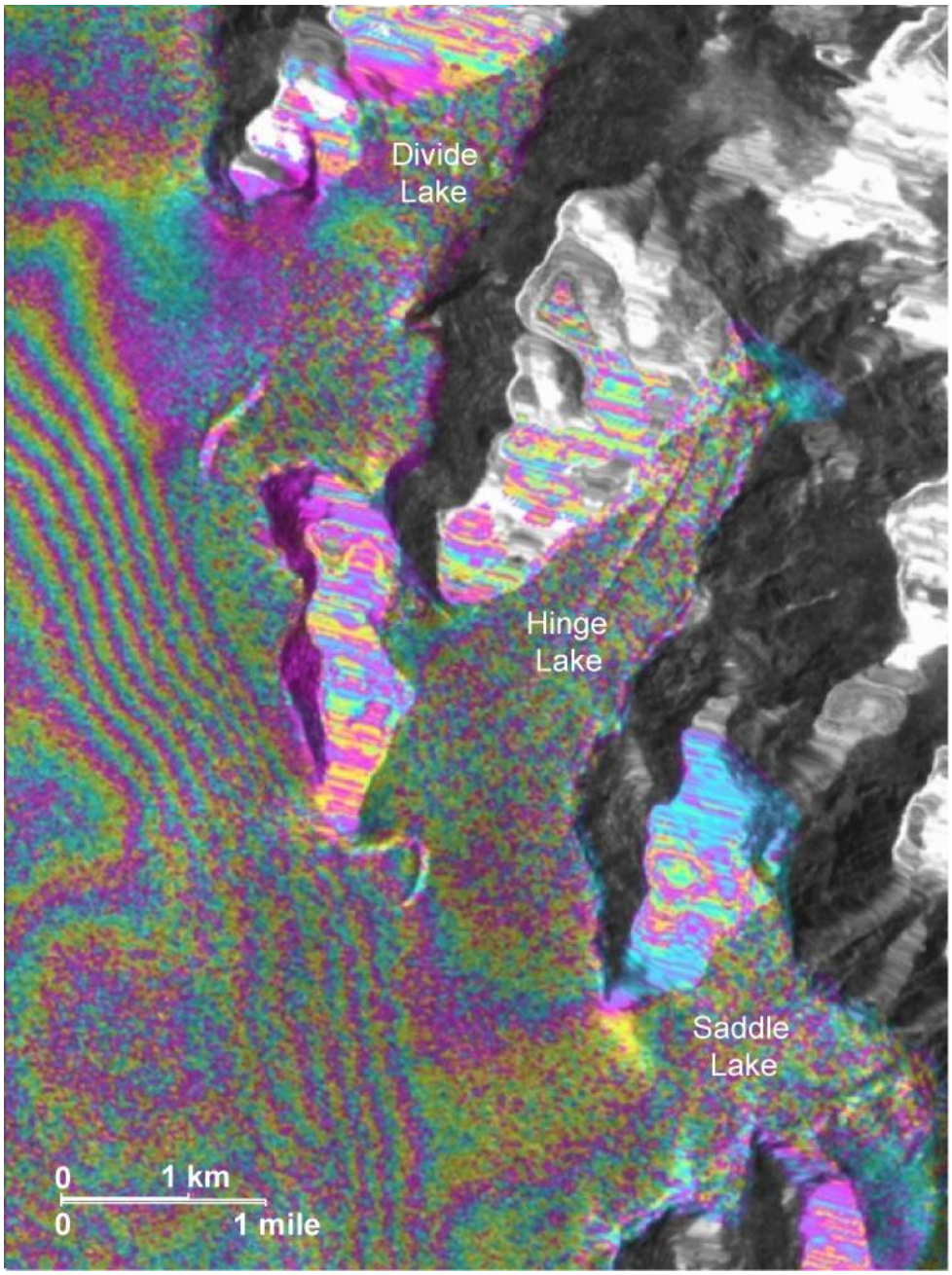

11 to 12 September 1995

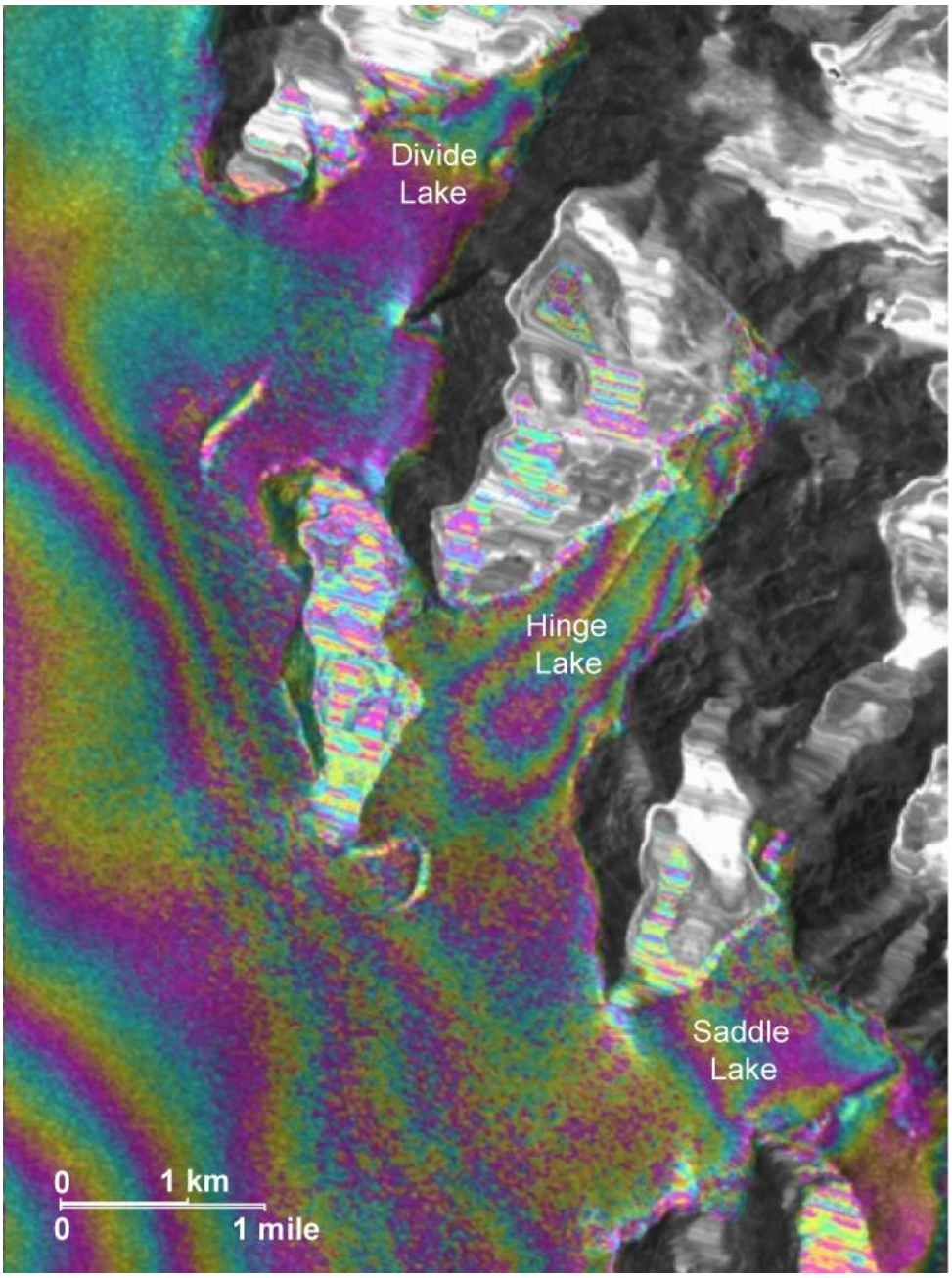

30 September to 1 October 1995

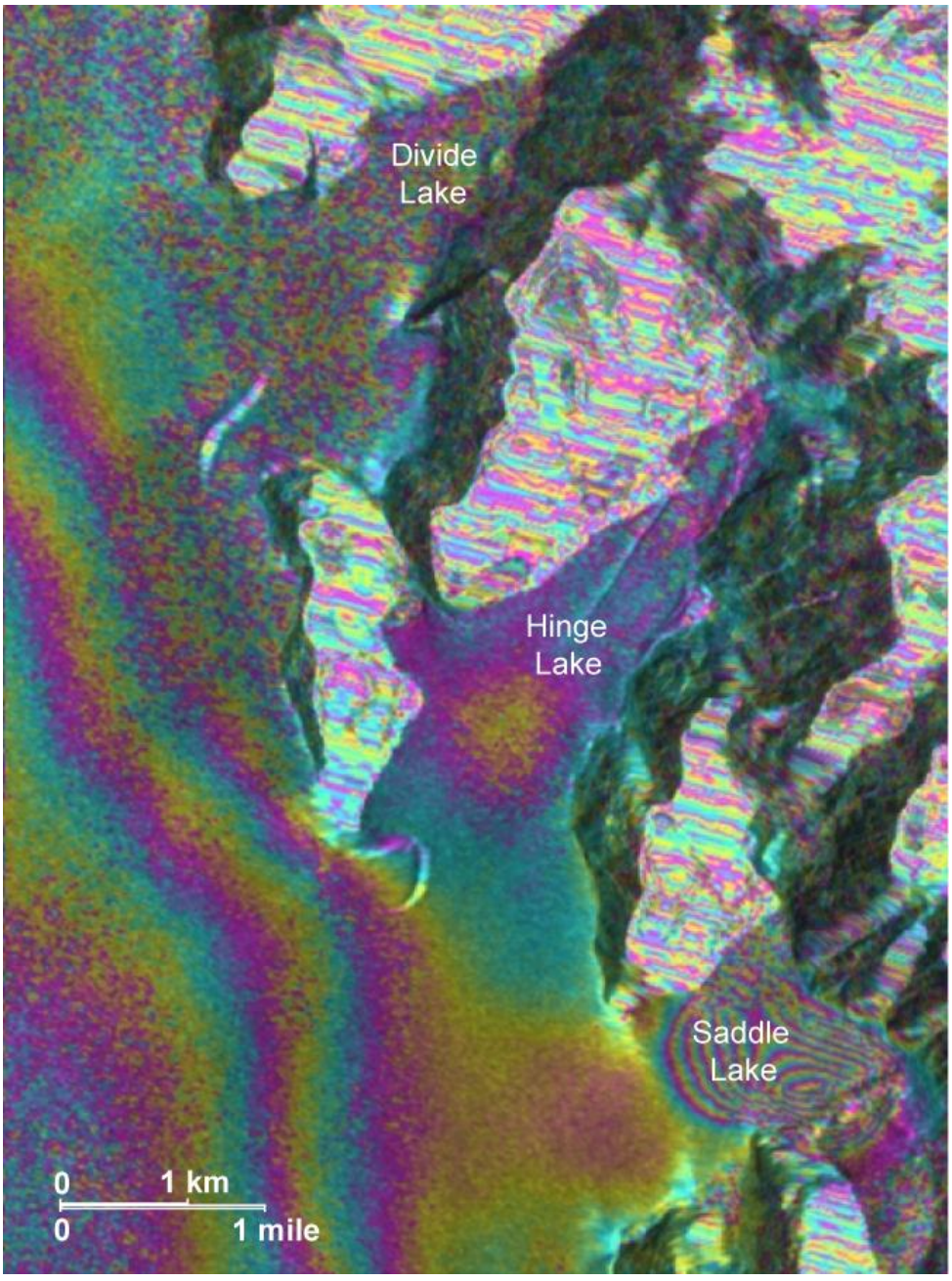

4 to 5 November 1995

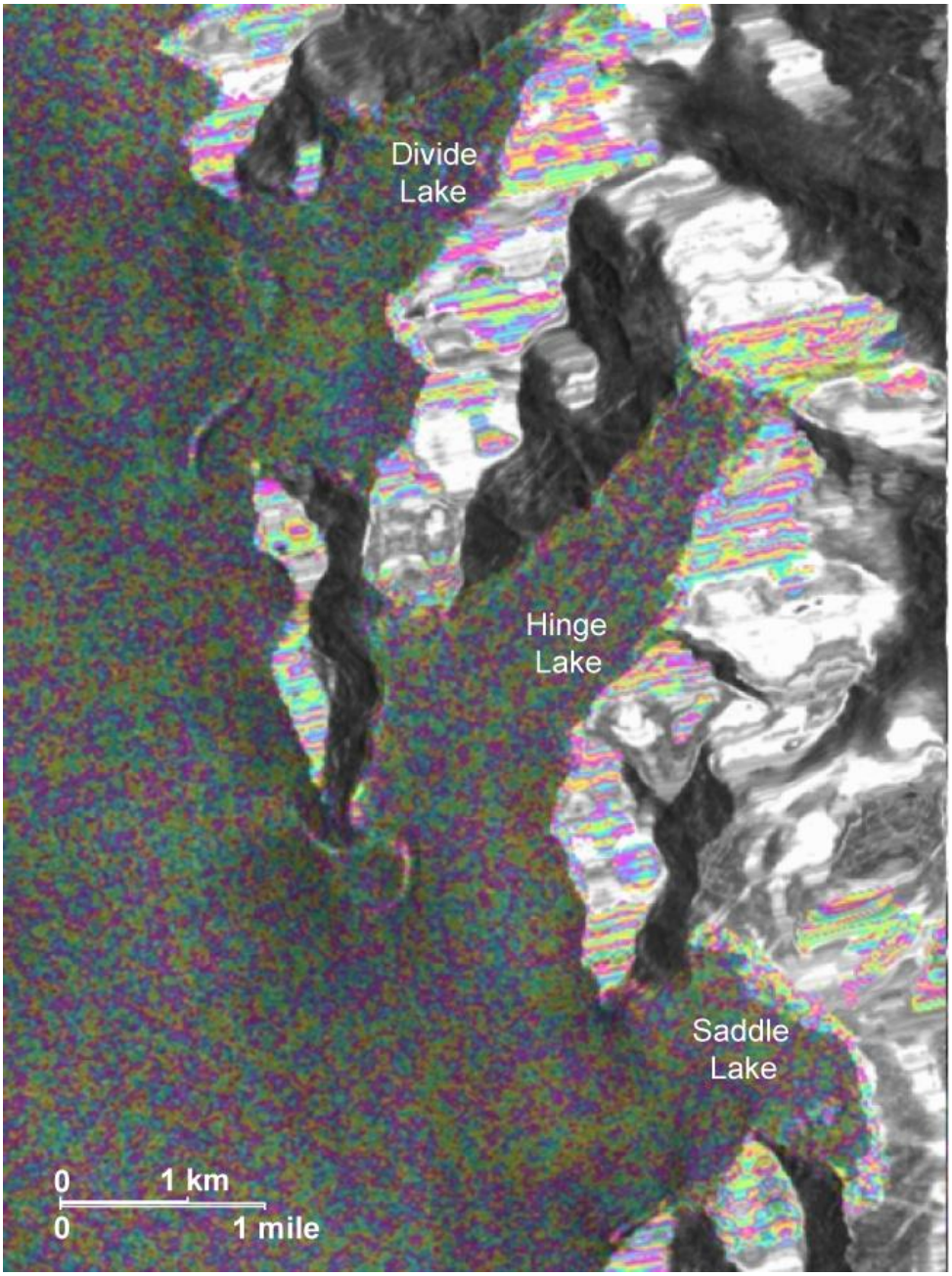

12 to 13 November 1995

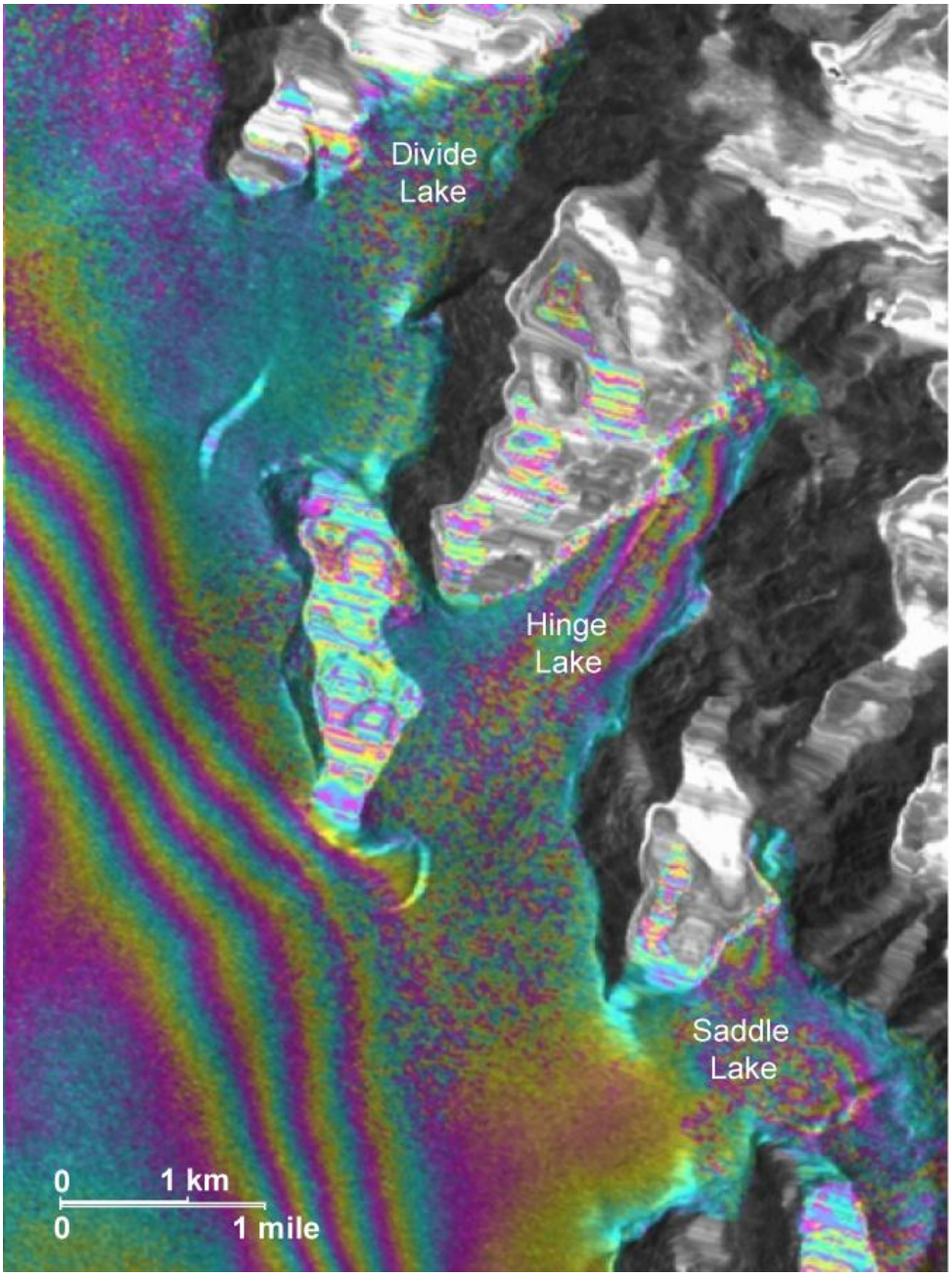

13 to 14 January 1996

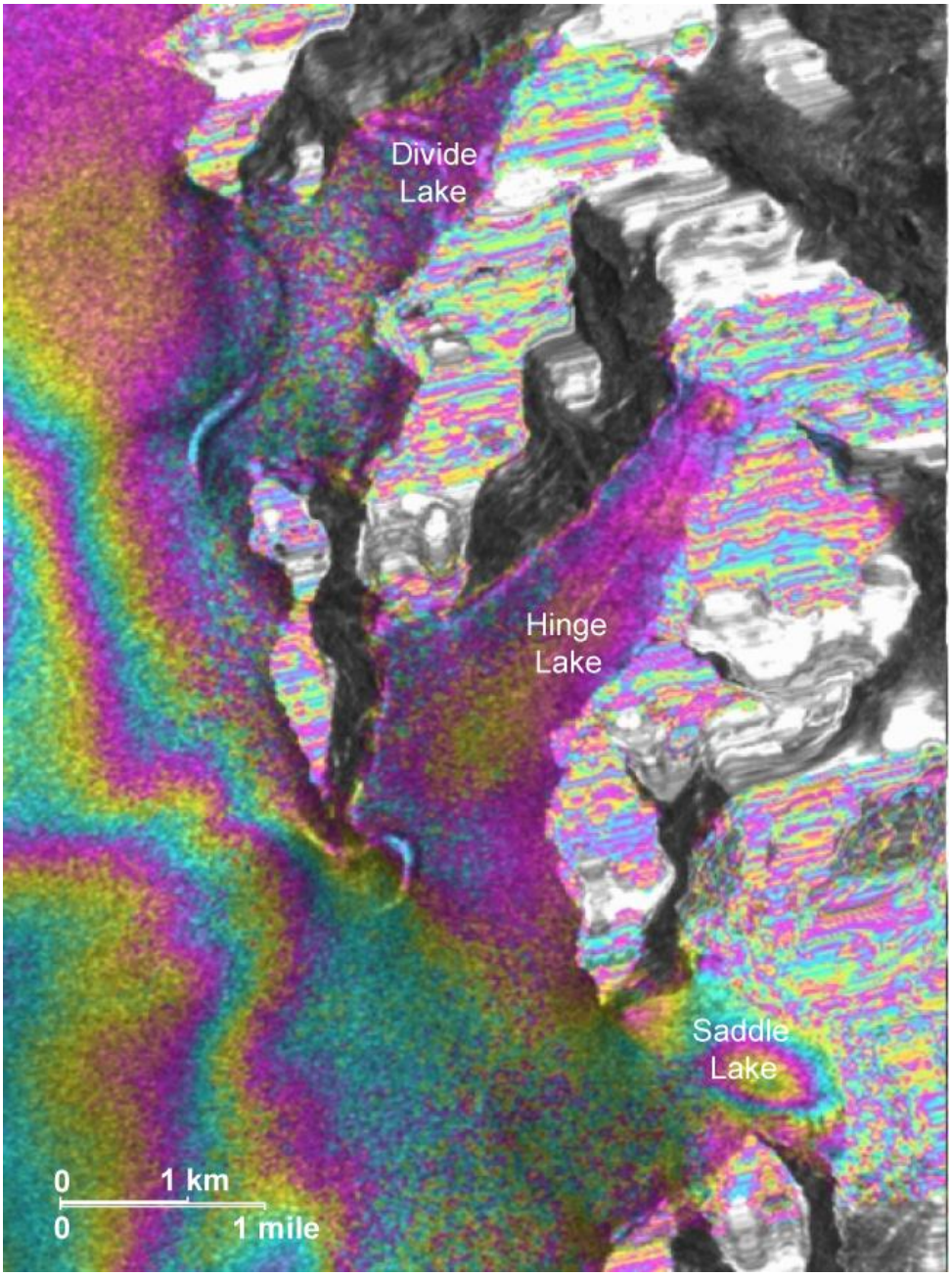

3 to 4 March 1996

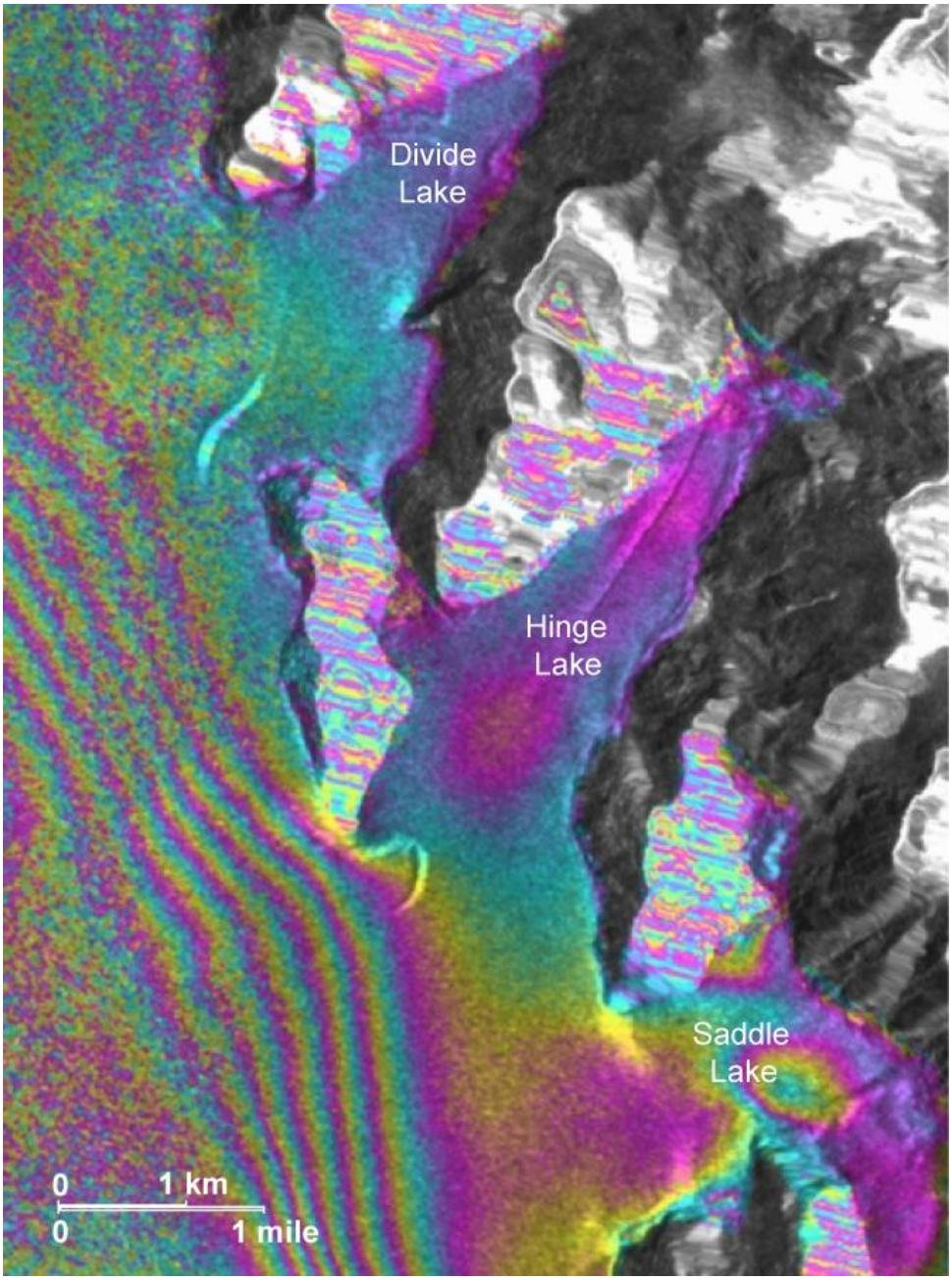

4 to 5 March 1996

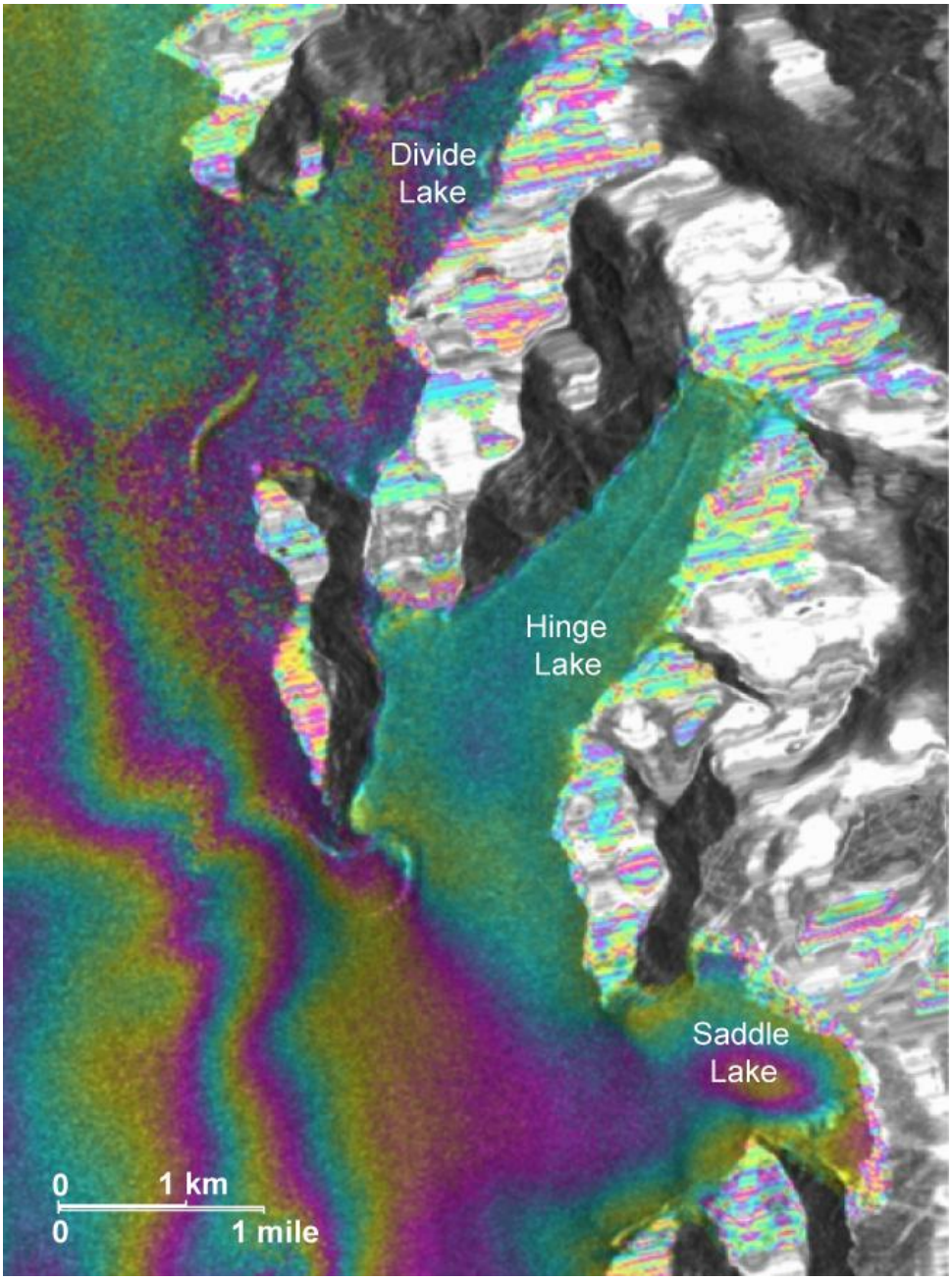

22 to 23 March 1996

Appendix B. Dendrochronology COFECHA output

CONTENTS:

Part 1: Options selected, summary, absent rings by series
Part 2: Histogram of time spans
Part 3: Bar plot of master ring series
Part 4: Correlation by segment of each series with Master ring series
Part 5: Descriptive statistics

PART 1: OPTIONS SELECTED, SUMMARY, ABSENT RINGS BY SERIES

RUN CONTROL OPTIONS SELECTED

1 Cubic smoothing spline 50% wavelength cutoff for filter in	32 years
2 Segments examined are:	50 years lagged successively by 25 years
3 Autoregressive model applied:	A Residuals are used in master dating series and testing
4 Series transformed to logarithms:	Y Each series log-transformed for master dating series
5 CORRELATION is Pearson (parametric, quantitative):	Critical correlation, 99% confidence level 0.3281
6 Master dating series saved:	N
7 Ring measurements listed:	N

Time span of master dating series:	1370 to 1861 (492 years)
Continuous time span:	1370 to 1861 (492 years)
Portion with two or more series:	1463 to 1846 (384 years)

```
**************************************
*C* Number of dated series           56
*O* Master series 1370-1861         492 yrs
*F* Total rings in all series      9510
*E* Total dated rings checked      9402
*C* Series intercorrelation       0.485
*H* Average mean sensitivity      0.237
*A* Segments possible problems       60
Mean length of series               169
**************************************

Ring series are listed hereafter by acronyms:
BG - Brady Glacier site
SL - Spur Lake site
NT - North Trick Lake site

ABSENT RINGS listed by SERIES: See Master Dating Series for absent rings listed by year

BG0718A     1 absent rings:   1773
BG0718B     3 absent rings:   1772 1813 1814
BG0720B     1 absent rings:   1752
BG0727A     2 absent rings:   1798 1799
BG0727B     1 absent rings:   1791
SL16        1 absent rings:   1753
            9 absent rings   0.095%
```

PART 2: TIME PLOT OF TREE-RING SERIES

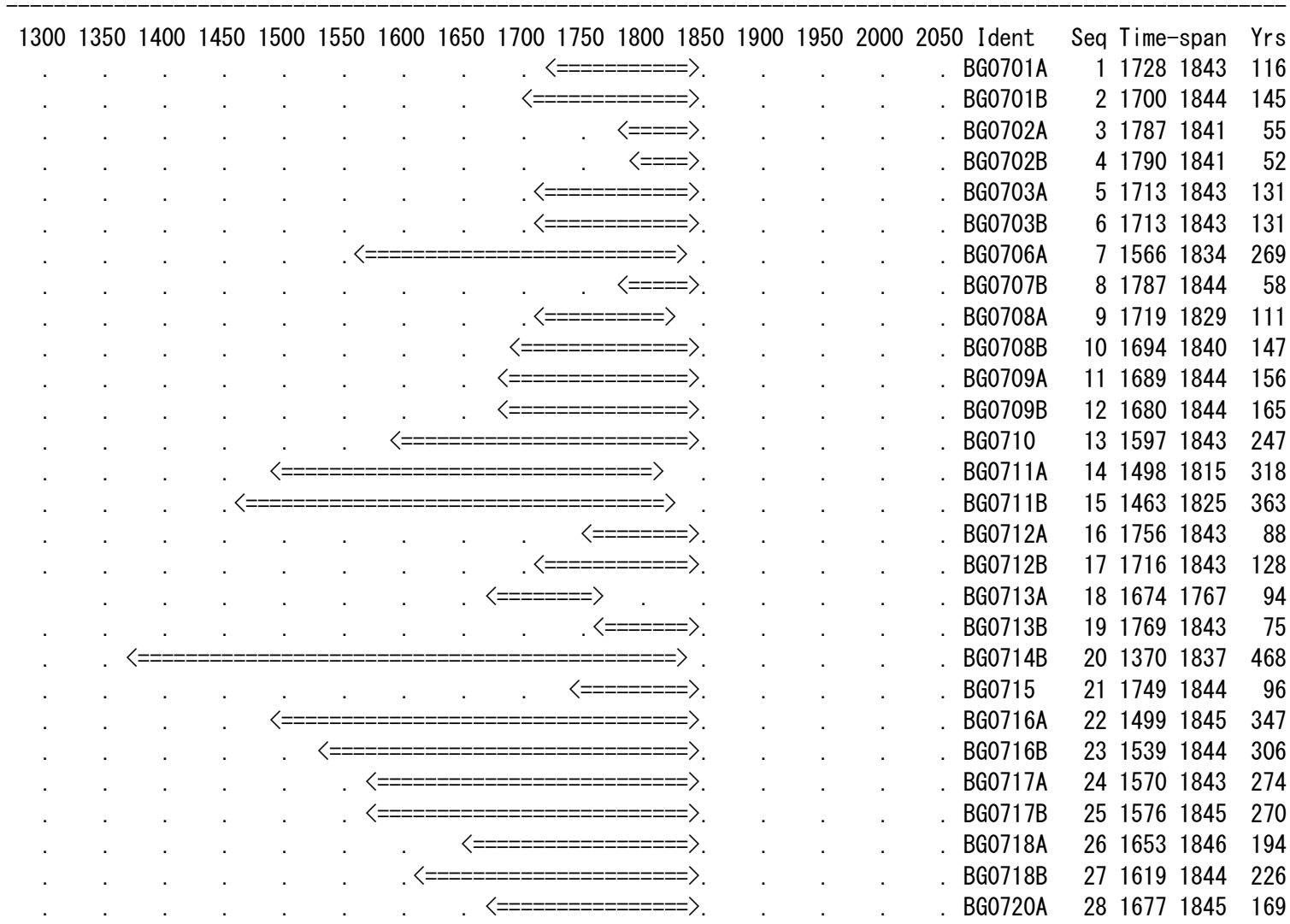

PART 2: TIME PLOT OF TREE-RING SERIES (continued)

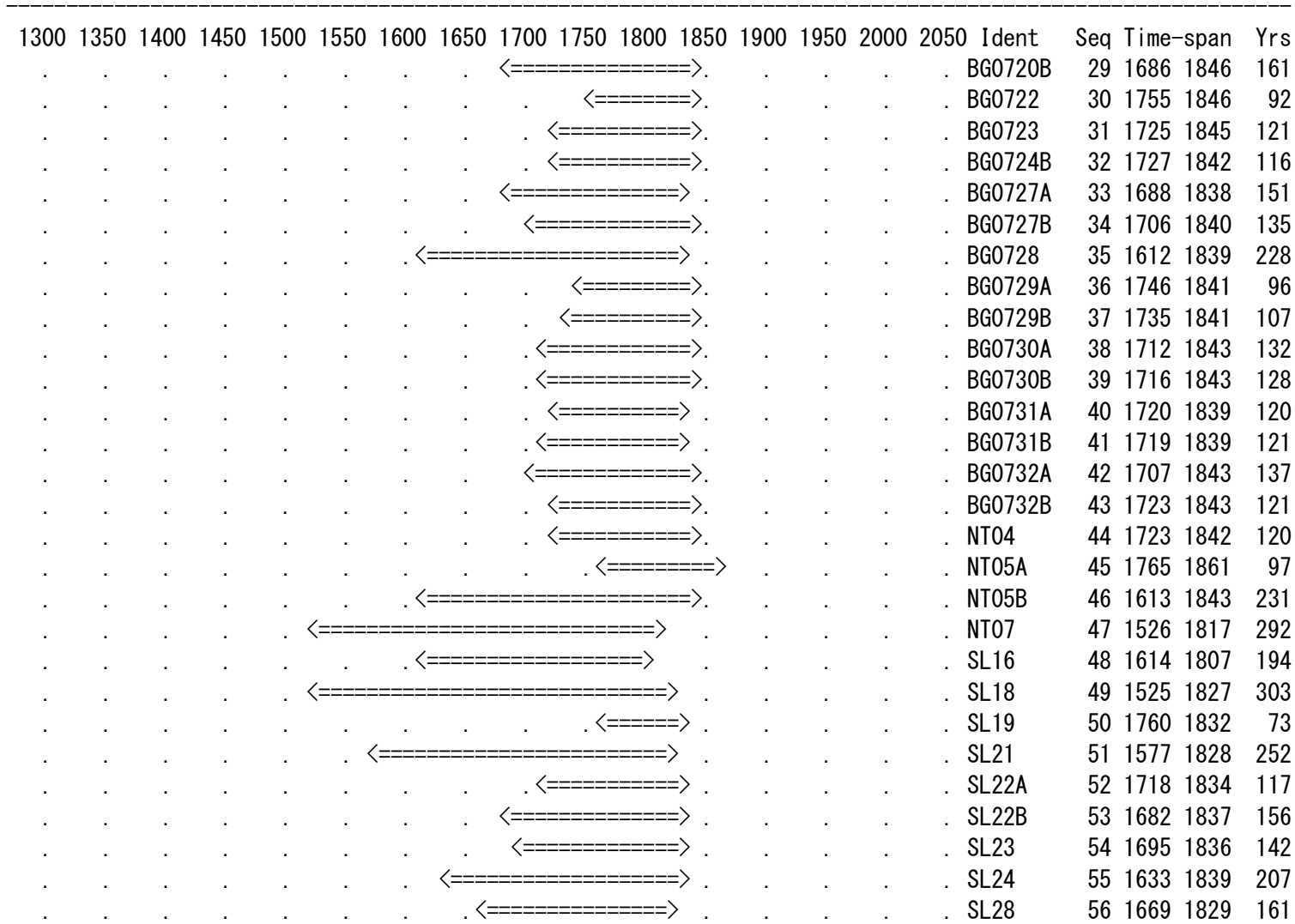

PART 3: Master Bar Plot

Length of line next to date indicates relative width of tree ring. Upper-case alphabetic characters represent rings that are wider than the mean and lower-case characters represent rings that are narrower than the mean. The "@" symbol represents a value very near the mean. The higher the upper-case letter, the wider the ring. The higher the lower-case letter, the narrower the ring. Each change in letter represents an additional 0.25 standard deviation departure from the mean (Grissino-Mayer, 2001).

Year	Rel value	Year	Rel value	Year	Rel value	Year	Rel value	Year	Rel value	Year	Rel value	Year	Rel value
1370	g	1442	o	1514	---------D	1586	-e	1658	-----@	1730	-----@	1802	-----A
1371	----------G	1443	l	1515	---------E	1587	-e	1659	--------C	1731	--------C	1803	--------C
1372	---a	1444	--b	1516	------A	1588	-d	1660	--c	1732	-----A	1804	----------E
1373	---------D	1445	-----@	1517	-----@	1589	-e	1661	-d	1733	----a	1805	----------F
1374	---------D	1446	--c	1518	------A	1590	--b	1662	--b	1734	-d	1806	---a
1375	----------I	1447	--b	1519	---------D	1591	--b	1663	---a	1735	------A	1807	------A
1376	-------B	1448	----a	1520	---------E	1592	---a	1664	--c	1736	-----@	1808	-----A
1377	------A	1449	-----@	1521	--------C	1593	----@	1665	---b	1737	---------D	1809	----a
1378	------A	1450	---------D	1522	--c	1594	--------C	1666	---a	1738	-----@	1810	-e
1379	--c	1451	-d	1523	-------B	1595	--------C	1667	--------C	1739	---------E	1811	-d
1380	--------C	1452	---------D	1524	-------B	1596	-----@	1668	--------C	1740	------A	1812	g
1381	g	1453	------A	1525	-----@	1597	---------D	1669	---------E	1741	----@	1813	g
1382	--c	1454	---------D	1526	-----A	1598	-------B	1670	-----A	1742	---a	1814	f
1383	-e	1455	-e	1527	h	1599	-----A	1671	-------B	1743	--b	1815	----a
1384	l	1456	--b	1528	--b	1600	----a	1672	---a	1744	--c	1816	--------C
1385	---a	1457	----------G	1529	g	1601	----a	1673	------A	1745	---a	1817	---a
1386	g	1458	----------F	1530	----a	1602	----@	1674	-------B	1746	------A	1818	-----A
1387	----@	1459	----------F	1531	-----@	1603	--b	1675	--------C	1747	-------B	1819	------A
1388	l	1460	----------I	1532	-------B	1604	------A	1676	--c	1748	---------D	1820	--------C
1389	f	1461	--------C	1533	--------C	1605	---a	1677	-f	1749	---------D	1821	-------B

1390--c
1391-------B
1392----------H
1393----------F
1394--c
1395----------E
1396---------C
1397----------G
1398----------E
1399---------D
1400------A
1401--------C
1402---------D
1403-------B
1404q
1405--c
1406-----@
1407--b
1408f
1409g
1410----------F
1411----------H
1412----------F
1413----------I
1414-------B
1415-d
1416----a
1417---------D
1462----------G
1463------A
1464-------B
1465-d
1466k
1467h
1468---b
1469-----A
1470----a
1471g
1472---a
1473----------G
1474-----@
1475----@
1476-------B
1477---a
1478------A
1479---------D
1480----------H
1481----------G
1482----------I
1483---------D
1484--c
1485g
1486--c
1487g
1488---b
1489-----@
1534------A
1535-d
1536---a
1537--------C
1538--------C
1539--c
1540---a
1541---------E
1542--------B
1543-------B
1544------A
1545---------D
1546-----@
1547---a
1548f
1549--c
1550-----@
1551-------B
1552---b
1553------A
1554---------E
1555----------E
1556------A
1557---a
1558----a
1559---------D
1560g
1561----@
1606--------C
1607------A
1608------A
1609--c
1610-----@
1611------A
1612---------D
1613-------B
1614----@
1615-----@
1616---------D
1617-----@
1618--c
1619--b
1620---a
1621-----A
1622-------B
1623------A
1624-------B
1625----a
1626--b
1627-----@
1628---a
1629-d
1630-----@
1631-----@
1632----@
1633--c
1678-----@
1679h
1680-d
1681-d
1682-----A
1683--------C
1684-------B
1685----------F
1686-------B
1687---------D
1688-----@
1689------A
1690----@
1691-----@
1692-----@
1693----a
1694---a
1695-------B
1696-----@
1697-d
1698i
1699-e
1700---a
1701------A
1702--------C
1703--------C
1704---------D
1705--------C
1750----------G
1751--------C
1752--c
1753-d
1754h
1755-e
1756-e
1757--b
1758-----A
1759-----@
1760---a
1761---------D
1762--------C
1763---------E
1764-------B
1765---------E
1766---------D
1767--------C
1768-d
1769--c
1770-d
1771-e
1772-e
1773--c
1774------A
1775-------B
1776-------B
1777---------D
1822----------E
1823---------D
1824--------C
1825---------D
1826---a
1827----a
1828--------C
1829---------D
1830--c
1831--c
1832-----A
1833-----A
1834--c
1835---b
1836--b
1837-----A
1838--------C
1839----a
1840-------B
1841-------B
1842------A
1843-e
1844-d
1845---b
1846-e
1847h
1848k
1849f

1418------A
1419-d
1420------A
1421n
1422-----@
1423-e
1424f
1425----------H
1426----------H
1427-----@
1428-------B
1429---------D
1430---a
1431--------C
1432------A
1433----------F
1434------A
1435--------C
1436---a
1437--------C
1438---------D
1439----------L
1440---------E
1441m
1490---b
1491-------B
1492---b
1493---b
1494g
1495--c
1496------A
1497---------D
1498-------B
1499---------D
1500---------D
1501--------C
1502---b
1503----------F
1504--c
1505g
1506--c
1507----@
1508---a
1509-e
1510-d
1511--------C
1512----@
1513---a
1562------A
1563-------B
1564----@
1565----a
1566-----@
1567----a
1568----@
1569-e
1570-d
1571-d
1572---a
1573-----@
1574----@
1575---------D
1576---------D
1577--------C
1578--------C
1579-------B
1580----a
1581-------B
1582---------D
1583---------D
1584------A
1585-e
1634---------E
1635--------C
1636---b
1637----a
1638--c
1639--b
1640----a
1641--c
1642--------C
1643-----@
1644--------C
1645-------B
1646------A
1647--------C
1648--------C
1649------A
1650--------C
1651-----@
1652----@
1653-----@
1654--c
1655------A
1656--b
1657------A
1706g
1707--------C
1708------A
1709-------B
1710--------C
1711-d
1712------A
1713-------B
1714---b
1715------A
1716---a
1717h
1718------A
1719---------D
1720----a
1721---------D
1722--------C
1723---------E
1724------A
1725----@
1726g
1727-d
1728--b
1729----a
1778--------C
1779--------C
1780---------E
1781------A
1782--------C
1783---b
1784------A
1785-------B
1786--c
1787-e
1788-----A
1789-e
1790g
1791-d
1792---a
1793-------B
1794--------C
1795---------D
1796-------B
1797--------C
1798--c
1799---b
1800-----A
1801------A
1850h
1851-e
1852---------D
1853-----A
1854-d
1855----@
1856-------B
1857--------C
1858---------E
1859---------E
1860----------E
1861j

PART 4: CORRELATION OF SERIES BY SEGMENTS

Correlations of 50-year dated segments, lagged 25 years
Flags: A = correlation under 0.3281 but highest as dated; B = correlation higher at other than dated position

Seq	Series	Time_span	1450 1499	1475 1524	1500 1549	1525 1574	1550 1599	1575 1624	1600 1649	1625 1674	1650 1699	1675 1724	1700 1749	1725 1774	1750 1799	1775 1824	1800 1849			
1	BG0701A	1728 1843												.62	.78	.75	.69			
2	BG0701B	1700 1844											.55	.67	.80	.72	.60			
3	BG0702A	1787 1841														.55	.43			
4	BG0702B	1790 1841														.76	.63			
5	BG0703A	1713 1843											.52	.49	.53	.66	.67			
6	BG0703B	1713 1843											.49	.47	.50	.57	.65			
7	BG0706A	1566 1834					.55	.63	.67	.43	.44	.59	.54	.42	.39	.46	.40			
8	BG0707B	1787 1844														.48	.50			
9	BG0708A	1719 1829											.70	.69	.66	.64	.65			
10	BG0708B	1694 1840										.39	.34	.61	.74	.54	.46			
11	BG0709A	1689 1844										.39	.42	.49	.53	.52	.69			
12	BG0709B	1680 1844										.40	.50	.54	.56	.50	.65			
13	BG0710	1597 1843						.00B	.01B	.17B	.41	.58	.51	.28A	.40	.51	.44			
14	BG0711A	1498 1815		.49	.52	.56	.67	.52	.49	.60	.61	.71	.69	.70	.67	.61				
15	BG0711B	1463 1825	.28B	.30B	.58	.59	.64	.31A	.42	.66	.64	.72	.65	.65	.59	.35	.36			
16	BG0712A	1756 1843													.64	.66	.67			
17	BG0712B	1716 1843											.69	.74	.73	.71	.69			
18	BG0713A	1674 1767									.63	.63	.50	.37B						
19	BG0713B	1769 1843													.63	.65	.53			
20	BG0714B	1370 1837	.17B	.19B	.24B	.30B	.42	.43	.50	.36	.59	.80	.78	.64	.30B	.06B	-.10B			
21	BG0715	1749 1844												.65	.65	.68	.36			
22	BG0716A	1499 1845		-.13B	-.09B	-.19B	-.03B	.13B	.04B	-.03B	.25A	.64	.61	.47	.51	.46	.36			
23	BG0716B	1539 1844				.17B	-.06B	-.33B	.03B	.32A	.32A	.55	.63	.60	.52	.46	.48			

PART 4: CORRELATION OF SERIES BY SEGMENTS (continued)

Seq	Series	Time_span	1450 1499	1475 1524	1500 1549	1525 1574	1550 1599	1575 1624	1600 1649	1625 1674	1650 1699	1675 1724	1700 1749	1725 1774	1750 1799	1775 1824	1800 1849
24	BG0717A	1570 1843					.38	.35	.35	.36	.43	.58	.58	.55	.52	.31B	.09B
25	BG0717B	1576 1845						.57	.55	.50	.50	.61	.61	.57	.53	.52	.43
26	BG0718A	1653 1846									.40	.51	.57	.61	.60	.59	.56
27	BG0718B	1619 1844							.06B	.11B	.56	.51	.57	.73	.53	.33B	.32A
28	BG0720A	1677 1845										.56	.44	.34	.36	.33B	.28B
29	BG0720B	1686 1846										.53	.51	.31A	.27B	.31B	.31B
30	BG0722	1755 1846													.55	.73	.55
31	BG0723	1725 1845												.50	.42	.62	.63
32	BG0724B	1727 1842												.43	.54	.65	.66
33	BG0727A	1688 1838										.61	.67	.68	.55	.41	.52
34	BG0727B	1706 1840											.72	.64	.42	.42	.58
35	BG0728	1612 1839							.52	.50	.74	.76	.69	.77	.78	.73	.43B
36	BG0729A	1746 1841												.60	.61	.56	.40
37	BG0729B	1735 1841												.38B	.64	.53	.36
38	BG0730A	1712 1843											.61	.58	.64	.61	.50
39	BG0730B	1716 1843											.57	.58	.70	.66	.62
40	BG0731A	1720 1839											.59	.53	.44B	.67	.58
41	BG0731B	1719 1839											.66	.59	.49	.71	.65
42	BG0732A	1707 1843											.38	.41	.62	.60	.63
43	BG0732B	1723 1843											.38	.39	.64	.62	.59
44	NT04	1723 1842											.39B	.40B	.57	.54	.40B
45	NT05A	1765 1861													.63	.67	.45
46	NT05B	1613 1843							.22B	.18B	.14B	.41	.49	.56	.60	.45	.40
47	NT07	1526 1817				.32A	.41	.32A	.17B	.11B	.35	.71	.51	.33A	.61	.66	
48	SL16	1614 1807							.45	.49	.60	.61	.60	.64	.58	.35	
49	SL18	1525 1827				.09B	.17B-	.09B-	.14B	.37	.68	.62	.54	.61	.68	.56	.55

PART 4: CORRELATION OF SERIES BY SEGMENTS (continued)

Seq	Series	Time_span	1450 1499	1475 1524	1500 1549	1525 1574	1550 1599	1575 1624	1600 1649	1625 1674	1650 1699	1675 1724	1700 1749	1725 1774	1750 1799	1775 1824	1800 1849		
50	SL19	1760 1832													.53	.54	.59		
51	SL21	1577 1828						.45	.46	.47	.47	.58	.53	.38	.57	.55	.57		
52	SL22A	1718 1834											.52	.45	.66	.59	.62		
53	SL22B	1682 1837										.65	.51	.46	.63	.48	.40		
54	SL23	1695 1836										.55	.51	.49	.54	.48	.50		
55	SL24	1633 1839								.60	.66	.64	.50	.60	.72	.71	.50		
56	SL28	1669 1829									.62	.64	.60	.52	.61	.55	.26B		
Av segment correlation			0.23	0.21	0.31	0.26	0.35	0.27	0.30	0.36	0.50	0.59	0.56	0.54	0.58	0.55	0.49		

PART 5: DESCRIPTIVE STATISTICS

Seq	Series	Interval	No. Years	No. Segmt	No. Flags	Corr with Master	Unfiltered Mean msmt	Unfiltered Max msmt	Unfiltered Std dev	Unfiltered Auto corr	Unfiltered Mean sens	Filtered Max value	Filtered Std dev	Filtered Auto corr	AR ()
1	BG0701A	1728 1843	116	4	0	0.676	1.56	3.68	0.602	0.793	0.180	2.81	0.540	0.036	2
2	BG0701B	1700 1844	145	5	0	0.637	1.57	3.00	0.578	0.785	0.197	2.57	0.453	0.019	1
3	BG0702A	1787 1841	55	2	0	0.419	1.71	2.50	0.446	0.667	0.175	2.48	0.463	-0.038	2
4	BG0702B	1790 1841	52	2	0	0.648	1.68	2.76	0.520	0.733	0.187	2.56	0.543	-0.042	1
5	BG0703A	1713 1843	131	5	0	0.582	1.42	2.54	0.396	0.737	0.170	2.76	0.534	0.031	1
6	BG0703B	1713 1843	131	5	0	0.538	1.30	2.11	0.341	0.756	0.153	2.62	0.506	0.024	1
7	BG0706A	1566 1834	269	11	0	0.471	0.74	5.08	0.679	0.799	0.326	2.92	0.262	-0.047	1
8	BG0707B	1787 1844	58	2	0	0.466	3.04	5.42	0.796	0.729	0.153	2.58	0.566	0.073	1
9	BG0708A	1719 1829	111	5	0	0.659	0.67	2.10	0.412	0.882	0.196	2.86	0.421	-0.014	2
10	BG0708B	1694 1840	147	6	0	0.512	0.71	2.47	0.473	0.890	0.212	2.87	0.475	0.068	1
11	BG0709A	1689 1844	156	6	0	0.514	0.64	1.88	0.369	0.860	0.211	2.76	0.406	0.020	1
12	BG0709B	1680 1844	165	6	0	0.512	0.73	1.54	0.278	0.778	0.206	2.48	0.354	0.001	1
13	BG0710	1597 1843	247	10	4	0.372	0.66	2.39	0.367	0.843	0.270	2.69	0.465	-0.028	1
14	BG0711A	1498 1815	318	13	0	0.588	0.63	2.25	0.454	0.927	0.228	2.52	0.311	-0.034	5
15	BG0711B	1463 1825	363	15	3	0.484	0.58	3.08	0.526	0.944	0.226	2.60	0.378	-0.018	5
16	BG0712A	1756 1843	88	3	0	0.663	1.15	2.17	0.470	0.831	0.201	2.56	0.445	0.045	1
17	BG0712B	1716 1843	128	5	0	0.684	0.93	2.11	0.424	0.855	0.208	2.56	0.385	-0.042	1
18	BG0713A	1674 1767	94	4	1	0.547	1.24	2.05	0.354	0.669	0.191	2.79	0.558	-0.020	1
19	BG0713B	1769 1843	75	3	0	0.522	0.77	1.30	0.237	0.761	0.149	2.68	0.450	-0.041	1
20	BG0714B	1370 1837	468	15	7	0.353	0.46	2.56	0.318	0.886	0.256	2.61	0.400	-0.015	1
21	BG0715	1749 1844	96	4	0	0.466	0.76	1.48	0.289	0.816	0.165	2.71	0.427	-0.094	1
22	BG0716A	1499 1845	347	14	8	0.228	0.64	2.60	0.511	0.896	0.265	2.64	0.357	-0.014	7
23	BG0716B	1539 1844	306	12	6	0.337	0.55	2.88	0.420	0.871	0.286	2.84	0.409	-0.014	7
24	BG0717A	1570 1843	274	11	2	0.385	0.42	3.50	0.364	0.863	0.283	2.61	0.343	-0.020	1
25	BG0717B	1576 1845	270	10	0	0.524	0.56	2.25	0.363	0.853	0.284	2.49	0.255	-0.060	1

PART 5: DESCRIPTIVE STATISTICS (continued)

Seq	Series	Interval	No. Years	No. Segmt	No. Flags	Corr with Master	//-------- Unfiltered -------- Mean msmt	Max msmt	Std dev	Auto corr	//---- Filtered ----- Mean sens	Max value	Std dev	Auto corr	AR ()
26	BG0718A	1653 1846	194	7	0	0.542	0.69	2.21	0.338	0.639	0.360	2.55	0.349	-0.020	1
27	BG0718B	1619 1844	226	9	4	0.467	0.63	2.29	0.334	0.709	0.352	2.66	0.405	-0.009	3
28	BG0720A	1677 1845	169	6	2	0.381	0.65	1.53	0.287	0.850	0.186	2.55	0.375	-0.020	3
29	BG0720B	1686 1846	161	6	4	0.391	0.75	1.75	0.390	0.883	0.217	2.35	0.278	0.020	1
30	BG0722	1755 1846	92	3	0	0.546	0.88	2.12	0.384	0.786	0.205	2.58	0.444	0.001	1
31	BG0723	1725 1845	121	4	0	0.561	0.52	1.48	0.214	0.834	0.196	2.84	0.529	0.038	1
32	BG0724B	1727 1842	116	4	0	0.521	0.76	2.08	0.351	0.813	0.252	2.60	0.367	0.000	1
33	BG0727A	1688 1838	151	6	0	0.588	1.34	3.68	0.777	0.788	0.322	2.64	0.353	0.042	1
34	BG0727B	1706 1840	135	5	0	0.548	1.37	3.61	0.807	0.817	0.342	2.72	0.427	0.024	1
35	BG0728	1612 1839	228	9	1	0.596	1.02	2.12	0.484	0.886	0.179	2.72	0.298	0.013	1
36	BG0729A	1746 1841	96	4	0	0.504	0.98	1.73	0.306	0.672	0.213	2.61	0.408	0.031	1
37	BG0729B	1735 1841	107	4	1	0.408	0.95	1.92	0.312	0.722	0.208	2.52	0.316	0.078	1
38	BG0730A	1712 1843	132	5	0	0.598	1.43	2.58	0.481	0.816	0.164	2.63	0.383	0.040	1
39	BG0730B	1716 1843	128	5	0	0.625	1.45	2.72	0.496	0.875	0.140	2.67	0.456	0.011	1
40	BG0731A	1720 1839	120	5	1	0.565	0.81	2.05	0.399	0.881	0.191	2.41	0.345	-0.069	2
41	BG0731B	1719 1839	121	5	0	0.626	0.82	1.83	0.400	0.871	0.191	2.53	0.381	-0.039	1
42	BG0732A	1707 1843	137	5	0	0.508	1.08	2.43	0.457	0.735	0.232	2.57	0.482	-0.050	1
43	BG0732B	1723 1843	121	5	0	0.507	1.05	2.16	0.419	0.772	0.208	2.39	0.325	0.015	1
44	NT04	1723 1842	120	5	3	0.438	1.80	3.54	0.652	0.763	0.199	2.67	0.532	0.059	1
45	NT05A	1765 1861	97	3	0	0.526	3.14	5.81	1.063	0.735	0.195	2.50	0.410	0.034	1
46	NT05B	1613 1843	231	9	3	0.404	0.39	1.14	0.185	0.813	0.235	2.58	0.342	-0.038	2
47	NT07	1526 1817	292	11	5	0.418	0.70	2.10	0.366	0.830	0.227	2.72	0.380	0.022	6
48	SL16	1614 1807	194	8	0	0.471	0.55	1.84	0.359	0.773	0.321	2.53	0.355	-0.057	1

PART 5: DESCRIPTIVE STATISTICS (continued)

Seq	Series	Interval	No. Years	No. Segmt	No. Flags	Corr with Master	Unfiltered Mean msmt	Unfiltered Max msmt	Unfiltered Std dev	Unfiltered Auto corr	Unfiltered Mean sens	Filtered Max value	Filtered Std dev	Filtered Auto corr	AR ()
49	SL18	1525 1827	303	12	4	0.358	0.67	3.31	0.464	0.852	0.269	2.58	0.347	-0.025	1
50	SL19	1760 1832	73	3	0	0.556	1.35	3.63	0.621	0.710	0.239	2.79	0.460	-0.086	2
51	SL21	1577 1828	252	10	0	0.483	1.04	2.99	0.615	0.885	0.200	2.71	0.425	0.055	1
52	SL22A	1718 1834	117	5	0	0.556	2.63	7.25	1.433	0.889	0.212	2.46	0.351	-0.036	2
53	SL22B	1682 1837	156	6	0	0.513	1.71	3.94	0.905	0.878	0.213	2.48	0.366	0.053	1
54	SL23	1695 1836	142	6	0	0.521	1.82	4.56	0.857	0.838	0.202	2.78	0.441	0.035	1
55	SL24	1633 1839	207	8	0	0.570	1.54	6.75	1.007	0.899	0.221	2.70	0.354	-0.002	2
56	SL28	1669 1829	161	7	1	0.447	19.81	63.97	13.705	0.836	0.268	2.47	0.279	-0.044	2
Total or mean:			9510	368	60	0.485	1.25	63.97	0.702	0.831	0.237	2.92	0.387	-0.006	